Coordination of Limb Bud Development: The Role of SHH in PD Limb Bud Patterning

5   Material and Methods   36

1 List of Abbreviations

ADH	Alcohol dehydrogenase		**GLI3**	GLI-Kruppel family member GLI3
AER	Apical ectodermal ridge		**GLI3R**	GLI3 repressor form
Alcam	Activated leukocyte cell adhesion molecule		**GLIA**	GLI activator form
			GLIFL	GLI full-length form
Aldh1a2	aldehyde dehydrogenase family 1, subfamily A2		**GREM1**	Gremlin 1
			Gria2	Glutamate receptor, ionotropic, AMPA2 (alpha 2)
AVE	Anterior visceral endoderm			
AP	Antero-posterior		**GSK3**	Glycogen synthase kinase 3
BAC	Bacterial artificial chromosome		**GST**	Glutathione-S-transferase
BMP	Bone morphogenetic protein		**HAND2**	Heart and neural crest derivatives expressed transcript 2
CASK	Calcium/calmodulin-dependent serine protein kinase			
			HC	Hypertrophic chondrocytes
Cdk6	Cyclin dependent kinase 6		**Hh**	Hedgehog
cDNA	Complementary DNA		**Hhip**	Hedgehog interacting protein
CK1	Casein kinase 1		**Hox**	Homeobox gene
CMV	Cytomegalovirus		**HRP**	Horse radish peroxidase
Cre	Cyclization recombination		**HSPG**	Heparan sulfate proteoglycan
Cxcr7	Chemokine (C-X-C motif) receptor 7		**Id**	Inhibitor of DNA binding
CYP26	Cytochrome P450 group 26		**IHH**	Indian hedgehog
DIG	Digoxigenin		**KIF7**	Kinesin family member 7
DHH	Desert hedgehog		**LPM**	Lateral plate mesoderm
DMEM	Dulbecco's modified Eagle medium		**loxP**	locus of X-over P1
DMSO	Dimethylsulfoxid		**MAPK**	Mitogen activated protein kinase
DNA	Deoxyribonucleic acid		**MBP**	Myelin basic protein
DTT	Dithiothreitol		**MEF**	Mouse embryonic fibroblast
DV	Dorso-ventral		**Meis**	Meis homeobox
EDTA	Ethylenediaminetetraacetic acid		**MFCS1**	Mammals-fish conserved sequence 1
ER	Endoplasmic reticulum		**NeoR**	Neomycin resistance
ES	Embryonic stem		**N-myc**	V-myc myelocytomatosis viral related oncogene, neuroblastoma derived
EtOH	Ethanol			
FCS	Fetal calf serum		**PBS**	Phosphate buffered saline
FGF	Fibroblast growth factor		**PBT**	PBS with 0.1% Tween 20
FGFR	FGF receptor		**Pbx1**	Pre-B-cell leukemia homeobox 1
FPC	Flat proliferating chondrocytes		**PC**	Proliferating chondrocytes
FRT	Flippase recognition target		**PCR**	Polymerase chain reaction
GFP	Green fluorescent protein		**PD**	Proximo-distal

PFA	Paraformaldehyde
PGK	Phospho glycerate kinase
PKA	Protein kinase A
PKC	Protein kinase C
PKDCC	Protein kinase domain containing, cytoplasmic
Prdm1	PR domain containing 1, with ZNF domain
PTCH	Patched
PZ	Progress zone
RA	Retinoic acid
RAA	Retinoic acid antagonist
RALDH	Retinaldehyde dehydrogenase
RAR	Retinoic acid receptor
Rb	Retinoblastoma
RBP4	Retinol binding protein 4
RDH	Retinol dehydrogenase
RMCE	Recombinase mediated cassette exchange
RNA	Ribonucleic acid
RT	Room temperature
RT PCR	Real time PCR
RXR	Retinoic X receptor
SDS	Sodium dodecyl sulphate
SGK493	Sugen kinase 493
SHH	Sonic hedgehog
SMO	Smoothened
Sox9	SRY-box containing gene 9
Spry	Sprouty
STRA6	Stimulated by retinoic acid gene 6
TALE	Three amino acid loop extension
TBST	Tris buffered saline with 0.1% Tween 20
TGF-ß	Transforming growth factor ß
TGN46	Trans-golgi network protein 2
VAD	Vitamin A deficiency
WISH	Whole mount *in situ* hybridisation
Wnt5a	Wingless-related MMTV integration site 5A
Wt	Wild-type
Zfhx	Zinc finger homeodomain
ZPA	Zone of polarizing activity

2 Summary

The limb bud serves as an excellent model to investigate the signals involved in diverse processes during embryonic development. Limb bud development is controlled by complex regulatory networks that instruct coordinated patterning and proliferation of mesenchymal progenitors along the dorso-ventral (DV), antero-posterior (AP) and proximo-distal (PD) limb axes. Over the last two decades many of the underlying molecular mechanisms instructing limb development have been described. Nevertheless, little is known about how these signals are integrated into the networks controlling limb bud development and how the cells respond to these signals to acquire their identity. Sonic hedgehog (SHH) is known to specify the AP limb bud axis and regulate its expansion as part of a larger self-regulatory signalling system. To analyze the genome-wide effects and to identify novel targets of SHH signalling in the limb bud, we have performed microarray analysis on *Shh*-deficient limb buds. From this analysis we have identified a novel kinase (*Pkdcc*), whose expression is up-regulated in *Shh*-deficient limb buds and that is dynamically expressed during development. Targeted deletion of the *Pkdcc* gene in mice shows that *Pkdcc* is essential for embryonic development. Furthermore, the transcriptome analysis uncovers an unexpected function of SHH in PD limb axis development as *Shh*-deficient mouse limb buds are proximalized. Expression of proximal genes and retinoic acid (RA) pathway activity are up-regulated and distally expanded in *Shh*-deficient limb buds. In parallel, the expression of the RA inactivating enzyme *Cyp26b1* is decreased in the distal mesenchyme. We have investigated the possible SHH-RA interactions using a combination of experimental manipulation, genetics and mathematical simulations. Our findings reveal a SHH-dependent signalling module that normally enhances RA clearance by increasing fibroblast growth factor (FGF) signalling in the apical ectodermal ridge (AER), which in turn up-regulates *Cyp26b1* expression in the distal mesenchyme. Disruption or reduction of CYP26b1-mediated RA clearance interferes with distal limb bud development leading to molecular proximalization of *Shh*-, AER-*Fgf*- and *Cyp26b1*-deficient limb buds. In addition, we provide molecular evidence for early specification of the PD axis by a mutually inhibitory interaction of RA with AER-FGFs. Subsequently AP and PD limb bud patterning becomes interlinked via SHH mediated regulation of the AER-FGF/CYP26b1/RA signalling module, which enables spatially coordinated progression of limb bud development.

3 Introduction

The tetrapod limb as a system to study organogenesis and the coordination of patterning with growth

Over the last 60 years the developing vertebrate limb has served as an excellent model to study how pattern formation and growth are controlled during embryogenesis. During the last two decades, many of the underlying molecular mechanisms that instruct the spatial organisation of undifferentiated limb cells have been described. Most of the key developmental signalling pathways are involved in the regulation of limb development. In general, these pathways are also of importance to the development of other structures than limbs. Their deregulation plays important roles in pathological circumstances.

The limb is a well-suited model structure to study these pathway interactions because changes of the limb skeleton provide a good readout for alterations in signals important during limb development. During evolution a large variety of limbs such as legs and wings were developed, but the basic organisation of the vertebrate limb skeleton is conserved. During its outgrowth the limb has to be correctly patterned along its three axes. These axes are the proximo-distal (PD) axis, running from the shoulder to the digits; the antero-posterior (AP) axis, from the thumb to the pinky and the dorso-ventral (DV) axis from the back of the hand to the palm. The three main skeletal elements of the PD axis are the proximal stylopod (humerus or femur), followed by the zeugopod (radius/ulna or tibia/fibula) and the distal autopod (digits and metacarpals). The skeletal elements of the zeugopod and the autopod provide the readout for the AP axis, with the radius and the thumb (digit 1) being the most anterior and the ulna and the pinky (digit 5) being the most posterior elements [**Figure 1A**].

Limb development begins with the formation of a limb bud. It starts with the appearance of a small bulge of mesodermal cells from the lateral plate mesoderm (LPM) at defined positions along the embryonic axis. This bulge is encased in ectoderm and rapidly grows along the PD axis. At the same time as the limb bud grows it is patterned along its three axes. Later this results in the formation of cartilage condensations with a proximal to distal sequence, which will give rise to the final skeletal elements. During these steps, patterning and formation of the skeletal elements along the three axes need to be coordinated with efficient outgrowth of the limb bud [**Figure 1**].

A

Mouse

Chicken

A: scapula, B: humerus, A: radius, C: ulna, 1-5: digits 1 to 5

B

E9.5 E10.5 E12 E14.5 E11.5

C

Fgf8 *Shh* *Rarb* (RA activity) *Gli3*
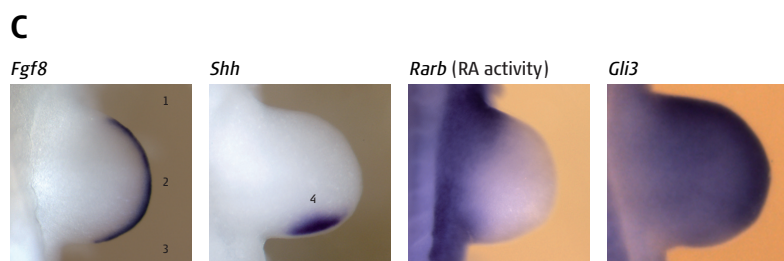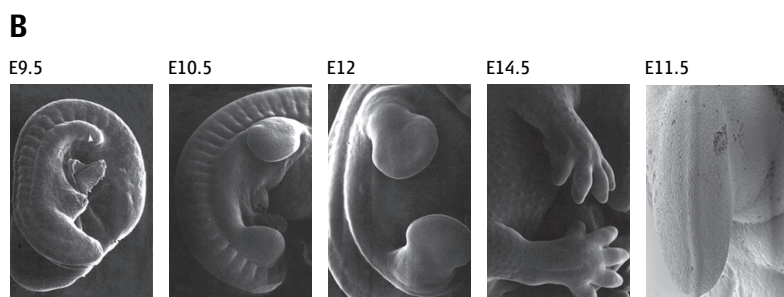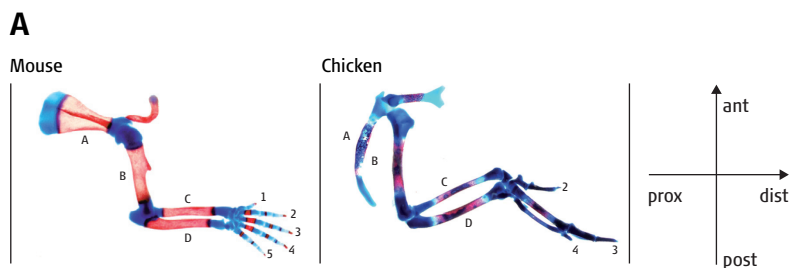
1: ant, 2: AER, 3: post, 4: ZPA

[**Figure 1**] The skeletal structure of tetrapod limbs and the main signalling centres involved in limb bud morphogenesis are shown. [**A**] The skeleton of a newborn mouse forelimb and of a chicken wing at day 15 of embryonic development are shown. The blue staining marks the cartilage and the red staining the bone. The names of the skeletal elements are indicated (from (Benazet and Zeller, 2009)). [**B**] Scanning electron microscopy (EM) pictures of E9.5 to E14.5 mouse embryos showing forelimb and hindlimb (from (Zuniga and Galli, 2005)). The last panel shows a scanning EM picture of the AER at E11.5 (from (Michos et al., 2004)). [**C**] In situ hybridisation on limb buds with probes visualizing different important structures or signals during limb development. All limbs are oriented with anterior (ant) to the top and posterior (post) to the bottom. The first panel shows the expression pattern of *Fgf8*, which is expressed in the AER. The second panel shows *Shh* expression, marking the ZPA. The third panel shows *Rarb* expression, which demarcates RA activity and the fourth panel shows *Gli3* expression, which creates an AP gradient of GLI3R (*Shh* expression image from J.D. Benazet and *Gli3* expression image from J. Lopez-Rios). AER: apical ectodermal ridge, ant: anterior, AP: antero-posterior, dist: distal, post: posterior, prox: proximal, ZPA: zone of polarizing activity.

Patterning along the proximo-distal (PD) axis

The AER is an important signalling centre for PD limb bud development – In the last 60 years experimental manipulations of chicken limb buds have led to the discovery of the two important signalling centres in the developing limb bud. These signalling centres produce the molecules that instruct the pattern of the limb skeletal elements. One of these centres is the apical ectodermal ridge (AER), which consists of a distinct thickening of the ectoderm along the distal limb bud tip at the DV border **(Figure 1B)**. In 1948 Saunders performed seminal experiments, in which he removed the AER from chicken limb buds at different stages of limb bud outgrowth and observed that this led to truncations in the developing skeleton. The earlier the AER was removed, the more proximal these skeletons would become truncated (Saunders, 1948). These experiments demonstrated that the AER produces a signal that is critical for limb bud outgrowth along the PD axis. These observations led to the proposal of the "progress-zone"-model (PZ-model) by Wolpert and colleagues (Summerbell et al., 1973). The progress zone was defined as the area underlying the AER. The PZ-model states that cells in the PZ are kept in an undifferentiated and proliferating state by signals from the AER and that they acquire their positional character according to the time they spend in this zone. Once a cell leaves the PZ it is no longer under the influence of the AER and its identity is determined. According to the PZ-model cells spending only a short time in the PZ and leaving it early during limb development will adopt a proximal identity, whereas cells spending a longer time under the influence of the AER will have more distal identities. This model incorporates the importance of both space and time in pattern formation [see Figure 3A, page 22].

FGF signalling: functions in outgrowth and specification of PD identities – The molecular signals expressed by the AER and mediating its effect are members of the fibroblast growth factor (*Fgf*) gene family [**Figure 1C**]. This was demonstrated by the fact that implantation of a bead soaked with FGF-4 rescues limb bud outgrowth and patterning after AER removal in chicken wing buds (Niswander et al., 1993).

FGF signalling pathway – *Fgfs* regulate fundamental developmental processes and are involved in the establishment of diverse embryonic structures. In addition, they play a physiological role in adults and are involved in pathologies. The *Fgf* family is composed of 18 ligands and four highly conserved transmembrane tyrosine kinase receptors (FGFR1 to

4). FGF ligands bind to their receptors with the help of heparan sulphate proteoglycans (HSPG). Ligand-induced dimerization leads to the activation of the intracellular kinase domain of the receptors, which then activate multiple signal transduction pathways (e.g. Ras, MAPK, PKC). The predominant signalling pathway activated by the FGFRs during development seems to be MAPK signalling (Corson et al., 2003). *Fgfs* regulate cell behaviours such as proliferation, survival, migration, and differentiation (reviewed by (Turner and Grose, 2010)).

   ***Fgf* functions during limb development:** Four *Fgf* ligands are expressed by the AER, *Fgf-4*, *Fgf-8*, *Fgf-9*, and *Fgf-17* (Sun et al., 2000). Of these, *Fgf8* is expressed the earliest. It is expressed at the time when the AER becomes specified, while expression of the others is activated later. *Fgf8* alone is sufficient for limb development, since mouse limb buds that do not express *Fgf4*, *Fgf9*, and *Fgf17* develop normal limbs (Mariani et al., 2008). Conditional removal of *Fgf8* during limb development leads to relatively mild skeletal phenotypes affecting the stylopod and the autopod (Lewandoski et al., 2000; Moon and Capecchi, 2000). Combined inactivation of *Fgf8* and *Fgf4* leads to an arrest of limb bud development and a complete lack of a limb skeleton. Transient expression of *Fgf4* and *8* in the early limb bud is sufficient to specify the entire PD axis, however the skeletal elements are reduced in size and malformed due to a decreased number of skeletal progenitor cells (Sun et al., 2002). The removal of *Fgf9* and *Fgf17* in *Fgf8*-deficient limb buds has shown that this leads to a relatively mild worsening of the phenotype observed in *Fgf8*-deficient limbs. All this genetic analysis has shown that the different AER-FGFs contribute to the function of the AER, *Fgf8* being the most important, most likely due to the fact that *Fgf8* is expressed in the AER for the longest time (Mariani et al., 2008). Furthermore, it was shown that in addition to sustaining cell survival, AER-*Fgfs* specify the distal domain by regulating the expression of PD patterning genes (Mariani et al., 2008). In summary, Mariani et al. have demonstrated the roles of AER-Fgfs both in controlling cell survival and specifying distal fates in the limb bud.

   Fgf-10 is expressed by the limb bud mesenchyme. It is involved in the induction of *Fgf8* expression in the AER during early limb bud development (Ohuchi et al., 1997). Embryos deficient for *Fgf10* do not develop limbs and limb bud outgrowth is arrested at a very early stage. Moreover, *Fgf8* expression is not induced in the AER (Min et al., 1998; Sekine et al., 1999). Based on the finding that *Fgf8* also up-regulates *Fgf10* expression, a positive feedback loop operating between *Fgf8* in the AER and *Fgf10* in the mesenchyme was proposed (Ohuchi et al., 1997).

RA signalling: a second signal involved in PD patterning? – Another signal that plays a role in PD limb development is retinoic acid (RA), although its exact function in this process is not fully understood. RA is produced in the flank of the embryo and diffuses into the limb bud [**Figure 1C**]. It is thought to be involved in the specification of proximal identities (Mercader et al., 2000; Niederreither et al., 1999; Tamura et al., 1997).
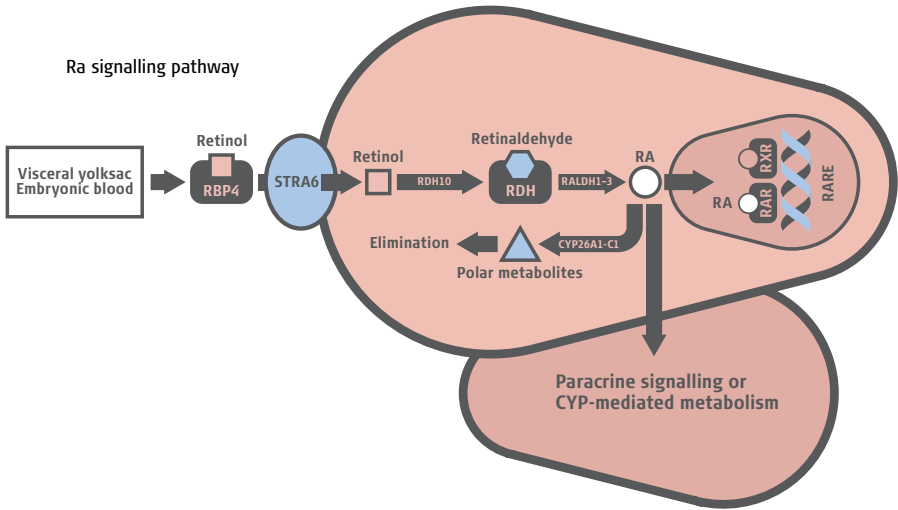
[**Figure 2**] The RA signalling pathway. Placental embryos receive retinol from their mother via the blood and oviparous species store retinol in the egg yolk. The retinol is transported to the embryos through the visceral yolk sac and later through the embryonic blood. In the embryo retinol is bound by RBP4 and taken up by the cell through the receptor STRA6. Within the cell retinol is transformed to retinaldehyde, mainly by RDH10. Retinaldehyde is then converted to RA by the enzymes RALDH1-3. RA then binds to its nuclear RAR receptors, which form heterodimers with nuclear RXR receptors. These heterodimers bind to RA response elements (RAREs) and regulate transcription of target genes. RA is metabolized to polar metabolites by the cytochrome P450 enzymes CYP26a1-c1. These polar metabolites are subject to further metabolism and elimination. RA can also function in a paracrine manner, signalling to neighbouring cells. RA: retinoic acid, RALDH: retinaldehyde dehydrogenase, RAR: retinoic acid receptor, RARE: retinoic acid response element, RBP4: retinol binding protein 4, RDH: retinol dehydrogenase, RXR: retinoid X receptor, STRA6: stimulated by retinoic acid 6, (adapted from (Niederreither and Dolle, 2008)).

The RA pathway – RA is the active metabolite of vitamin A (retinol), which is taken up with the nutrition. Placental embryos receive vitamin A from their mother. Within the embryo retinol is bound by the retinol binding protein 4 (RBP4) and cellular uptake is mediated by the cell-surface receptor stimulated by retinoic acid gene 6 (STRA6). Within the cell retinol is converted into retinoic acid by two sequential reactions. First, retinol is transformed to retinaldehyde by alcohol dehydrogenases (ADHs) and retinol dehydrogenases (RDHs). The second step is the oxida-

tion of retinaldehyde to RA by three retinaldehyde dehydrogenases (RALDH1 to 3); the corresponding genes are called *Aldh1a1-3* (from now on referred to as *Raldh1-3*). RA interacts with the nuclear retinoic acid receptors (RARs), which form heterodimers with retinoic X receptors (RXRs) to elicit a transcriptional response by binding to RA response elements (RARE). Furthermore, RA is metabolized to the inactive forms 4-hydroxy-RA and 4-oxo-RA by the cellular cytochrome P450 26 enzymes (CYP26a1, b1 and c1), which where first identified as RA-inducible gene products [**Figure 2**] (White et al., 1996) (reviewed by (Niederreither and Dolle, 2008)).

RA functions during embryogenesis – During embryonic development RA is involved in a wide variety of processes, ranging from the regulation of embryonic AP patterning and patterning of the spinal cord to heart morphogenesis (Niederreither et al., 1999). The importance of RA during development becomes evident from both gain- and loss-of-function studies in embryos. Vitamin A deficiency in mothers during pregnancy leads to severe fetal malformations (VAD syndrome)(Wilson et al., 1953), while an excess of RA is teratogenic (Ross et al., 2000). This illustrates that the amount and distribution of RA needs to be strictly controlled during development. From the metabolic pathway of RA it becomes evident that the distribution of RA can be efficiently controlled by the spatial restriction of expression of genes involved in synthesis and degradation of RA. Indeed, many of the factors involved in the RA pathway show restricted expression patterns (see e.g. (MacLean et al., 2001; Niederreither et al., 1997)). RDH10 seems to be the most important enzyme performing the conversion of retinol to retinaldehyde, because embryos deficient for *Rdh10* display phenotypes reminiscent of VAD (Sandell et al., 2007). Of the enzymes involved in the second reaction of RA synthesis RALDH2 seems the most essential. *Raldh2*-deficient mouse embryos die at E9.5 from severe cardiac defects and suffer multiple developmental abnormalities including hindbrain and somite patterning defects and a lack of limb buds (Niederreither et al., 1999). In addition, targeted disruptions of RARs and RXRs lead to developmental defects reminiscent of VAD in structures where these receptors have a function (reviewed by (Mark et al., 2009)). Embryos deficient for the RA degrading enzymes *Cyp26a1* and *b1* display phenotypes reminiscent of the teratogenic effects of excess RA, which shows that these enzymes are important for controlling the amount of RA in the embryo (Abu-Abed et al., 2001; Yashiro et al., 2004).

RA function in the developing limb bud – During limb development, RA is produced in the flank mesoderm by RALDH2 and diffuses into the proximal limb bud mesenchyme. The distribution of RA in the limb bud can be visualized by the expression pattern of the RA receptor *Rarb*, because the promoter of *Rarb* contains a RARE, and thus is a direct positive transcriptional target of RA signalling (de The et al., 1990; Rossant et al., 1991; Sucov et al., 1990). The expression pattern of *Rarb* demonstrates that RA signalling is active across the AP axis in the proximal limb bud [**Figure 1C**]. *Cyp26b1* is the only *Cyp26* enzyme expressed during the patterning phase of limb development (i.e. E9.5 to E11.5). It is expressed in the distal limb bud mesenchyme and non-AER ectoderm (MacLean et al., 2001). Targeted loss of *Cyp26b1* leads to severe malformations of the limb skeleton including shortening of the PD axis that can be phenocopied by an excess of RA during limb development. Therefore, the phenotype of *Cyp26b1*-deficient limbs is most likely caused by an excess of RA activity due to the absence of a RA degrading activity in the distal limb bud (Yashiro et al., 2004). These findings indicate among others that RA levels need to be strictly controlled during normal limb bud development.

Analysis of the function of endogenous RA in the limb bud has proved difficult, because embryos deficient for the enzyme responsible for its synthesis in the flank (*Raldh2*) die at E9.5, precluding limb bud analysis. At the time these embryos die, they show no sign of a forelimb bud (Niederreither et al., 1999). Oral RA supplementation of pregnant females can rescue these embryos and significantly restores forelimb outgrowth, but results in digit AP patterning defects, suggesting that RA functions in both PD and AP axis patterning (Niederreither et al., 2002). Contradicting this view, a recent publication suggests that RA is completely dispensable for PD and AP limb bud patterning and that it is only important for limb bud induction. In this study they use mouse embryos lacking *Raldh2* and *Raldh3*, which are RA deficient. Limb bud induction in these embryos needs to be restored by maternal RA supplementation. These limb buds express *Shh* and *Meis* genes (see below) but show no sign of RA activity in limb buds as the corresponding LacZ reporter is not expressed. The authors thus conclude that RA signalling is dispensable for limb bud patterning (Zhao et al., 2009).

Grafting experiments in chicken limb buds have shown that distal limb bud tissue that has been treated with RA develops into more proximal structures than expected (Tamura et al., 1997). This raised the question what target genes of RA signalling mediate this effect in the limb bud. RA has been shown to positively regulate the expression of *Meis* genes. A bead soaked in RA induces strong up-regulation of *Meis*

expression in the chicken limb bud (Mercader et al., 2000). *Meis* genes are initially expressed throughout the limb bud, but during limb bud outgrowth their expression becomes restricted to the proximal limb bud mesenchyme. Ectopic distal overexpression of *Meis* genes causes distal to proximal transformations of skeletal elements (Capdevila et al., 1999; Mercader et al., 1999; Mercader et al., 2009). Furthermore, Mercader et al. have shown that *Meis* expression is negatively regulated by FGFs, because reduction of FGF signalling causes distal expansion of the *Meis* expression domain and *Meis* expression was reduced around beads soaked in FGFs. Genetic evidence in mice supports these interactions as the distal *Meis1*-negative domain is reduced in limb buds deficient for *Cyp26b1* or for AER-*Fgfs* (Yashiro et al., 2004) (Mariani et al., 2008). These observations led to the proposal that RA specifies proximal cell fates. Taken together, these studies indicate that RA is synthesized in the flank and spreads into the limb bud, where it is actively degraded in the distal compartment by CYP26b1. These events are thought to result in a PD gradient of RA activity controlling specification of proximal cell fates by high levels of RA.

It is important to keep in mind that in addition to functioning during limb bud patterning, RA is also important for chondrocyte maturation and endochondral ossification. RA has been shown to both stimulate and inhibit chondrocyte maturation depending on the time of exposure (Adams et al., 2007). This additional function of RA might in part explain the severe skeletal phenotype observed in *Cyp26b1* mutant limbs (Yashiro et al., 2004).

Several models for PD limb bud patterning – Substantial progress has been made in revealing the molecular signals and their interactions during limb bud development since the original proposal of the "progress-zone"-model (PZ-model) [**Figure 3A**]. Several of these observations do not fit entirely with the PZ-model, which was originally proposed to explain the AER-removal experiments. For example the fact that *Fgf8*-deficient limb buds display a phenotype in the stylopod but not in the zeugopod is hard to reconcile with this model. In addition, to date no molecular evidence for a clock-like mechanism in the undifferentiated distal zone that affects limb patterning or determines identity has been described. Interestingly, one publication describes cyclic expression of *hairy2* in distal mesenchyme of chicken limb buds, but the functional relevance of these observation are not clear (Pascoal et al., 2007).

Results of classical experiments that were explained in the context of the PZ-model have recently been reinterpreted. For example, X-ray irradiation experiments in developing chicken limb buds induce

phocomelia, which is a malformation in which limb bones are severely shortened and proximal limb elements are more affected than distal ones (Wolpert et al., 1979). These patterning defects were initially viewed as evidence supporting the PZ-model. Irradiation-induced cell death leads to a smaller limb bud, which was thought to cause proximal cells to be under the influence of the AER for longer than usual. According to the PZ-model this would cause more distal specification of proximal cells and lead to phocomelia. A recent study revaluated these classical x-ray experiments and showed that markers for PD patterning were not affected in irradiated limb buds. Instead, irradiation caused the death of chondrogenic progenitor pools, which are generated in a proximal to distal sequence, and therefore proximal structures are more affected than distal ones (Galloway et al., 2009). Furthermore a study performed in chicken limb buds has shown that truncations after AER removal are caused by cell death in the region under the AER rather than by an arrest in specification. Cell labelling and transplantation experiments indicated instead that limb bud cells are specified along the PD axis relatively early during development and are then expanded by proliferation (Dudley et al., 2002).

These discrepancies led to the formulation of new models for PD axis formation. The observations by Dudley et al. lead to the proposal of the early specification model [**Figure 3B**]. According to this model cells are specified early and are subsequently expanded by proliferative signals by AER-FGFs. However, no markers demonstrating this early specification have been described so far. Furthermore, the experiments performed by Mercader et al. (Mercader et al., 2000) lead to the proposal of a two-signal-model, which states that the PD axis is patterned by a distal and a proximal signal with opposing effects (**Figure 3C**). RA activity from the flank is the proximal signal that specifies proximal fate at least in part by its effect on *Meis* gene expression. Counteracting the RA pathway, FGF signalling from the AER promotes distalization of the limb bud. Identities along the PD axis would then be specified as a consequence of cells integrating the amount and time they were exposed to these opposing signals. This model is also supported by the distal expansion of *Meis1* expression in mutants lacking expression of several *Fgfs* in the AER (Mariani et al., 2008). In fact, this two-signal-model could provide an explanation for the molecular basis of the early-specification model. However, clear evidence for a proximal RA signalling centre is lacking and the function of RA in patterning of the developing limb bud is not supported by all experimental evidence (Zhao et al., 2009).

In an effort to include all current genetic and molecular data, Tabin and Wolpert (2007) proposed the differentiation-front model [**Figure 3D**].

A

Progress-zone model

B
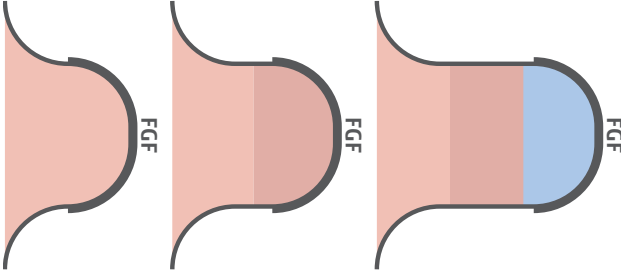
Early specification model
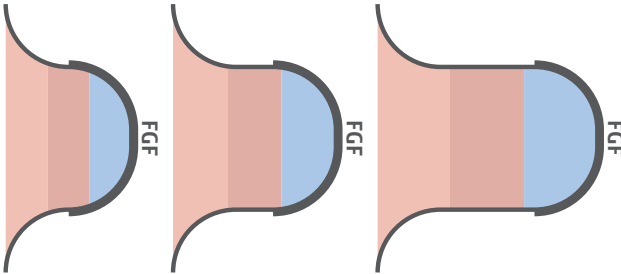
This model states that during limb bud outgrowth the distal limb bud mesenchyme is kept in an undifferentiated state by AER-FGFs. As proximal cells leave this undifferentiated zone at the proximal border, called the differentiation front, they will become determined and initiate chondrogenic differentiation by activating *Sox9* expression. Cells leaving the undifferentiated proliferating zone will acquire their PD identity according to the specific combination of genes that are expressed at the time the cells leave this zone. The two-signal model is integrated into the differentiation-front model to explain the regulation of gene expression patterns that will denote the different PD domains formed during limb bud outgrowth (Tabin and Wolpert, 2007).

C

Two-signal model

D

Differentiation-front model
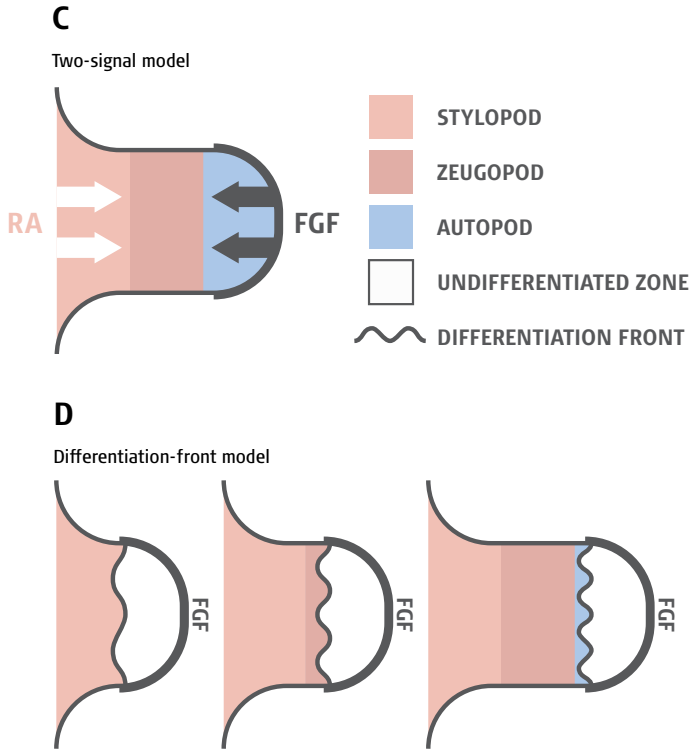
[**Figure 3**] Models for PD limb bud development. [**A**] The progress-zone model: the cells in the progress zone in the distal limb bud are kept in an undifferentiated state by FGF signals from the AER. As cells leave the PZ their identities are determined. Cells spending only a short time in the PZ will have proximal identities, whereas cells spending a longer time under the influence of the AER will have more distal identities. [**B**] Early specification model: identities along the PD axis are specified early during limb development and are then expanded by proliferative signals from the AER. [**C**] Two-signal model: the PD axis is patterned by two opposing signals: a proximal to distal RA gradient from the flank specifies proximal identities while a distal to proximal FGF signalling gradient from the AER specifies distal identities. [**D**] Differentiation-front model: the distal limb bud mesenchyme is kept in an undifferentiated state by FGF signalling from the AER. As proximal cells leave the undifferentiated zone at the proximal border (differentiation front), they will become determined according to the specific combination of genes that are expressed at the time the cell leaves this zone and initiate chondrogenic differentiation. AER: apical ectodermal ridge, FGF: fibroblast growth factor, PD: proximo-distal, RA: retinoic acid. (adapted from (Zeller et al., 2009)).

Patterning along the antero-posterior (AP) axis

The ZPA is the signalling centre controlling AP patterning during limb bud development – As mentioned before, two important signalling centres control limb bud outgrowth and patterning. The first signalling centre that was discovered is the AER, which was described above. The second signalling centre is composed of a group of cells located in the posterior limb bud mesenchyme. Transplantation of these posterior cells to the anterior margin of the limb bud leads to the formation of mirror image duplications of all digits (Saunders and Gasseling, 1968), demonstrating that this centre can instruct AP limb bud patterning [Figure 4A]. This posterior region is a classical embryonic organizer of the limb bud and was named the zone of polarizing activity (ZPA) or the polarizing region [Figure 1C].

To explain these observations, Wolpert formulated the French-flag model, which proposes that the ZPA cells secrete a diffusible morphogen that patterns the AP axis of the limb bud corresponding to different specific thresholds of morphogen concentrations [Figure 4B]. According to this model cells in the posterior mesenchyme near the polarizing region will be exposed to high morphogen concentrations and form posterior digits, while cells in the anterior mesenchyme are exposed to lower concentrations and form more anterior digits. The model was named the French-flag model to illustrate the three thresholds that were assumed to be created by the morphogen signal, corresponding to the three digits of the chicken wing [Figure 4B] (Wolpert, 1969). Support for this model was provided by experiments showing that the number and identity of extra anterior digits depended on the number or the amount of time of ZPA cells grafted to the anterior limb bud. More cells and longer exposure led to more posterior digit formation and more complete duplications (Smith, 1980; Tickle, 1981). RA was the first diffusible molecule identified that was able to induce the same mirror-image duplications as ZPA-grafts and was thus assumed to be the morphogen secreted by ZPA cells (Tickle et al., 1982), but it was subsequently shown that rather than being the morphogen itself, RA induced anterior cells to become morphogen-secreting ZPA cells. RA itself was not active in ZPA cells (Noji et al., 1991; Wanek et al., 1991). In 1993, the ZPA morphogen was finally identified by Riddle et al. as sonic hedgehog, a vertebrate homolog of the *Drosophila* hedgehog gene. They showed that *Shh* is expressed by the ZPA [Figure 1C] and that cells expressing *Shh* can induce mirror-image digit duplications (Riddle et al., 1993). In addition, they showed that RA soaked beads induce *Shh* expression in the anterior limb bud mesenchyme.

A Zone of polarizing activity

AER ZPA
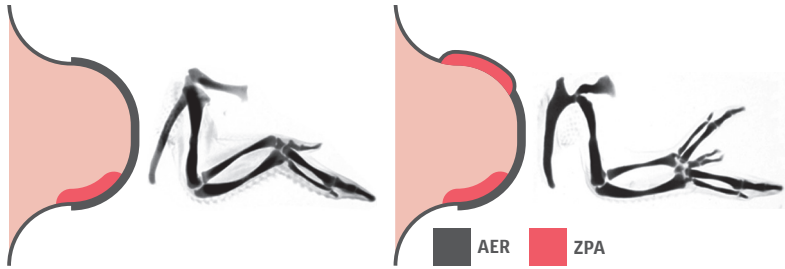
B French flag

C SHH loss-of function

D Prepattening

GLI3R

5'HOXD HAND2

FGF

GLI3R

HAND2

Shh

E Temporal gradient

1 2 3 4 5

Not exposed to SHH

Longrange SHH

Shh-descendants

Shh
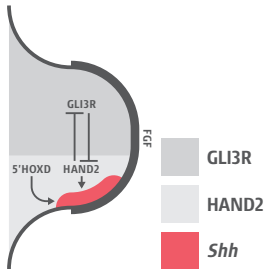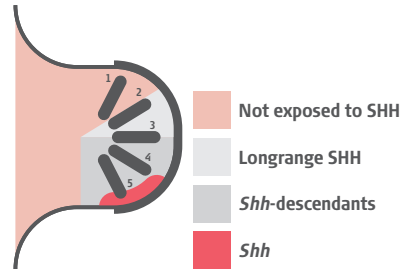
[**Figure 4**] AP patterning and SHH signalling during limb bud development. [**A**] Anterior grafts of the ZPA, which consists of a group of cells in the posterior limb bud mesenchyme, results in mirror image duplications in chicken wings. [**B**] The French-flag model was proposed to explain the effect of the ZPA. This model proposes that ZPA cells secrete a diffusible morphogen that patterns the AP axis of the limb corresponding to specific thresholds of morphogen concentrations. The model was named the French-flag model to describe the three thresholds, corresponding to the three digits of the chicken wing. [**C**] Skeleton of a *Shh*-deficient limb at newborn stage. Formation of the AP limb bud axis is disrupted in the zeugopod and the autopod. Only one zeugopod bone and the most anterior digit 1 are present in *Shh*-deficient limbs. [**D**] Prepatterning of the early limb bud along the AP axis: the limb is prepatterned by antagonistic interactions between the transcription factors GLI3R in the anterior limb bud and HAND2 in the posterior limb bud. Posteriorly restricted HAND2 and 5'HOXD transcription factors are involved in the activation of *Shh* expression in the ZPA. [**E**] Next to a spatial gradient of SHH (as proposed by the French-flag model) also a temporal gradient is involved in SHH limb bud patterning: cells originating from cells expressing *Shh* (*Shh*-descendants) contribute to parts of digit 3 to digit 5. Specification of the different posterior digits is dependent on the exposure time of cells to SHH rather than only the SHH concentration. Long-range SHH signalling is important for patterning of digit 2/3. Specification of digit 1 is SHH independent. AER: apical ectodermal ridge, AP: antero-posterior, GLI3R: GLI3 repressor, SHH: sonic hedgehog, ZPA: zone of polarizing activity. (Adapted from (Benazet and Zeller, 2009)).

Early establishment of the limb bud AP axis upstream of SHH – Before activation of SHH signalling, polarized gene expression patterns along the AP limb bud axis are already observed. The transcription factors *Gli3* and *Hand2* are expressed in the anterior and in the posterior limb bud mesenchyme respectively. *Hand2* and *5'Hoxd* (see below) expression during the onset of limb bud outgrowth was shown to be restricted posteriorly by the repressor form of GLI3 (GLI3R) (te Welscher et al., 2002a; Zuniga and Zeller, 1999). In the absence of *Gli3* both *Hand2* and *5'Hoxd* expression is expanded over the entire limb bud mesenchyme. On the other hand, *Gli3* expression is expanded posteriorly in the absence of *Hand2* (Galli et al., 2010). These results indicate that the limb bud is prepatterned along the AP axis by the antagonistic interactions between *Hand2* and *Gli3* before activation of SHH signalling [**Figure 4D**]. Indeed limbs deficient for both *Hand2* and *Gli3* lack AP asymmetry along the entire PD axis and display polydactyly with a complete loss of AP identities (Galli et al., 2010).

Establishment of the ZPA in the posterior limb bud mesenchyme – Expression of *Shh* in the posterior forelimb bud mesenchyme is activated at E9.5 (around 26 somites) and remains expressed until E12 (Zhu et al., 2008). *Shh* expression is only activated in the posterior limb bud after limb bud outgrowth has started, raising the questions which factors in the limb bud are involved in establishment of the ZPA. *5' Hoxd* and *5' Hoxa* genes (*Hoxd/a 10* to *13*) are expressed in the posterior limb bud mesenchyme (see below) and have been shown to be essential for activation of *Shh* expression in the ZPA, because *Shh* expression is lost in the absence of the whole *HoxA* complex and *Hoxd10* to *13* (Tarchini and Duboule, 2006). The basic helix-loop-helix transcription factor *Hand2* is also required for the activation of *Shh* in the posterior limb bud. In fact, absence of *Hand2* during limb development leads to the same phenotype as is observed in *ShhΔ/Δ* limbs [**Figure 4C+D**] (Galli et al., 2010). RA and *Fgf8* might also be involved in activation of *Shh* expression in the ZPA. In mouse limb buds mutant for *Fgf8*, *Shh* expression is delayed but it is eventually expressed (Lewandoski et al., 2000). As previously mentioned, RA can induce ectopic *Shh* expression in the anterior limb bud (Riddle et al., 1993). Furthermore, RA might be involved in posterior restriction of Shh expression together with *Hand2* (Niederreither et al., 2002).

Shh expression in the ZPA is controlled by an enhancer element (called mammals-fish conserved sequence 1 (MFCS1)) located 1 Mb upstream of the transcriptional start site of *Shh* (Lettice et al., 2003). Targeted deletion of this sequence in mouse leads to a complete absence of *Shh* expression in the developing limb and to a *Shh*–deficiency phenotype of the limb skeleton (see below) [**Figure 4C**], while the mice develop normally otherwise

(Sagai et al., 2005). It was shown that 5'HOXD and HAND2 proteins directly bind to the *Shh* limb enhancer and activate expression of a reporter gene (Capellini et al., 2006; Galli et al., 2010). In addition, HAND2 was shown to associate with HOXD13 and together they tansactivate expression of a reporter construct more strongly than alone (Galli et al., 2010). In summary, regulation of *Shh* expression by the ZPA is a rather complex process involving a variety of different transcriptional regulators.

The Hedgehog signalling pathway – The hedgehog gene was originally discovered in Drosophila as a segment-polarity gene (Nusslein-Volhard and Wieschaus, 1980). The three homologues *Shh*, indian hedgehog (*Ihh*), and desert hedgehog (*Dhh*) have been identified in human and mouse. These three hedgehog proteins (Hh) act as morphogens controlling the development of different embryonic tissues, but *Shh* has been shown to be the most important during embryonic development (Chiang et al., 1996) (Varjosalo and Taipale, 2008). SHH signalling is involved in a variety of organogenetic processes, including neural patterning along the DV axis, lung branching, and cerebellar growth. The main components of the hedgehog pathway were identified using Drosophila genetics and the homologues were subsequently found in vertebrates. Even though these pathways are highly conserved between invertebrates and vertebrates, some notable differences between these signal transduction pathways exist. Here the vertebrate Hh pathway will be discussed.

In the Hh-producing cells the Hh precursor is cleaved and a cholesterol and palmitoyl-moiety are attached to the C- and the N-terminus respectively. The Hh signalling protein is then released into the extracellular space, where it can move over long distances to create a gradient [**Figure 5**]. Several proteins are involved in the modification and release of the Hh protein [**see Figure 5**] (reviewed by (Varjosalo and Taipale, 2008)). In the absence of Hh signalling the twelve-pass transmembrane Hh-receptor patched (PTCH) localizes to the cilium and prevents the seven-pass transmembrane protein smoothened (SMO) from accumulating in the cilium. In addition, PTCH represses SMO function by an unknown mechanism. The transcriptional effectors of Hh signal transduction are the GLI transcription factors. In the absence of Hh signalling, these proteins are phosphorylated by the kinases PKA, CKI and GSK3 and thus targeted to the proteasome. This leads to proteolytic processing of full-length GLI proteins (GLIFL) to a shorter repressor form (GLIR). These repressor then translocate to the nucleus where they repress Hh target genes [**Figure 5**] (reviewed by (Wilson and Chuang, 2010) (Jiang and Hui, 2008)). In responding cells, Hh binds to its transmembrane receptor

PTCH. Binding of Hh to PTCH triggers opposite trafficking of PTCH and SMO, with PTCH moving out of the cilium and SMO accumulating in the cilium. In addition binding of Hh to PTCH inhibits its repression of SMO. Once SMO inhibition is released, it becomes activated which leads to Hh signal transduction. GLI proteins are not targeted to the proteasome and the full-length GLI proteins are activated (GLIA). The GLIAs then move to the nucleus and positively regulate transcription of Hh target genes. In vertebrates there are three homologues of GLI proteins, GLI1, GLI2 and GLI3. GLI1 lacks the repressor domain and functions only as an activator, but it is expressed only after Hh pathway activation thus reinforcing activation of the pathway. GLI2 seems to function mainly as an activator in Hh signalling while GLI3 is responsible for most of the repressor activity. A variety of factors are involved in the intracellular signal transduction of the Hh signal, but the function of most factors has not been completely elucidated [**Figure 5**] (reviewed by (Varjosalo and Taipale, 2008) and (Wilson and Chuang, 2010)).

Shh **function during limb bud development and digit patterning** – Both gain and loss of function studies in mouse and chicken have demonstrated the importance of *Shh* for AP patterning of the limb. The mirror image duplications induced by ectopic anterior *Shh* expression (see above) have shown that SHH can instruct AP identity [**Figure 4A**]. *Shh* deficiency disrupts the formation of the AP limb bud axis in distal skeletal elements, as only one zeugopodal bone and the most anterior digit 1 develop in these limbs [**Figure 4C**] (Chiang et al., 2001; Kraus et al., 2001). SHH signal transduction is mediated by the GLI transcriptional regulators (GLI1 to GLI3), which are all expressed in the limb bud mesenchyme. Only *Gli3* is essential for limb development, as *Gli1*- and *Gli2*-deficient limbs are patterned normally with 5 digits (Mo et al., 1997; Park et al., 2000). Strikingly, *Gli3*-deficient mouse limbs display polydactyly with up to 8 digits and a loss of digit identity (Johnson, 1967). *Gli3* is expressed widely in the limb bud with strongest expression in the anterior part [**Figure 1C**] (Mo et al., 1997). In the absence of SHH signalling the full-length GLI3 protein is processed to a shorter repressor form (GLI3R) [**Figure 5**]. In presence of SHH signalling GLI3 processing in the posterior limb bud is inhibited and the GLI3 activator (GLI3A) is formed leading to a gradient of high anterior to low posterior levels of Gli3R in the limb bud (Wang et al., 2000). Limb buds lacking both *Shh* and *Gli3* display the same polydactylous phenotype as *Gli3* mutant limb buds, demonstrating that one major function of *Shh* during limb development is to counteract GLI3R-mediated repression (Litingtung et al., 2002; te Welscher et al., 2002b).
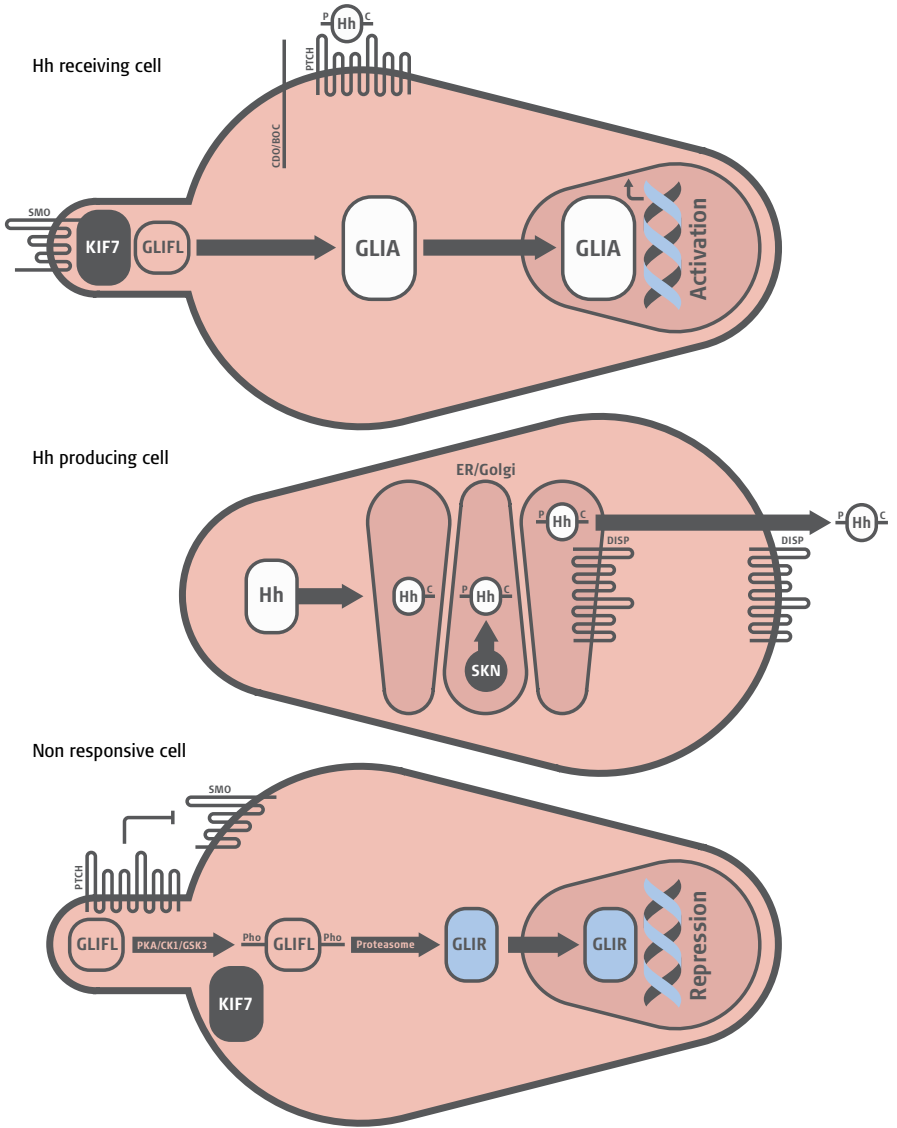
[**Figure 5**] The hedgehog pathway. Hh producing cell: The Hh precursor enters the ER/Golgi secretory pathway. The precursor undergoes autoproteolytic cleavage to release the N-terminal fragment responsible for signalling activity of Hh. It carries a cholesterol moiety linked to its C-terminus. HH is then palmitoylated at the N-terminus by the acyltransferase skinny hedgehog (SKN). HH is released from the cell with the help of dispatched (DISP). Hh receiving cell: In responding cells, Hh binds to its receptor patched (PTCH). Additional Hh binding proteins CDO and BOC positively regulate Hh reception at the cell surface. Binding of Hh to PTCH triggers PTCH to move out of the cilium and SMO to accumulate in the cilium. SMO inhibition by PTCH is released, leading to Hh signal transduction. The kinesin-motor-domain protein KIF7 is involved in ciliary localization of GLI proteins. The full-length GLI proteins (GLIFL) are activated (GLIA) and move to the nucleus where they activate Hh target genes. Non-responsive cell: In the absence of Hh signalling PTCH localizes to the cilium and prevents SMO from moving to the cilium. KIF7 is localized to the base of the cilium and the GLIFL transcription factors are phosphorylated by PKA, CK1, and GSK3, targeting them to the proteasome where they are processed to repressor forms (GLIR). GLIRs translocate to the nucleus and repress target genes. C: cholesterol, CK1: casein kinase 1, GSK3: glycogen synthase kinase 3, Hh: hedgehog, KIF7: kinesin family member 7, P: palmitate, Pho: phosphate, PKA: protein kinase A.

AP patterning of the limb bud by *Shh* is thought to be achieved by the formation of a SHH protein gradient across the limb bud leading to the GLI3R and GLIA gradients described above. Two possible mechanisms to establish graded SHH activity have been proposed: either a spatial gradient of SHH protein across the limb bud or variation of the exposure time of the cells to SHH could result in graded SHH activity. The SHH signalling response can be visualized by the expression of the direct SHH target genes *Gli1* and *Ptch1* in a broad domain in the posterior limb bud (Marigo et al., 1996a; Marigo et al., 1996b). Evidence for the existence of a gradient has been provided by experiments in chicken limb buds showing that the amount of anterior duplicated digits and their identity depends on the amount and time of exposure to SHH (Yang et al., 1997). Furthermore, the SHH activity across the limb bud can be changed by modification of the SHH lipid-moieties. Loss of the C-terminal cholesterol leads to increased spreading of the SHH protein across the limb bud resulting in reduced GLI3 repressor formation and preaxial polydactyly (Li et al., 2006). On the other hand loss of palmitoylation leads to decreased spreading of the SHH protein in the limb bud and to a loss of digits (Chen et al., 2004). These results show that the SHH protein indeed creates an AP gradient across the developing limb bud. A study using a conditional Cre-line allowing removal of *Shh* at specific time points during limb development has shown that in the mouse limb bud, SHH seems to specify AP digit identities very early, i.e. during the first 12 hours of *Shh* expression (Zhu et al., 2008). Furthermore, genetic cell-lineage labelling experiments have demonstrated that cells originating from cells once expressing *Shh* (*Shh*-descendants) contribute directly to parts of digit 3 to digit 5. Long-range SHH signalling is necessary only for partial patterning of digit 3 and for digit 2. Specification of the thumb (digit 1) is SHH independent, because this digit still forms in *Shh*-deficient limbs. Thus, it seems that the specification of the different posterior digits is dependent on the exposure time of the cells to SHH rather then the concentration of SHH alone. Cells at the posterior margin in the ZPA expressing *Shh* the longest will give rise to the most posterior digit 5, while cells moving away from the ZPA will form digits 3 and 4. This shows that the SHH gradient in the limb bud is both a temporal and a spatial gradient [**Figure 4E**] (Ahn and Joyner, 2004; Harfe et al., 2004). Furthermore, limiting the time or the amount of Shh signalling during limb development showed that a short time of *Shh* expression leads to the formation of only anterior digits. Conversely, decreasing the levels but not the time of *Shh* expression affects only formation of digit 2, showing that the time of SHH exposure is crucial for posterior digits (Scherz et al., 2007). Taken together, these experiments suggest that both time

and diffusion are important in generating a graded response to SHH signalling in the limb bud.

Hox **genes during limb development** – *Hox* genes have been shown to be essential for limb development during multiple processes. Four *Hox* gene clusters exist in vertebrates, the *HoxA*, *B*, *C*, and *D* clusters. During limb development, the *HoxA* and the *HoxD* clusters seem to be most important because deletions of the whole *HoxB* or *HoxC* complexes do not result in limb phenotypes (Medina-Martinez et al., 2000; Suemori and Noguchi, 2000). Limbs mutant for both *HoxA* and *HoxD* complexes display severe truncations of distal elements and only the proximal third of the stylopod is formed (Kmita et al., 2005). *5' Hoxa* and *Hoxd* genes seem to be especially important as deletion of *Hoxa13* and *Hoxd13* leads to the absence of the autopod (Fromental-Ramain et al., 1996) and deletion of *Hoxa11* and *Hoxd11* affects zeugopod development (Davis et al., 1995). *Hox* genes are expressed in two waves during limb development. During the first early wave of *HoxA* and *HoxD* gene expression, genes are activated in a sequence following their genomic topography (*Hox1* paralogues to *Hox13* paralogues), leading to a gradient in *Hox* gene expression in the limb bud, such that *Hoxd1* is expressed throughout the limb bud and *Hoxd13* is expressed only in a small posterior domain. *Hoxa/d10* to *13* genes all show posteriorly restricted expression patterns. This expression is similar to the collinear expression of the *Hox* genes in the embryonic trunk (reviewed by (Zakany and Duboule, 2007)). This expression pattern is thought to be regulated by two genomic regions, one 3' of the *Hox* cluster regulating temporal collinearity and a second one 5' of the cluster, which restricts *5'Hox* genes posteriorly through repression (Tarchini and Duboule, 2006). This early posterior restriction of the *5'Hox* genes is thought to be involved in activation of *Shh* expression (see above). The second wave of *Hoxd* gene expression during limb development is dependent on SHH signalling (Chiang et al., 2001; Panman et al., 2006). During the second wave *5'Hoxd* genes are expressed in the presumptive digit domain in reverse collinearity. This means that *Hoxd13* shows most anterior expansion and *Hoxd12*, *11* and *10* are restricted more posteriorly (reviewed by (Zakany and Duboule, 2007)). This asymmetry in expression will be translated into digit identities along the AP axis. The expression of the *5'Hoxd* genes in the digit domain is regulated by a global control region 5' of the *HoxD* cluster (Spitz et al., 2003). *5' Hoxa* genes are also expressed in a second wave. *Hoxa13* expression marks the future autopod domain and *Hoxa11* expression marks the future zeugopod (reviewed by (Zakany and Duboule, 2007)).

Integration of patterning and outgrowth

Many of the specific signals and underlying pathways involved in limb bud patterning have been described in the last two decades. It has become clear that many of the central developmental signalling pathways (SHH, FGF, RA, BMP) are involved in this process. Nevertheless, little is known about how these different signals interact and are coordinated to control the development of such a complex three-dimensional structure. In the last few years a few studies have started to explore these complex interactions (reviewed by (Zeller et al., 2009).

Shh **function integrates patterning and proliferation** – Two recent studies have demonstrated the crucial role of SHH for the proliferative expansion of the limb bud mesenchyme in addition to patterning digit identities across the limb bud (Towers et al., 2008; Zhu et al., 2008). Towers et al. have shown that SHH controls the expression of positive cell-cycle control genes in chicken wing buds. Treatment of limb buds with cyclopamine, which is an antagonist of SHH signal transduction, led to formation of only anterior digits, due to reduction of both proliferation and patterning by SHH. Conversely, blocking proliferation specifically by using cell-cycle inhibitors led to the formation of posterior digits only, because the limb field is not expanded and the cells remain under the influence of a high concentration of SHH. This demonstrates that SHH-controlled proliferation is crucial for appropriate patterning of the autopod and the zeugopod (Towers et al., 2008). In addition, Zhu et al. have shown that SHH has two sequential functions in the mouse limb bud. Early during its activity, SHH specifies digit identities (see above) and afterwards it is essential for controlling proliferation in the distal limb bud to generate a sufficient number of cartilage progenitor cells (Zhu et al., 2008). In fact, the idea that growth and specification are controlled by the same or by different signals from the polarizing region has been around since quite a long time, at least since Cooke and Summerbell observed in 1980 that anterior grafts of the ZPA enhanced proliferation in the mesenchyme (Cooke and Summerbell, 1980). It seems that the process by which SHH controls digit patterning and growth is a complex mechanism integrating space, time and growth and only the correctly controlled combination of all three dimensions leads a perfectly patterned autopod and zeugopod.

Interlinked feedback loops control coordinated limb bud out-growth and patterning – It has been long known that the two signalling centres controlling limb bud development along the AP axis (ZPA) and the PD axis (AER) are somehow linked to enable limb bud development. Early evidence for such a linkage came from the fact that duplications mediated by ZPA grafts took place only if the ZPA was grafted close to the AER (Zwilling, 1956). Once the molecular signals underlying the function of the ZPA and the AER were identified, it was shown that maintenance of *Shh* expression by the ZPA depends on FGF signalling from the AER and in turn continued *Fgf* expression in the AER is dependent on the presence of SHH signalling (Laufer et al., 1994; Niswander et al., 1994). This positive feedback loop is essential for coordinated patterning and outgrowth during limb development. The positive feedback loop was shown to be indirect, because the BMP antagonist GREM1 was identified to be necessary to relay the signal from the mesenchyme to the AER (Zuniga et al., 1999). In the absence of GREM1 mediated BMP antagonism in the limb bud mesenchyme, AER-FGFs are in fact induced normally but progression of AER formation is defective, leading to a disruption of the SHH-FGF feedback-loop (Khokha et al., 2003; Michos et al., 2004). The distal limb bud is not expanded in *Grem1*-deficient limb buds and AP patterning is defective leading to fusion of the ulna and radius and digit loss. During limb development three members of the BMP family *Bmp2*, *Bmp4*, and *Bmp7* are expressed in the mesenchyme and ectoderm (Robert, 2007). Early during limb bud outgrowth BMPs have been shown to be important for appropriate formation of the AER [**Figure 6A**] (Ahn et al., 2001; Benazet et al., 2009; Pizette et al., 2001). BMP activity is down-regulated after the initial function in AER-formation and it was shown that this happens by a rapid up-regulation of *Grem1* expression by the BMPs themselves (mainly BMP4) (Benazet et al., 2009; Nissim et al., 2006). GREM1-mediated BMP antagonism then allows establishment of the SHH/GREM1/FGF feedback-loop and progression of distal limb development. It was shown that the two interlinked feedback loops of SHH/GREM1/FGF and BMP4-GREM1 provide robustness during limb development, allowing the system to buffer disturbances in gene dosage [**Figure 6B**] (Benazet et al., 2009). Later during limb development the SHH/GREM1/FGF feedback loop needs to be terminated to control limb size [**Figure 6C**]. *Shh* expressing cells and *Shh*-descendants have been shown to become unable to express *Grem1*, leading to an increasing gap between the ZPA and *Grem1*-expressing cells and finally to termination of the feedback loop (Scherz et al., 2004). Furthermore, an inhibitory FGF-*Grem1* feedback loop was described. GREM1-induced increase of FGF signalling by the AER eventually inhibits *Grem1* expression in the
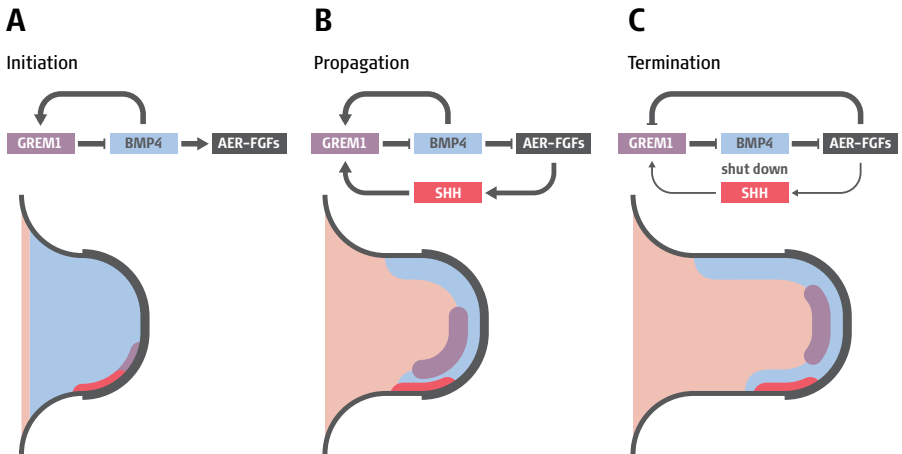
[**Figure 6**] Interlinked feedback loops controlling coordinated limb bud development. Blue areas schematically show the *Bmp4* expression domain, red indicates the *Shh* expression domain, and purple *Grem1*. The thickening of the line around the limb bud depicts the AER. The AER expresses *Fgfs*. [**A**] Initiation: BMP4 is involved in the induction of the AER and at the same time up-regulates expression of its antagonist *Grem1*. Independently *Shh* expression is activated in the posterior mesenchyme. [**B**] Propagation: Establishment and action of the ectodermal-mesenchymal feedback loop that enables distal progression of limb bud development. SHH up-regulates *Grem1* expression. GREM1-mediated BMP antagonism reinforces AER-FGFS, which maintain and up-regulated *Shh* expression in the posterior mesenchyme (SHH/GREM1/FGF feedback loop). [**C**] Termination: An increasing gap between the *Shh*-expressing and the *Grem1*-expressing cells and inhibition of *Grem1* expression in the distal mesenchyme by FGF signalling from the AER eventually results in self-termination of the positive SHH/GREM1/FGF feedback loop. AER: apical ectodermal ridge, BMP4: bone morphogenetic protein4, FGF: fibroblast growth factors, GREM1: gremlin1, SHH: sonic hedgehog (adapted from (Zeller et al., 2009)).

distal mesenchyme resulting in self-termination of the positive SHH/ GREM1/FGF feedback loop (Verheyden and Sun, 2008). In conclusion, limb bud development starts out with high BMP4 activity, which induces AER formation. BMP4 up-regulates at the same time its own antagonist GREM1 and thus BMP activity is rapidly down-regulated, allowing the establishment of the ectodermal-mesenchymal feedback loop integrating AP and PD limb bud patterning. Finally, the induction of high levels of FGFs leads to inhibition of *Grem1* and to termination of the feedback loop [**Figure 6C**] (Benazet et al., 2009).

4 Aim of the Thesis

Embryonic development is a highly fascinating process. The fact that a single cell will develop into a complex organism is amazing and hard to grasp. From a single cell an incredible array of different cell types will arise and each cell type has to fulfil its unique but absolutely necessary function in intricate interactions with neighbouring cells. These different cell types have to be organized into complex three-dimensional structures to give rise to an organism. Each time an organism develops every structure within the embryo is formed faultlessly to give rise to a living being that functions perfectly.

The idea of studying this amazing process is what fascinated me when I started my PhD project with Dr. Aimée Zuniga in the group of Prof. Rolf Zeller. In our laboratory we study development of the mouse limb, which serves as an excellent model structure to investigate the signals involved in diverse processes during embryonic development. During my project I wanted to study the role of SHH during limb bud development. SHH is a morphogenetic signalling molecule that is essential for many aspects of vertebrate development and studying its function during limb development can give insights into the function of SHH in other structures as well. During limb bud development, SHH has been shown to be important for patterning along the AP axis. SHH is thought to mediate this effect by counteracting the formation of a transcriptional repressor (GLI3R). Many other factors like FGFs, BMPs, RA and the *Hox* genes have also been shown to be essential for the development of the limb. Even though these signals have been described to be crucial for limb development using mouse genetics and experimental manipulation in chick embryos, still not much is known about how these signals interact and how they are regulated to generate the complex three-dimensional structure and function of the limb.

I started my project on the basis of a genome-wide microarray analysis performed by Aimée Zuniga. This analysis compared the transcriptome of *Shh*-deficient limb buds with wild-type limb buds, asking the question what gene networks and mechanisms act downstream of SHH signalling during limb development. With the aim of identifying novel targets and functions of SHH Aimee Zuniga, Rushikesh Sheth, and I performed a large in situ hybridisation screen analyzing the spatial distribution of genes identified by the microarray analysis. This screen has led to the two main projects of my thesis.

In the first part of my project I investigated the function of a novel gene during mouse development. This gene was found to be downstream

of SHH signalling by the microarray analysis. To study the requirement of this gene during development, I created a conditional targeted deletion in mice and I combined molecular with cell-biochemical analysis to establish its function. The second part of my project was to examine the global changes we observe in the limb buds of *Shh*-deficient embryos to describe novel functions of SHH during limb development. In collaboration with Conradin Kraemer, Dagmar Iber and Aimée Zuniga I combined genetics, molecular analysis, experimental manipulation of limb buds, and mathematical modelling to describe novel interactions of SHH during limb bud development.

5 Material and Methods

Homologous recombination in mouse embryonic stem cells

For the generation of the mice carrying the *Pkdcc* conditional null allele, male R1 (10th passage, 129 hybrid background) embryonic stem (ES) cells were used. ES cells were fed every day. During most of the procedure ES were grown on a mouse embryonic fibroblasts (MEF) feeder layer.

Thawing and culturing of MEFs – MEFs were conserved in liquid nitrogen. To prepare MEFs to use them as feeder cells for ES cells one vial was defrosted in a waterbath at 37 °C. The freezing medium was washed away by transferring the MEFs in 10 ml freshly made prewarmed MEF culture medium (see recipe below), centrifuged (5 min, 1200 rpm) and resuspended in 6 ml of warm medium (pipet up and down several times smoothly with 3 ml and add 3 more ml). MEFs were seeded in 10 cm dishes (10 ml/dish) and 6 cm dishes at a dilution of 1/6 to 1/8. MEFs can be passaged only twice after thawing. After 2 to 3 days of growth, cells reached confluency and were either passaged to generate more plates or were mitomycin-C treated to use as feeder cells for ES cells.

MEF culture medium: 500 ml Dulbecco's modified Eagle medium (DMEM) + 4.5 g/l glucose (Gibco 41966029), 10% fetal calf serum (FCS), 0.1 mg/ml penicillin-streptomycin (Sigma P-0781), 200 mM L-glutamine (Sigma G-7513).

Passaging of MEFs – Trypsinization: a 10 cm dish was rinsed with 4 ml trypsin, 3 ml trypsin was added and the dish was incubated at 37 °C for 5 min. Cells were collected with 7 ml MEF medium and spun down 5 min at 1200 rpm. The supernatant was removed and the pellet was resuspended in a small volume, diluted and seeded at a dilution of around 1:5-1:6.

Mitomycin-C treatment of MEFs – Stock solution: (stored at 4 °C in foil-wrapped tube, stable for approx. 2 weeks): mitomycin-C (Sigma M-0503) was dissolved in PBS at 1 mg/ml, this means 2 ml PBS were introduced in a 2 mg vial, using a syringe and a needle through the rubber cap. Mitomycine-C is very toxic, avoid contact with the powder/solution.

Treatment of MEFs: confluent plates of MEFs were treated with MEF medium containing 10 mg/ml mitomycin-C (5 ml medium and 50 µl of mitomycin-C stock for a 10 cm plate). The plates were incubated at 37 °C for 2 hours (not longer than 2.5 hours). The medium was removed, cells were rinsed 3 times with 12-15 ml PBS, fresh medium was added and cells were returned to the incubator or ES-cells were seeded on them.

The MEFs can be kept for approximately one week after the mitomycin-C treatment, with medium changes (every 3 days) but if not used within this period of time, they should be discarded (always check under microscope before use). These cells were used directly on 10 cm dishes or they were trypsinized and split on another type of plate (10 cm plate = 48-well plate or 24-well plate or 6-well plate or three 6 cm plates). To prevent cell clumping and uneven plating, cells should not be overgrown at time of trypsinization and/or treatment. The cells were allowed to attach for at least a couple of hours before using. After overnight plating, they should form a confluent monolayer.

ES cell thawing, expansion and electroporation – The medium of a 10 cm mitomycin-C treated MEF plate was removed and 10 ml of ES medium (see below) were added to the plate. A vial of ES cells was quickly thawed at 37 °C and as soon as the last crystals disappeared, the cells were transferred into a 15 ml falcon tube containing 10 ml of prewarmed complete ES medium. The cells were spun down 5 min at 1200 rpm and the medium except for 100–200 µl liquid was removed. 3 ml of ES medium were added and the cells were resuspended and plated onto the MEF plate. The plate was incubated at 37 °C, 7.5% CO_2 for 24 hours. The next day the medium was changed. On day 2 the cells were split as described below onto 4 x 10 cm plates. The next day the medium was changed and on day 4 each plate was split 1:4-1:7 depending on confluency of the cells. Depending on the transfection planned not all plates need to be split. In this case, the other plates were frozen (see below). On day 5 the medium was changed. On the day of electroporation seven 10 cm dishes with ES cells were treated with trypsin and collected in two 50 ml falcon tubes. Cells were counted at a 1:10 dilution, then they were centrifuged for 5 min at 1200 rpm and resuspended at the desired concentration of 18.75×10^6 cells/ml (15×10^6 cells/0.8ml) in PBS. 3 cuvettes were filled with 0.8 ml of the cell suspension each. Two

of the cuvettes were electroporated with 35 mg of targeting vector and one cuvette was electroporated with a water control. These cells were used to assess the efficiency of the subsequent antibiotic selection. Cells were electroporated (capacitance 475 µlF, voltage 0.24 V) and set on ice for 20 min. For recovery cells were then transferred into a falcon tube containing complete ES medium, they were mixed well and plated at a dilution of 1/10 and 1/5 onto gelatinized (see below) 10 cm dishes. Cells were left to recover for two days before antibiotic selection.

ES cell medium: DMEM + 4.5 g/l glucose (Gibco 41966029), 15% FCS (not heat inactivated), 0.1 mg/ml penicillin-streptomycin (Gibco 15140-122), 200 mM L-glutamine (Gibco 25030-024), 50 mM ß-mercapto-ethanol (Gibco 31350-010), 10^7 u/ml leukaemia inhibitory factor (LIF) (EsGRO LIFTM Gibco 13275-029), 1x non essential amino acids (Gibco 11140-035), 1x sodium pyruvate (Gibco 11360-039).

Splitting ES cells – Plates were quickly rinsed with trypsin/EDTA (Sigma T-3924), prewarmed or RT (4 ml for 10 cm plate, 2 ml for 6 well-plate, 300 µl for 24 well-plate, 75 µl for 48 well-plate). Then trypsin/EDTA was added to the plate/well (3 ml for 10 cm plate, 1 ml for 6 well-plate, 150–200 µl for 24 well-plate, 75 µl for 48 well-plate) and the plate was returned to the incubator for 15 min. Cells were then resuspended in trypsin by pipetting up and down 7–10 times with a 2 ml pipette for a 6 cm dish and a 5 ml pipette for a 10 cm dish (check under microscope that cells are not clumping). Cells were resuspended in medium and pipetted up and down 4–5 times (no bubbling) (7 ml for 10 cm plate, 4 ml for 6 well-plate, 1 ml for 24 well-plate, 300 µl for 48 well-plate). Dishes were left 15 minutes in the hood to preplate in order to get rid of the MEFs, the supernatant was transferred to a 15 ml falcon tube and spun at 1200 rpm for 5 min. For 24 and 48 well-plates, no centrifugation step was performed and cells were transferred directly to a new plate (6 and 24 well-plate, containing 5 and 1 ml media respectively, this will dilute the trypsin enough). After spinning, the medium was removed and the cells were resuspended well in fresh medium (2 ml for a 6 cm plate and 4 ml for a 10 cm plate) and transferred to a new plate with medium (4–5 ml for a 6 cm plate and 8–10 ml for a 10 cm plate).

Gelatine coating of ES cell culture plates – Stock solution: a 0.1% gelatine (Sigma G-2500) solution was made in double distilled water and stored at 4 °C (or RT). Coating plates: enough gelatine solution was used to cover the surface of the plates, which were placed for 5–10 min at RT, the gelatine solution was aspirated leaving a thin film on the plates, which was left to dry 5–10 min before use.

Antibiotic selection of transfected ES cell clones – Transfected mouse ES cells were cultured in the presence of G418 at a concentration of 180 μg/ml to 200 μg/ml (the right concentration of G418 was previously determined) and left to grow. Medium was changed every day. After 4 to 5 days the cells electroporated without DNA should die.

Colony picking – After 8 and 9 days of selection ES cell colonies were picked in PBS using a P-200 Gilson pipette and single colonies were transferred into 48-well plates containing MEFs and ES medium without G418. Colonies were broken up by pipetting up and down a few times. Colonies of similar size were put into the same 48-well plate. From now on the cells were kept without selection.

Expansion and freezing of ES cell clones – Medium was changed every day. Every two days the clones were either tryplated onto a new MEF 48-well plate or split onto a MEF and a gelatine-coated 48-well plate depending on confluency of the colonies. Cells on MEF-coated plates were grown for 1 to 3 days and frozen after reaching confluency. To freeze the cells, the medium was removed from the wells and the plate was placed on ice. 400 μl of freezing medium (25% FCS, 10% DMSO in plain DMEM) was added carefully without disturbing the monolayer and the plate was wrapped in parafilm, put in a plastic bag and placed into a stryrofoam box in the -80 °C freezer. The cells on the gelatine plates were grown to confluency in ES medium without LIF and used to prepare DNA for southern blot analysis.

Thawing ES cell clones – For this project, four positive clones were thawed and expanded to several 10 cm dishes, which were frozen. The plates containing the positive clones were removed from the -80 °C freezer, wiped with 70% ethanol and 400 μl of prewarmed ES medium was added to the wells containing the positive clones and placed at 37 °C. As soon as only a few crystals are left, the medium was carefully removed with a Gilson P1000 and 300–400 μl of warm medium was added to melt the last crystals. The medium was changed twice again to rinse all traces of DMSO. If cells completely detached as a monolayer, they were broken up into pieces by pipetting up and down and replated onto new feeders. The next day the medium was changed. At this stage many of the cells (a majority!) were dead. Cells were fed every day for the next 3–4 days (max 10 days) until colonies were growing. The cells were then passaged on onto 24 well-plates containing MEFs and further expanded. When there were several 10 cm dishes they were frozen. For this, the medium was changed 2 to 3 hours before the freezing. Cells were trypsinized, centrifuged and

all medium except 200 μl was removed. Cells were resuspended in the desired amount of freezing medium (40% FCS, 10% DMSO and 50% cold ES medium without LIF, filtered) and distributed into cryovials (3 to 5 vials per 10 cm dish), which were transferred to the -80 °C freezer in bubble-wrap and a styrofoam box. The next day, cells were transferred to liquid nitrogen.

Analysis of ES clones

Preparing DNA from ES cell clones in multiwell plates – This was done on the bench outside of the hood. When ES cells were grown to 80-100% confluency on gelatine, the medium was removed and cells were washed 3 times with 750 μl PBS (regular PBS, not tissue culture grade) carefully so the layer of cells doesn't come off. After this the cells can be frozen at -20°C (wrap with parafilm). To proceed, 250 μl lysis buffer (100 mM Tris-HCl pH 8.5, 5 mM EDTA pH 8, 0.2% SDS, 200 mM NaCl) containing 100 μg/ml of proteinase K was added per well without disturbing the cell monolayer (i.e. on the side of the wells). Cells were incubated at 55 °C overnight in a wet box in an oven. On day 2 500 μl of absolute ethanol was added to each well without disturbing the mono-layer and the plate was left overnight at RT to precipitate the DNA. The next day the plate was inverted to remove the liquid, tapped onto tissue paper and the wells were washed 3 times with 750 μl 70% ethanol (again carefully). DNA was dried at RT overnight on tissue paper. Then 100 μl digestion mix (H2O, buffer 1x, RNAse A 100μg/ml, enzyme (30 units)) per well was added directly to the DNA. DNA was digested overnight in a wet box at 37 °C. The next morning the reaction was spiked with 10 units of enzyme in 5 ml of buffer. Loading buffer was added directly to the digests (20 μl of 10X loading buffer) and the plate was heated at 55 °C for 20 min before loading half of the digest on an agarose gel for southern blot analysis.

DIG Southern blot protocol – Half of the sample from a 48-well plate was loaded on a thick 1% agarose gel and the DNA was separated overnight at 30 V. The following morning the gel was run until DNA was sufficiently separated. Slots were cut along the sides of the gel to mark the location of markers and a photograph alongside a fluorescent ruler was taken. The gel was prepared for transfer by a 10 min depurination wash in 0.25 M HCl, 2 times 15 min wash in denaturation solution (0.5 M NaOH, 1.5 M NaCl), 2 times 15 min wash in neutralization solution (0.5 M Tris HCl pH 7.5, 1.5 M NaCl) and it was equilibrated in 20x SSC (3M NaCl,

150 mM sodium citrate, pH 7.0). Between each step the gel was rinsed with H2O quickly. Capillary transfer was performed in 20X SSC with a positively charged nylon membrane (Boehringer Mannheim, Roche, roll 1417240). A piece of membrane the size of the gel was pre-soaked in H2O and equilibrated in 2x SSC before setting the transfer stack. The transfer stack was left overnight, the next day tissue papers were exchanged and the transfer was left to continue for another few hours. After transfer the membrane was washed in 2x SSC for 5 min and left to dry at RT for 1 hr and baked at 80 °C for 2 hrs. At this stage the membrane can be stored at RT. To continue, fresh hybridization solution was prepared (5X SSC, 50% deionized formamide, 0.1% N-lauroylsarcosine, 0.02% SDS, 2% Blocking Solution in maleic acid buffer (0.1 M maleic acid (not the disodium salt), 0.15 M NaCl, pH 7.5)) and prewarmed at 42 °C. The membrane was placed in a rolling bottle and the hybridization solution was added and the membrane was prehybridized for at least 30 min in the hybridization oven. Subsequently, the prehybridization solution was replaced with hybridization solution containing the probe (either freshly prepared or reused, in which case the probe was heated 10 min at 68 °C) and the membrane was incubated overnight at 42 °C. The next day, the membrane was washed 2 times 15 min in 2x SSC, 0.1% CHAPS at RT and 2 times in 0.2x SSC, 0.1% CHAPS at 68 °C in the rolling bottle. The membrane was then rinsed quickly in maleic acid wash buffer (0.1 M maleic acid (not the disodium salt), 0.15 M NaCl, pH 7.5, 0.3% Tween-20) at RT and then the membrane was blocked for 30 min to 3 hours in 1% blocking solution (1% blocking reagent (Roche) in maleic acid buffer). The blocking solution was then replaced by antibody diluted 1:20'000 in 1% blocking solution for 30 min. After the antibody incubation the membrane was removed from the bottle and placed into a plastic tray and washed 3x 15min in maleic acid wash buffer and incubated 2 min in detection buffer (0.1 M NaCl, 0.1 M TrisHCl pH 9.5). To develop the signal, the membrane was placed on a surface and detection buffer containing 6 μl/ml CDP Star (Roche, cat. 12 041 677 001) was added onto the membrane for 5 min. The membrane was then exposed to film (Kodak BioMax MR Film: MR-1, size 8 X10 in.; cat. 8701302) for 2 hrs to overnight.

DIG northern blot protocol

A northern blot from Clontech containing total RNA from E7.5, E11.0, E15.0, and E17.0 embryos was used for performing this experiment. Premade hybridisation buffer (Expresshyb) was supplied with the membrane by Clontech. The membrane was prehybridized in Expresshyb solution in a plastic bag for 45 min at 68 °C in a shaking water bath. 0.7 µl probe was added to 50 µl H2O and heated at 99 °C for 10 min and quenched on ice and added to 7 ml Expresshyb solution. The prehybridization solution was exchanged with the probe solution and the membrane was hybridized with the probe for 1 hour at 68 °C. After hybridization the probe was recovered, the membrane was removed from the bag, placed in a tray and rinsed in 2x SSC (see above) with 0.1% SDS. The membrane was washed twice in this solution for 15 min at RT and twice in 0.1x SSC, 0.1% SDS at 68 °C (these hot washes were performed in rolling bottles in the hybridization oven). After this step the Southern protocol was followed. Finally the membrane was exposed to film overnight.

Mouse colony management

Genetic crosses of mouse strains – *Gli3XtJ/+* (Hui and Joyner, 1993), *ShhΔ/+* (St-Jacques et al., 1998) and *ShhΔL/+* (Sagai et al., 2005) alleles were kept in NMRI background. To obtain *Gli3XtJ/XtJ* and *ShhΔ/Δ* embryos heterozygous parents were mated.

Genetic analysis of *Pkdcc* interactions with SHH pathway components – The *Pkdcc* alleles (*floxedneo/+* and *Δ/+*) were kept in a mixed 129;C57BL/6 genetic background and *Gli3Δ/+* (J. Lopez-Rios), and *PtchΔ/+* (Goodrich et al., 1997) alleles were kept in C57BL/6 genetic background. *PkdccΔ/Δ;ShhΔ/+*, *PkdccΔ/Δ;ShhΔ/Δ*, *PkdccΔ/Δ;Gli3Δ/+*, *PkdccΔ/Δ;Gli3Δ/Δ*, *PkdccΔ/Δ;PtchΔ/+* and *PkdccΔ/Δ;PtchΔ/Δ* compound mutant embryos were generated by mating *PkdccΔ/+;ShhΔ/+* or *PkdccΔ/+;Gli3Δ/+* or *PkdccΔ/+;PtchΔ/+* males and females. All mice and embryos were genotyped by PCR amplification of diagnostic fragments (for primers see [Table 1]) using DNA prepared from ear punches for mice at weaning and head tissue or extra-embryonic membrane for embryos.

Staining embryos for cartilage and bone

Embryos were dissected in PBS, eviscerated and placed into 95% ethanol for at least 3 days (use glass vials). If the embryos were older than E14.5, the skin was removed before placing them in ethanol as follows. The embryos were first placed in tap water for 1 to 24 hrs, then they were put in 70°C tap water for 20 to 30 seconds and the skin was peeled off using forceps. After the 95% ethanol step, the embryos were placed in Alcian blue stain (0.3 g/l alcian blue 8GX (Sigma A3157), 80% EtOH, and 20% acetic acid) for 24 hours. Embryos were rinsed twice in 95% EtOH and left in 95% EtOH overnight. The next day the embryos were placed in 1% KOH for 10 – 30 min and then switched into Alizarin red stain (50 mg/l Alizarin Red (Sigma A5533) in 1% KOH) to stain the bones. The incubation time depended on the age of the embryo (E14.5 2-3 hours, newborns overnight). Subsequently, the embryos were cleared in a glycerol series: 0 to a few hours in 1%KOH, one to several days in 80% 1%KOH / 20% glycerol, several days in 50% 1%KOH / 50% glycerol, and several days in 20% 1%KOH / 80% glycerol. Embryos were photographed and kept in 80% glycerol / 20% water indefinitely.

gene	forward primer	reverse primer	allele
Shh	GAAGAGATCAAGGCAAGCTCTGGC	GGACACCATTCTATGCAGGG	Wt
	ATGCTGGCTCGCCTGGCTGTGGAA		null
	GACCAATTATCCAAACCATC GGCTATTCGGCTATGACTGG	TAACACTAAGCAGCACTTCC GAGATGACAGGAGATCCTGC	ΔL Wt ΔL mut
Gli3	GGGTGAACAGCATCAAAATGGAG TACCCCAGCAGGAGACTCAGATTAG	ATAGCCATGTGGTGGTGCCCATG AAACCCGTGGCTCAGAGCAAG	XtJ Wt XtJ mut
Cyp26b1	CTACAGCATTAGAATCCCAGC	AAGTGCTTCAATCTGCAAGCC	XtJ
	AGCAGCCTCTGTTCCACATAC		mut
Pkdcc	TTGCTATCTCACTCCTAATGGTT	GTGGTGGAACAGCTCCATAGTTG	Wt
	AAGCGCCTCCCCTACCCGGTA		Floxedneo
	CACACGCTCAATCATACCACACC	GGTCATTAGGTCACAGGGTAGGG	Wt
		GTGGTGGAACAGCTCCATAGTTG	null
Ptch	CTGCGGCAAGTTTTTGGTTG TGTCTGTGTGTGCTCCTGAATCAC	AGGGCTTCTCGTTGGCTACAAG TGGGGTGGGATTAGATAAATGCC	Wt null
Cre	GCCTGCATTACCGGTCGATGCAACGA	GTGGCAGATGGCGCGGCAACACCATT	Tg

Table 1: genotyping primers

Tissue culture

Cell lines were propagated as monolayers in DMEM with the appropriate amount of fetal calf serum (FCS) and kept at 37 °C and 5% CO_2. Immuno-cytochemistry experiments were performed in COS cells (african green monkey kidney fibroblast-like cell line, ATCC CRL-1650). Overexpression of proteins was performed in HEK293T cells (human embryonic kidney cells, ATCC CRL-1573). Both cell lines were cultured in high glucose DMEM containing 10% FCS, 0.1mg/ml penicillin-streptomycin (Gibco 15140-122) and 200 mM L-glutamine (Gibco 25030-024).

Transient expression of proteins

Transient protein expression experiments with plasmid constructs were performed using Lipofectamine™ 2000 (Invitrogen, cat. 12566-014). Lipofectamine™ 2000 reagent is a cationic lipid that leads to high transfection efficiencies and thus high protein expression levels. It can be used in a broad range of mammalian cells. Transfection was performed following the supplier's protocol.

Protein purification and in vitro kinase assay

Purification of GST fusion proteins for in vitro kinase assays

10 cm dishes containing HEK293T cells were transfected as described above. After 24 hours, cells were washed 3 times with ice-cold PBS and harvested by the addition of 200 ml of lysis buffer per 10 cm dish (20 mM TrisHCl pH8.0, 138 mM NaCl, 2.7 mM KCl, 5% glycerol, 1% NP40, 1 mM DTT, 40 mM NaF, 2 mM Na_3VO_4 and complete protease inhibitor from Roche). The samples were kept on ice for 15 min and then centrifuged for 15 min at full speed. The supernatant was transferred to new tubes and gluthatione-beads (glutathione sepharose 4B, GE Healthcare, cat. 17-0756-01) were added to the lysate (approximately 20 μl 50% slurry, wash the beads in lysis buffer twice before using) and rotated for 3 hrs at 4 °C. The GST-fusion proteins will by then have bound to the beads. The beads were quickly spun down and washed twice with lysis buffer, one time with 0.1 M Tris HCl pH7.4, 0.5 M LiCl2 and twice in kinase buffer (see below) if used for in vitro kinase assay. Otherwise sample buffer (25% 0.5 M tris base pH6.8, 2% SDS, 5% ß-mercapto-ethanol, 20% glycerol, 0.0025% bromophenolblue) was added to the purified proteins and the samples were used for western blot analysis.

Coomassie blue staining of protein gels – After separation of proteins on a SDS-polyacrylamid gel the gel was incubated in fixative for 30 min (45% ethanol, 7.5% acetic acid). Then the gel was stained for 30 min or longer in coomassie blue stain (45% methanol, 7.5% acetic acid, 0.12% Serva blue R). The gel was destained in fixative and or H_2O (takes longer) until the background was sufficiently reduced.

Western blot analysis – HEK293 cells were transfected with the GST fusion constructs as described above. After 24 hours, the cells were washed 3 times in ice-cold PBS and lysis buffer (RIPA buffer: 50 mM TrisHCl pH7.5, 150 mM NaCl, 1% NP40, 0.5% Sodium Deoxycholate, 0.1% SDS, 1:1000 pefabloc, complete protease inhibitor Roche) was added to the cells. Cells were removed from the dish and the lysate was transferred to an eppendorf tube; the tube was maintained at constant agitation for 30 min at 4 °C. The tube was then centrifuged for 20 min at 13'000 rpm at 4 °C and the supernatant was transferred to a new tube. At this step the sample can be frozen and stored. The samples were prepared for SDS-PAGE by addition of sample buffer and boiling at 98 °C in a heat block for 10 min. Proteins were separated on a SDS-polyacrylamid gel (8% polyacrylamide) and blotted on a membrane (immobilon–P transfer membrane, Millipore, cat. IPV00010) that was activated briefly in methanol and equilibrated in transferbuffer (25 mM Tris; 192 mM glycine; 20% methanol). Wet transfer was performed at 4 °C at 100 V for 75 to 90 min. After transfer the membrane was blocked for at least 1 hr in 5% milk in TBST (10 mM Tris pH8.0, 150 mM NaCl, 0.05% Tween 20) and incubated with the primary α-GST antibody in 5% milk in TBST (rabbit α-GST 1:15'000, Bethyl labs). The membrane was washed 3 times 10 min in TBST and incubated with the HRP-linked secondary antibody (goat α-rabbit-HRP 1:10'000). Finally the bands were detected using Pierce ECL western blotting substrate (cat. 32109) and the membrane was exposed to Hyperfilm ECL films (GE Healthcare).

Kinase assay – The constructs for expression of the desired fusion-proteins were expressed in HEK293T cells (one 10cm dish for two reactions) and purified (see above). The purified proteins (attached to the beads) were washed twice in 1x kinase buffer (50 mM HEPES pH7.4, 0.03% Triton X100) and 20 μl were distributed to tubes for different reaction conditions. Then 25 μl of 1.2x kinase buffer including 2x supplements (60 mM HEPES pH 7.4, 0.036% Triton X100, 20 mM MgCl2 or 20 mM MnCl2, 2 mM DTT) were added and 1 μl of substrate if used. Samples were warmed to 30 °C for 2 min. Finally, 5 μl of ATP-mix (100 μM ATP in H_2O containing 2 or 5 μCi of [³²P]-ATP for each tube) were added to each

tube. Tubes were incubated for 20 min at 30 °C with shaking. The reaction was stopped by the addition of 14 μl of sample buffer. Samples were separated by SDS PAGE (autophosphorylation gel: 8% polyacrylamide, substrate phosphorylation gel: 15% polyacrylamide) (see above). The gels were stained with Coomassie blue (see above), dried, and exposed to film for approximately 5 hrs.

Immunocytochemistry

COS cells were transfected in 12-well or 6-well dishes containing round glass cover slips. After 24 hours, the cells were rinsed 3 times with PBS and fixed in 4% paraformaldehyde (PFA) in PBS for 20 min at RT. The cells were washed 3 times 3 min in PBS and then treated with 0.1% TritonX-100 for 10 min. Cells were rinsed once with PBS and blocked in 10% goat serum in PBS. Antibodies were diluted in 1% goat serum (rat α-Grp94 1:30, rabbit α-bovine PD1 1:500, sheep α-human TGN46 1:100, mouse α-myc 1:500). To apply the antibody to the cells, drops of 70 μl of the antibody solution were pipetted onto parafilm. The cover slips were then removed from the wells, were placed upside down onto the drops and left to incubate for 2 hrs. Cover slips were returned to a fresh 12-well plate and rinsed 3 times 5 min in with PBS 0.1% Tween-20 (PBT). Cover slips were incubated with a fluorescin-conjugated secondary antibody on parafilm for 1 hr (FITC-goat α-rat IgG 1:200, Cy2 α-rabbit IgG 1:200, FITC-rabbit α-sheep IgG 1:200, Cy3 α-mouse IgG 1:100). Cells were again washed 3 times 5 min in PBT, incubated with HOECHST in PBS for 5 min, washed 3 times in PBS, once in H2O to remove salt and then mounted on a microscope slide using mowiol. The mowiol was left to harden at 4°C before microscopy.

Whole mount in situ mRNA hybridization

Whole mount in situ hybridization (WISH) was done after a modified protocol from David Wilkinson (Wilkinson, 1993). All steps were carried out in 2 ml tubes. Embryos were collected in PBS and fixed overnight at 4 °C in 4% PFA in PBS and dehydrated in a 25%, 50%, 75%, 2x 100% methanol/PBT series and stored in methanol at -20 °C. On day one of the WISH, the embryos were rehydrated in the reverse methanol/PBT series. Embryos were bleached 15 min in 6% H_2O_2 in PBT and washed 3 times 5 min in PBT. Embryos were then treated with 10 μg/ml in proteinase K in PBT for 15 min for detection of mesenchymal probes and with 5 μg/

ml for 4 min for ectodermal probes. To inactivate the proteinase K the embryos were incubated in 2 mg/ml glycine in PBT for 5 min and then washed twice 5 min in PBT. The embryos were refixed for 20 min in freshly prepared 4% PFA in PBT with 0.2% glutaraldehyde and washed twice 5 min in PBT. Embryos were transferred into hybridization buffer (see below) at 70 °C and prehybridized for at least 1 hour at 70 °C in a rotating hybridisation oven. After prehybridization the solution was replaced by prewarmed hybridization buffer containing 10 µl/ml of digoxigenin-labelled RNA probe and incubated overnight at 70 °C in the oven (to prepare the probe heat it for 5 min at 85 °C and then add 10 µl probe to 1 ml prewarmed hybridisation mix).

The next day, embryos were brought through a series of 100%, 75%, 50%, 25% prehybridization mix/2x SSC (0.3 M NaCl, 0.03 M Sodium citrate, pH4.5), followed by two 30 min washes in 2x SSC, 0.1% CHAPS at 70 °C. To remove any unbound single stranded RNA probe embryos were incubated with RNAse A (20 µg/ml) in 2X SSC, 0.1% CHAPS during 45 min at 37 °C. Then embryos were washed in maleic acid buffer (100 mM maleic acid, 150 mM NaCl pH7.5) twice for 10 min at RT and twice for 30 min at 70 °C. Embryos were washed 3 times 5 min at RT in TBST (140 mM NaCl, 2.7 mM KCl, 25 mM Tris HCl pH7.5, 0.1% Tween). Embryos were blocked with 10% sheep serum in TBST for at least one hour. After this the blocking solution was replaced by the α-digoxigenin AP antibody (Fab fragments, Roche) in 1% sheep serum in TBST at a concentration of 1:5000 and the embryos were incubated with the antibody at 4°C overnight.

On the third day of WISH, the embryos were washed 3 times 5 min and 5 times 1 to 1,5 hour in TBST at RT. Finally they were washed in TBST overnight at 4°C.

On day four, embryos were washed three times 10 min in freshly made NTMT (100 mM NaCl, 100 mM Tris HCl pH9.5, 50 mM MgCl2, 0.1% Tween-20) and were incubated in BM Purple (Roche) to develop the colour. The reaction was stopped by several washes in PBT. Pictures were taken in PBT using a silicon dish. For storage embryos were fixed in 4% PFA, 0.1% glutaraldehyde in PBS for one hour at RT, washed in PBS twice at RT and kept in 0.05% sodium azide in PBS at 4°C.

Hybridization buffer: 50% formamide (deionized, extra pure), 5x SSC pH 4.5 (use 20x stock solution), 2% Blocking Reagent (Roche), 0.1% Tween 20, 0.5% CHAPS, 5 mM EDTA 50, 50 µg/ml yeast tRNA, and 50 µg/ml heparin.

Grafting and culturing of mouse limb buds (trunk cultures)

Generally all material used was sterile and tissue culture grade. Embryos were isolated at E10.25 to E10.5 (32 to 38 somites) in PBS (GIBCO). Embryos were then placed into equilibrated serum free culture medium (see below) at 6.5% CO_2 and 37 °C in a tissue culture incubator. Then one by one the embryos were prepared for culture and grafted: head and posterior trunk were removed as well as the heart and all other internal organs to isolate the trunk fragments with attached forelimb buds. The trunk was pinned with the dorsal side up and by using a tungsten needle, a small hole was made in the limb bud at the site where the bead will be placed. Using the tungsten needle a bead soaked in the desired protein or chemical (see below) was picked up from a dish and inserted into the limb bud. After inserting the bead, the embryos were transferred to a 24-well cell culture dish and pinned on inverted V-shaped stainless steel grids using sterile insect pins. Using a pipette, medium was removed so that the trunk was just covered with medium. This allows growth at the medium–air interface. The 24-well dish was then placed into the incubator and embryos were cultured for the desired time. The insect pins were removed carefully and trunks were removed from the wells and washed 3 times 5 min in PBS, fixed overnight in 4% PFA in PBS at 4 °C and then processed for WISH.

Culture medium: this medium is prepared fresh on the day of use.

— 500 ml Dulbecco's Modified Eagle Medium (1x), liquid (high glucose) (Cat. 41966-029, Gibco)
— 5 ml L-glutamine (Cat. 25030-024, Gibco)
— 2.5 ml penicillin-streptomycin (Cat. 15140-122, Gibco)
— 5 ml non-essential amino acids (Cat. 11140-035, Gibco)
— 5 ml sodium pyruvate (Cat. 11360-039, Gibco)
— 5 ml D-glucose (45% solution) (Cat. G8769, Sigma)
— 0.5 ml L-ascorbic acid [1] (Cat. A4034, Sigma)
— 5 ml lactic acid [2] (Cat. L4388, Sigma)
— 0.5 ml d-biotin/vitamin B12 [3] (Cat. B4639 and V6629 respectively, Sigma)
— 0.5 ml PABA [4] (Cat A9878, Sigma)

1. Dissolve 1 gram of L-ascorbic acid in 5 ml PBS, filter though 0.22 μm filter and add 0.5 ml to the medium. Make fresh.
2. Dissolve 0.2 gram of lactic acid in 5 ml of DMEM, filter through 0.22 μm filter and add 5 ml to the medium. Make fresh.
3. Make stock of 0.2 mg d-biotin and 40 μg vitamin B12 per ml DMEM. Filter through 0.22 μm filter. Make 0.5 ml aliquots and store at –20 °C
4. Make a stock of 2 mg PABA per 1 ml of PBS. Filter through 0.22 μm filter. Make 0.5 ml aliquots and store at -20 °C.

Prior to use, it is important that the medium is pre-warmed and pre-equilibrated with CO2 by placing the bottle (lid ajar) in the TC incubator. For this study, as a source of *Shh* deficient embryos for trunk cultures we crossed *Shh*Δ/+ females to males heterozygous for the limb specific *Shh* mutant allele (Δ*L* allele, (Sagai et al., 2005)). *Shh*Δ/Δ*L* limb buds are indistinguishable from *Shh*Δ/Δ limb buds, however *Shh*Δ/Δ*L* embryos are better suited for limb cultures as their trunks are healthy in contrast to the trunks of *Shh*Δ/Δ embryos. Wild-type controls correspond to either *Shh*Δ/+, *Shh L*/+ or +/+ embryos. AGX 1-2 beads were soaked in RA (Sigma, 1 mg/ml, dissolved in DMSO) or the retinoid antagonist BMS493 (a gift from Prof. Miguel Torres, 2 mg/ml, dissolved in DMSO), heparin beads were soaked in recombinant FGF4 (R&D Systems, 1mg/ml in PBS/0.1% BSA) and Affigel-blue beads in recombinant SHH protein (R&D Systems, 5 mg/ml in PBS/0.1% BSA). Beads loaded with molecules or protein were grafted into the right forelimb bud, while the contralateral forelimb bud was not grafted to serve as an internal control. In addition, a small number of limb buds grafted with beads alone (either soaked in DMSO or in PBS) were analyzed, but no alteration of gene expression was observed (data not shown). FGF signal transduction was blocked by supplementing the culture medium with 10 μM SU5402 (dissolved in DMSO). Trunks were cultured between 6 and 20 hours.

Mouse forelimb bud isolation and Affymetrix GeneChip analysis (performed by Aimée Zuniga)

Pairs of forelimb buds from littermates in the same genetic background were carefully dissected from their trunks at 35-36 somites (E10.5) and stored in RNAlater (Ambion). Three pairs of forelimb buds per genotype of the same sex were individually processed for RNA isolation. RNA was extracted using the RNeasy micro kit (Qiagen) following homogenisation by passing the RNAlater lysate through a 27g needle. On average 2.5 μg of total RNA were obtained per sample and integrity was confirmed using

RNA Nano 6000 Chips (2100 Bioanalyzer, Agilent). Target synthesis was performed starting from 200 ng total RNA using the WT expression kit (Ambion, Cat# 4411974). On average 53 μg (± 5 S.D.) of cRNA from each reaction was obtained. Then for each sample 10 μg was used to generate cDNA. On average 8.0 μg (± 0.1 S.D.) of cDNA from each reaction was obtained. For the following steps, the WT Terminal Labeling Kit (Affymetrix, Cat# 900671) was used: 5.5 μg cDNA was fragmented and fragments were monitored with the Bioanalyzer using the RNA Nano 6000 Chip. All synthesis reactions were carried out in 0.2 ml tubes using a PCR machine (TProfessional, Biometra, Gottingen, Germany) to ensure the highest possible degree of temperature control. A Nano-drop (NanoDrop ND-1000 Spectrophotometer, Thermo scientific, USA) was used to determine all RNA and DNA concentrations. The hybridization cocktail (85 μl) containing fragmented biotin-labelled target DNA at a final concentration of 25 ng/μl was transferred into Affymetrix GeneChip MoGene-1_0-st-v1 (Affymetrix, Cat#901168) and incubated at 45 °C on a rotator in a hybridization oven 640 (Affymetrix) for 17 h at 60 rpm. The arrays were washed and stained on a Fluidics Station 450 (Affymetrix) by using the Hybridization Wash and Stain Kit (Affymetrix, Cat# 900720) using the Fluidics Procedure FS450_0007. The GeneChips were processed with an Affymetrix GeneChip® Scanner 3000 7G (Affymetrix). DAT image files of the microarrays were generated using Affymetrix GeneChip Command Console (AGCC, version 0.0.0.676, Affymetrix). Quality control showed that the experimental output was thoroughly valid as the only significant source of variation in gene expression between samples was the genotype and that therefore potential differences would be significant.

Data analysis – Data analysis was performed using Partek Genomic Suite 6.5 (6.10.0212). Triplicates were run for each condition. Affy CEL files were normalized according to RMA method and data were log 2 transformed. To select differentially expressed genes a 2-way ANOVA model by using Method of Moments (Eisenhart, 1947) was applied. Genes were further filtered on the basis of a p-value lower than 0.03. To analyse the pathways affected in *Shh*-deficient limb buds the Ingenuity Pathway Analysis (IPA) program was used.

Quantitative real time PCR analysis
(performed by Aimée Zuniga)

Pairs of forelimb buds from littermates in the same genetic background were collected as described above and cDNA was synthesized using Superscript III (Invitrogen). Transcript levels were quantified by real time PCR using the BIO-RAD CFX96 Real Time System in combination with the iQ™ SYBR® Green Supermix (BIO-RAD; primers are listed in [Table 2]). Relative transcript levels were normalized using transcripts of the mouse hydroxy-methyl-bilane synthase (HMBS) gene as internal standard. Transcript levels in mutant forelimb buds are shown relative to the ones of wild-type forelimb buds (mean value set at 100%). Each result represents the mean of 7 to 10 independent samples per genotype (+/- standard deviation). The statistical significance of all differences was assessed using the two-tailed, non parametric Man-Whitney test.

cDNA	forward primers	revers primers
Rarb	5'-CACCGGCATACTGCTCAA-3'	5'-CAAACGAAGCAGGGCTTG-3'
Meis2	5'-TGGAAGCTCCAAGTCAGATCA-3'	5'-TTGCGTCATCGTGGTCTC-3'
Pbxl	5'-GCCAGACAGGAGGATACAGTG-3'	5'-GTGAGGATCAGTAGGTTCTTGACA-3'
Pkdcc	5'-CAAGCTGCTCAAAGAGATGGT-3'	5'-TGGTAGCAATAGCCATAGAGCTG-3'
Cyp26b1	5'-ACATCCACCGCAACAAGC-3'	5'-GGGCAGGTAGCTCTCAAGTG-3'

Table 2: Primers used for RT-PCR

Mathematical modelling
(performed by Conradin Kraemer and Dagmar Iber)

A spatio-temporal model for the PD core regulatory network – To simulate the core signalling interactions that regulate PD axis formation during limb bud outgrowth [**Figure 25**], we solved a set of reaction-diffusion type partial differential equations for FGF (F), CYP26b1 (C), RARb (B), and RA (R) on a growing 2-dimensional domain (AP and PD directions).
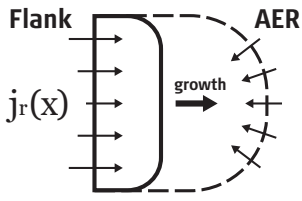
$$\frac{\partial F}{\partial t} = D\Delta F - kF \qquad\qquad \frac{\partial \beta}{\partial t} = \mu\, \frac{R^n}{R^n + K_b^n} - k\beta$$

$$\frac{\partial C}{\partial t} = \mu\, \frac{F^n}{F^n + K_f^n} - kC \qquad \frac{\partial R}{\partial t} = D\Delta R - kC\cdot R - kR$$

The expression of *Cyp26b1* and *Rarb* is enhanced by AER-FGF and RA signalling respectively up to a maximal rate μ, and RA is inactivated by CYP26b1 at rate k. All variables decay linearly at rate k. RA is produced in the flank while FGFs are produced by the AER and both diffuse with diffusion constant D into the limb bud mesenchyme. The influx of RA and FGFs were described using Neumann boundary conditions.

$$\left.\frac{\partial R}{\partial y}\right|_{\text{flank}} = -\, j_r(x)$$

$$\left.\frac{\partial F}{\partial n}\right|_{\text{AER}} = j_f \cdot \frac{K_r^n}{R^n + K_r^n}\left(1 + \theta(t)\ \frac{F^n}{F^n + K_s^n}\right)$$

Zero-flux conditions were applied to all other variables and boundaries. The experimentally observed lower RA influx in the centre of the flank was captured by a linear 8-fold increase in the RA influx rate from the centre to the anterior and posterior edges. The predicted and experimentally confirmed negative regulation of AER-Fgf expression by RA was captured by an inhibitory Hill-type function, while the SHH-dependent

positive feedback of AER-FGFs on its own expression was described by a self-activating Hill-type function. Multiplication with a step function in time, θ(t), ensured that *Shh* expression is activated with a delay in comparison to the other factors. For the simulations of *Shh* deficient limb buds θ = 0 was used for all t. For simulations AER-*Fgf mut* limb buds, the expression rate μ was reduced to 1/3 of the wild-type levels. All parameters are listed in table 3 and the values are justified below.

Prediction and validation of a novel negative feedback interaction between RA and AER-*Fgfs* – The first mathematical simulations were done assuming that the genetically identified regulatory interactions between RA (R), RARB (b), CYP26b1 (C), and AER-FGF (F) would be sufficient to reproduce the experimentally observed gene expression and activity domains. In particular, it was expected that the inactivation of RA by CYP26b1 and positive regulation of CYP26b1 by AER-FGFs [**Figure 25B**] would suffice to simulate the changes in gene expression in mutant limb buds. These two regulatory interactions can be described by the set of coupled reaction-diffusion type partial differential equations described previously. The boundary condition for FGF is given by:

$$\frac{\partial F}{\partial n}\bigg|_{AER} = j_f \cdot \left(1 + \theta(t)\ \frac{F^n}{F^n + K_s^n}\right)$$

Note that this boundary condition differs from that described above: here it was assumed that FGF is produced at a rate independent of RA but still dependent on the SHH-FGF positive feedback loop. While these initial simulations (using the equations shown above) reproduced many aspects of the experimentally observed expression and activity domains there were important discrepancies: in *Shh*-deficient limb buds, *Rarb* distribution was unchanged contrary to the *in situ* data, and the expression domains of *Cyp26b1* and AER-*Fgf* extend proximally in both *Shh*-deficient and wild-type limb buds [**Figure 26 and data not shown**]. To reproduce the experimental data observed in wild-type, *Shh* and *AER-Fgf mut* deficient limb buds, we had to invoke an additional inhibitory interaction by which high RA activity negatively regulates AER-FGFs [**Figure 25B, red inhibitory line**], which was done by introducing the inhibitory Hill-type function in the boundary condition (see above).

Parameter values – Instead of absolute values only the relative distributions of activities were considered for the mathematical simulations, no absolute values were required. Moreover, the same value was used for all diffusion constants to reduce unnecessary degrees of freedom. However, one could argue that functionally relevant differences exist, as the diffusion of RA might be much faster than AER-FGFs due to the large difference in molecular weight. Therefore, we verified that all simulations are stable even if diffusion constants are varied 10-fold. Given this robustness of the qualitative predictions to variations in parameter values, the set of equations could be simulated using only 6 relative parameter values (instead of 14)[**Table 3**]. These are: the diffusion constant D, the protein production rates μ, the degradation rates k, the Hill constants K_r, K_b, K_f, and the Hill coefficient n. The ratio between diffusion constants and degradation rates determines the characteristic length scale over which a morphogen gradient decays, which is known from experimental analysis. The Hill constants define the concentration ranges for which activating or inhibiting effects can be observed and thus scales with the protein production and decay rates. The relative values of the Hill constants reflect the relative strengths of activating and repressive effects. The Hill factors were set to 2 and reasonable alterations in this parameter did not qualitatively affect the outcome of the simulations, corroborating the robustness of the simulations.

Parameter	Value
D/k	0.056 L^2
$\mu/(k \cdot K_f)$	25
$\kappa \cdot \mu/k$	1
K_b/K_r	2
n	2
j_r^c/K_b	4 L^{-1}

Table 3: Parameter values used in the numerical simulations. L refers to the maximal length of the limb bud in AP direction. j_f^c denotes the minimum rate of RA influx; the RA influx rate j_r increases 8-fold from the centre to the anterior and posterior edges.

Simulations of mutant phenotypes – To simulate the effects of the AER-*Fgf*, and *Cyp26b* deficiencies [**Figures 25 and 26**] the AER-*Fgf* and the *Cyp26b1* expression rates were altered (jf in the boundary conditions of F and μ in the equations for C respectively) while all other parameters values remained the same. *Shh* mutants are simulated by removing the positive feedback by setting $\theta = 0$. AER-*Fgf* mutants were simulated by

lowering the parameter jf in the differential equation for F 3-fold. For simulating *Cyp26b1*-deficient limb buds, the expression rate μ in the differential equation for C was set to a 10-fold lower rather than zero buds because experimental analysis revealed low levels of precocious *Cyp26a1* expression in *Cyp26b1*-deficient limb buds (Yashiro et al., 2004). As a consequence of this compensatory effect by *Cyp26a1*, FGF activity remains in the distal-most part of the limb bud in the spatial simulations [**Figure 26**] as is observed by experimental analysis (Yashiro et al., 2004).

Modelling on a growing domain – To include growth in the model also the influence of the moving tissue on the spatial morphogen distribution has to be considered. The reaction-diffusion-equations for the concentration c on a medium with local fluid velocity u is given by:

where R(c) denotes the reaction part. For simplicity uniform outgrowth is assumed. The geometrical shape of the limb bud is stretched

$$\frac{\partial c}{\partial t} = \nabla \cdot (uc) = D\Delta c + R(c),$$

in proximal-distal direction but otherwise not changed over time. Instead of solving the equations on a geometry with moving boundaries the problem can be reduced to a fixed domain problem by means of a coordinate transformation. There the real coordinates x are related to the coordinates on a fixed domain via $x = \alpha(t) \cdot \tilde{x}$ and the velocity is given by $u = \dot{\alpha} \cdot \tilde{x}$. The equation on the fixed domain is then given by:

$$\frac{\partial c}{\partial t} = S \cdot (c + \tilde{x}\tilde{\nabla}c) = \frac{1}{\alpha^2} D\tilde{\Delta}c + R(c)$$

The term S can be interpreted as growth rate and is defined as $S = \nabla \cdot u = \dot{\alpha}/\alpha$. In the simulation the AER-FGF source is incorporated in form of a Neumann boundary condition, where the influx is set proportional to the expression term used in the static model. For the growth parameter α(t) a linear function with fivefold change over the considered time period has been assumed. Furthermore the impact of SHH signaling on *Fgf* expression was considered as time dependent; hence in the term for *Fgf* expression μ is not constant but also a function of time. In the simulation the onset of SHH signaling was described in form of a sigmoid function μ(t).

6 The novel kinase *Pkdcc* is essential during embryogenesis and *Pkdcc*$^{\Delta/\Delta}$ embryos exhibit skeletal defects

---

Results

***Pkdcc* expression is up-regulated in *Shh*-deficient limb buds and is dynamically expressed during embryogenesis** – SHH signalling by the ZPA is crucial for antero-posterior (AP) patterning and proliferative expansion of specified progenitors during limb bud development (reviewed by (Benazet and Zeller, 2009)). Although many genes that are positively regulated by SHH during limb bud development are known, only little is know about genes negatively regulated by SHH. In addition, it is important to understand how the diverse signals involved in morphogenesis of the limb are organized into regulatory gene networks. To address these questions we have performed transcriptome analysis of *Shh*-deficient limb buds at E10.5 (see chapter 7). Surprisingly about half of the genes that are changed ≥1.2 fold in *Shh*-deficient limb buds were found to be up-regulated, showing that SHH inhibits the expression of many genes during limb bud development. Among these genes with increased expression in *Shh*-deficient limb buds we identified also several unknown genes and genes that are not known to have a function during limb development. Therefore, we performed an in situ hybridisation screen to identify interesting novel genes with spatially restricted expression patterns in limb buds (data not shown).

One of the novel genes, the EST AW548124 (from now on called *Pkdcc*, (Imuta et al., 2009)), showed a restricted expression pattern in wild-type limb buds [**Figure 7 and 8**]. At E10.5 it is expressed in the proximal limb bud in an anterior and a posterior domain in a similar fashion to the *Meis* genes (Mercader et al., 1999). *In situ* hybridisation analysis confirmed that its expression is up-regulated and showed that it is distally expanded in *Shh*Δ/Δ limb buds [**Figure 7**]. One of the major functions of SHH during limb bud development is the counteraction of GLI3 repressor formation and *Shh* and *Gli3* are thought to have opposing functions during AP patterning of the limb bud (te Welscher et al., 2002b). In contrast to the observed distal expansion in *Shh*-deficient limb buds, the expression pattern of *Pkdcc* is unchanged in *Gli3XtJ/XtJ* mutant limb buds [**Figure 7**].

Since this gene showed an interesting expression pattern in limb buds, we further analyzed its expression during development in wild-type embryos. *Pkdcc* is expressed at E6.5 in the anterior part of the embryo in
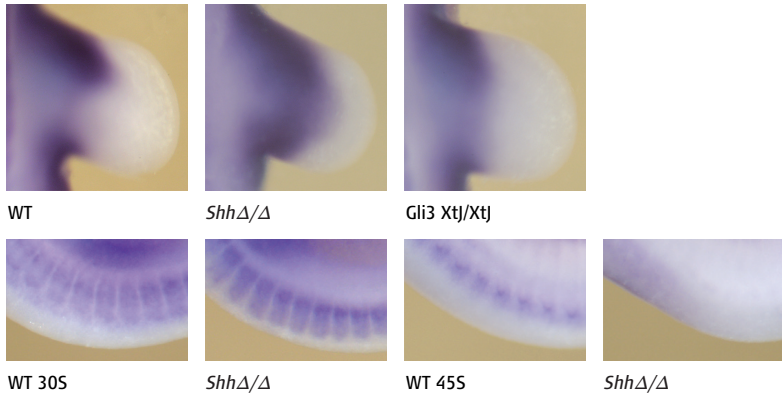
[**Figure 7**] Expression of *Pkdcc* is affected in *Shh*-deficient limb buds. All panels show *Pkdcc* expression. *Pkdcc* transcription is increased and distally expanded in *ShhΔ/Δ* limb buds (39 somites). Its expression is not changed in *Gli3XtJ/XtJ*-deficient limb buds. In *ShhΔ/Δ* somites the expression of *Pkdcc* is also changed when compared to wild-type somites (at 30 and 45 somites).
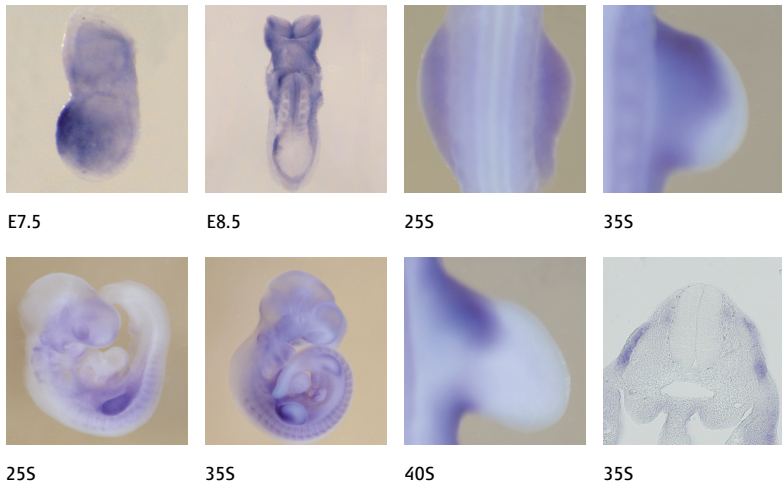
[**Figure 8**] *Pkdcc* is dynamically expressed during embryonic development. The expression pattern of *Pkdcc* is shown in whole embryos and limb buds. Expression in somites is shown on a section at the level of the forelimb buds.

the anterior visceral endoderm (AVE) and in the region of the node and the primitive streak (data not shown and (Imuta et al., 2009; Kinoshita et al., 2009)). At E7.5 and E8.5 *Pkdcc* is expressed in the anterior part of the embryo, while at E9.5 (25 somites) it is most strongly expressed throughout the mesenchyme of the emerging limb buds (**Figure 8**). It is also expressed in other parts of the embryo e.g. the somites, the head and the branchial arches. By E10.5 (35 somites), the expression in the limb buds is restricted to the proximal part of the limb bud and expres-

sion is stronger in the anterior domain than the posterior domain. In the somites expression is observed in the dermamyotome. By E11.0 (40 somites), the expression domains in the limb bud are separated by an expression-free domain in the middle of the limb bud [**Figure 8**]. The expression pattern observed in the somites is changed in *Shh*-deficient embryos. At E10.0 (30 somites), *Pkdcc* expression is expanded towards dorsal and at E11.5 (45 somites), no expression is observed in the somites of *Shh∆/∆* embryos whereas *Pkdcc* is still expressed in wild-type somites [**Figure 7**]. This analysis shows that *Pkdcc* is expressed dynamically and in restricted areas during embryonic development. The observed expression patterns indicate that *Pkdcc* might be important for normal embryonic development downstream of SHH signalling.

A
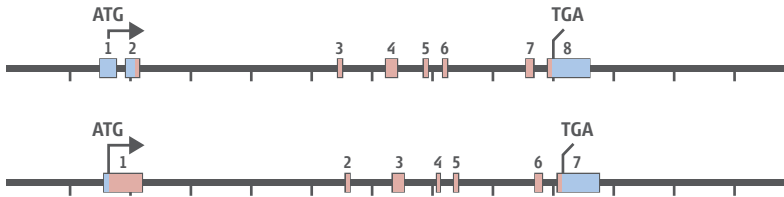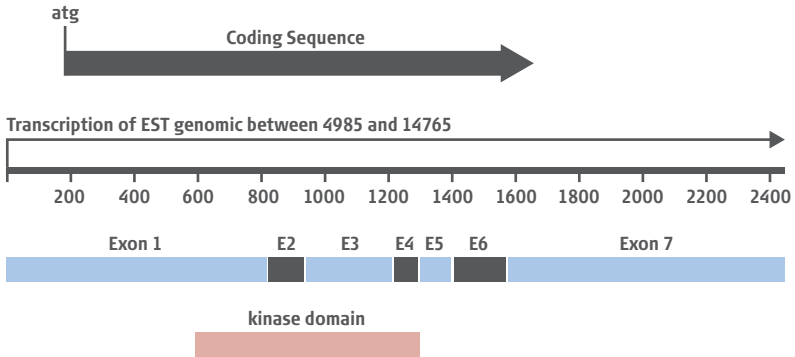
Identification of a full-length *Pkdcc* transcript – In online databases (NCBI, MGI), the predicted PKDCC protein is 293 amino acids long and contains part of a putative kinase domain. Because the N-terminal part of the kinase domain was lacking in this sequence, we reasoned that there might be alternative transcripts generated from this genomic locus. Intriguingly, exon 1 and exon 2 are separated by a very small intron and if this intron would be included to exon 1 and exon 2, resulting in

one longer exon 1, the predicted protein sequence would contain a full protein kinase domain [**Figure 9A**]. To identify alternative transcripts we performed 5' race on RNA from an E10.5 embryo. Indeed using a reverse primer close to the 5' end of the annotated RNA we were able to amplify a sequence that corresponds to the predicted sequence where exon 1 and exon 2 are actually one exon (data not shown). In addition we analyzed the transcript size of *Pkdcc* by northern blot analysis on embryo tissue. At E7.5 a single transcript of approximately 2.5 kb was detected [**Figure 9B**], corresponding in length to the predicted longer transcript that is 2454 nucleotides long. These data provide evidence that the *Pkdcc* gene indeed encodes this longer transcript. This transcript encodes a protein of 492 amino acids, which contains a full kinase domain.

B
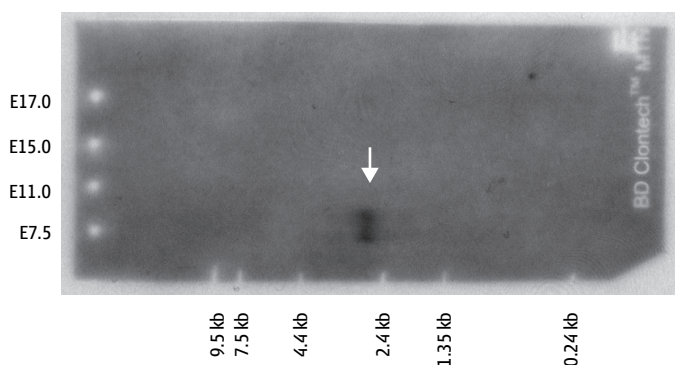
[**Figure 9**] Identification of a full-length *Pkdcc* transcript. (A) The genomic region of the *Pkdcc* gene is shown. The upper genomic region indicates the exons predicted by online databases, while the lower version depicts the newly identified exon 1 consisting of exon 1, exon 2, and intron 1 of the previously predicted gene. Below the newly identified transcript is illustrated. The exons, coding sequence, and kinase domain are indicated. (B) Northern blot analysis of the *Pkdcc* transcript on E7.5, E11.0. E15.0, and E17.0 embryonic RNA. In the E7.5 lane a faint band at approximately 2.5 kb is detected (arrow).

Performing a Blast of the protein sequence reveals that PKDCC has orthologues in some invertebrate species and that it is well conserved in vertebrates. An alignment of the sequences of mouse, human and zebrafish PKDCC proteins demonstrates the high degree of conservation between these species. Mouse and human orthologues display 92% and mouse and zebrafish 55% sequence homology [**Figure 10**].

```
Mouse       MRRRRAAVAAGFCASFLLGSVLNVLFAPGSEPPRP-----------------GQSPGSSA
Human       MRRRRAAVAAGFCASFLLGSVLNVLFAPGSEPPRP-----------------GQSPEPSP
Zebrafish   MKRRKMVVAAGFCVSFILGTLMNLLFIPGFEHHSERVHRHHHHHEKHTDAPARLQIDDSP
            *:**:  .*****.**:**:::*:**  **   *               .     *.

Mouse       APGPGRRGGRGELARQIRERYEEVQRYSRGGPGPGAGRPERRRLMDLAPGGPGLQRPRPP
Human       APGPGRRGGRGELARQIRARYEEVQRYSRGGPGPGAGRPERRRLMDLAPGGPGLPRPRPP
Zebrafish   PVEPATVGRLSELQRQIRERLDEVLRY-RQAHWLGTGPLERRRLMDLEQRSEWELYKGIE
            .  *.  *  .** **** *  :** **  .   *:*  *******   .

Mouse       RVRSPPDGAPGWPPAPGPGSPGPGPR---LGCAALRNVSGAQYVGSGYTKAVYRVRLPGG
Human       WARPLSDGAPGWPPAPGPGSPGPGPR---LGCAALRNVSGAQYMGSGYTKAVYRVRLPGG
Zebrafish   KINHYDPSRSTPAVSIATKSHREITRESGLGCGSIDNVTNVQYLGSGYTKAVYRAALNSS
            .   . .  :.. *   .*  ***.:: **:..**:*********. *  .

Mouse       AAVALKAVDFSGHDLGSCVREFGARRGCYRLAAHKLLKEMVLLERLRHPNVLQLYGYCYQ
Human       AAVALKAVDFSGHDLGSCVREFGVRRGCYRLAAHKLLKEMVLLERLRHPNVLQLYGYCYQ
Zebrafish   FSVALKSVDFGGHDMENCVKKYASSADCYKLASFKIIKEMTLMERLQHPNILKLYGSCYQ
            :****:***.***: .**:::.  .**:**:.*::***.*:***:***:*:*** ***

Mouse       DSEGIPDTLTTITELGAPVEMIQLLQTSWEDRFRICLSLGRLLHHLAHSPLGSVTLLDFR
Human       DSEDIPDTLTTITELGAPVEMIQLLQTSWEDRFRICLSLGRLLHHLAHSPLGSVTLLDFR
Zebrafish   DSNDIKETVTAITELGSPLEMIQLLQTPWEERFRICLSLMRLLHYLAHSPLGSVTLLDFR
            **:.  :*:*.*****:*:********* **:********  ****:************

Mouse       PRQFVLVNGELKVTDLDDARVEETPCTSSA--DCTLEFPARNFSLPCSAQGWCEGMNEKR
Human       PRQFVLVDGELKVTDLDDARVEETPCAGST--DCILEFPARNFTLPCSAQGWCEGMNEKR
Zebrafish   PRQFVLVDGVLKVTDLDDASVEETPCSKSAPQDCLMEFPARNFTLPCHKG-RCQGINQKR
            *******:* ********* ******: *:  **  :********:*** *   *:*:*:**

Mouse       NLYNAYRFFFTYLLPHSAPPSLRPLLDSIVNATGELAWGVDETLAQLETALHLFRSGQYL
Human       NLYNAYRFFFTYLLPHSAPPSLRPLLDSIVNATGELAWGVDETLAQLEKVLHLYRSGQYL
Zebrafish   NLYNAYRFFFTYLLPHSAPSALRPLLDKIVNSTGELMWGTDETLAHLEKVLDIYRNGHYL
            *******************.:******.***:**** **.*****:**..*..:*.*:**

Mouse       QNSTSSR-AEYQRIPDSAITQEDYRCWPSYHHGGCLLSVFNLAEAIDVCESHAQCRAFVV
Human       QNSTASSSTEYQCIPDSTIPQEDYRCWPSYHHGSCLLSVFNLAEAVDVCESHAQCRAFVV
Zebrafish   KNNTRMHKTEYKRVSDSSISAENYRCWPSYQHDGCLLSVYSVDEAVDVCESHVQCRAFVM
            :*.*   :**: :.**:*. *:*******:*.  *****.:.: **:****** .******:

Mouse       TNQTTWTGRKLVFFKTGWNQVVPDAGKTTYVKAPG---
Human       TNQTTWTGRQLVFFKTGWSQVVPDPNKTTYVKASG---
Zebrafish   TNHTTWTGHQLVLFKTGASSMSAAPGKLSYVRLGETES
            **:*****:**:**:****  ..:  ..* :**:
```

[**Figure 10**] Alignment of the predicted mouse, human, and zebrafish PKDCC protein sequences using 'multiple sequence alignment' by CLUSTALW.

Cell biological analysis of PKDCC – The newly identified full-length transcript codes for a complete kinase domain. However, some of the highly conserved motives common to protein kinases are not conserved in the PKDCC kinase domain, suggesting that this kinase might not function as a classical kinase. To establish if PKDCC has kinase activity we performed *in vitro* kinase assays with a C-terminal GST-fusion protein of PKDCC overexpressed in HEK293 cells. Since its targets are not known we assayed for autophosphorylation and the phosphorylation of histone 2B and myelin basic protein (MBP). Histone and MBP were not phosphorylated by PKDCC in the chosen conditions (+Mg or +Mn, data not shown). In the autophosphorylation assay a faint band was detected at the level of PKDCC-GST at 80 kDa [arrow in Figure 11A], which was absent in the GST control [GST band at 26 kDA, Figure 11A]. However, compared to the signal of the catalytic domain of protein kinase C (PKC) at 70 kDa, the positive control, the signal of PKDCC autophosphorylation was very weak. These results were therefore inconclusive.

A

PKDCC-GST · GST · PKDCC-GST · GST · PKC-GST

100 kD
75 kD
50 kD
25 kD

PKDCC-GST
PKC-GST
GST

PKDCC-GST + Mg · GST +Mg · PKDCC-GST + Mn · GST +Mn · PKC-GST + Mg

100 kD
75 kD
50 kD
25 kD

Enlargement of area

B
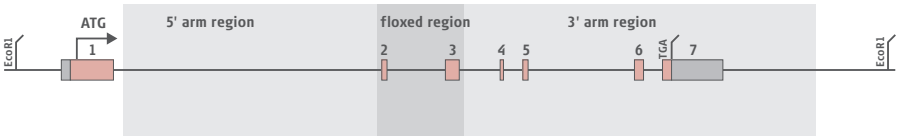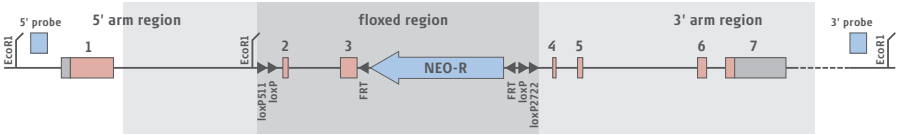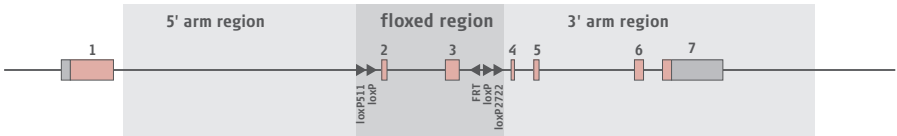
PKDCC

TGN46 (Golgi)

PKDCC + TGN46

PKDCC + PD1 (ER)

[**Figure 11**] Cell biological analysis of PKDCC. [**A**] Kinase assay with a C-terminal PKDCC-GST fusion protein. HEK293 cells were transfected with the PKDCC fusion protein, GST alone and a PKC-GST fusion protein. All proteins were purified and incubated with [^{32}P]-ATP to assay for autophosphorylation. Proteins were then separated by SDS-PAGE and the gel was exposed to film. Coomassie staining of the gel and the exposed film showing incorporation of [^{32}P]-ATP are shown. PKDCC-GST runs at 80 kDa (arrow), GST at 26 kDa and PKC-GST at 70 kDa. On the coomassie stained gel the proteins can be seen at the expected sizes. Some background bands are present as well. On the film a faint band is detected in the PKDCC-GST lanes (+Mg and +Mn) at the level of PKDCC-GST (80 kDa), whereas this band is absent in GST control lanes. This area is shown enlarged below the whole film. No band is detected in the GST control lanes at the level of GST (26 kDa). A very strong signal is detected for PKC-GST autophosphorylation. [**B**] Immunofluorescence on COS cells transfected with PKDCC-myc using antibodies against myc to detect the PKDCC protein and antibodies against golgi apparatus or ER proteins. The PKDCC-myc protein (red) overlaps with the golgi apparatus protein TGN46 (green, TGN46 panel) in some domains (orange on PKDCC + TGN46 panel). It does not overlap with the ER protein PD1 (green, PKDCC + PD1 panel).

61

To investigate the subcellular localization of PKDCC, we overexpressed myc-tagged PKDCC in COS cells. PKDCC-myc localized to the secretory system of the cell [**Figure 11B**]. We performed double immunostainings with anti-myc and antibodies against Golgi and ER proteins to identify its precise subcellular localization. The signal for PKDCC overlapped partly with a marker for the golgi apparatus (TGN46) in most transfected cells, but only in few cells with two markers for the ER [**PD1 and GDF 46**, **Figure 11B and data not shown**]. This suggests that PKDCC localizes preferentially to the golgi apparatus but might also be present in the ER and other compartments at certain stages during the cell-cycle.

Homologous recombination at the *Pkdcc* locus and generation of *PkdccΔ/Δ* mice – To establish the essential functions of *Pkdcc* in vivo we decided to generate a conditional targeted deletion of the gene in mice by homologous recombination in embryonic stem cells (ES). *Pkdcc* is located on mouse chromosome 17 and consists of 7 exons (described above) [**Figures 12A**]. The open reading frame spans all 7 exons, while the kinase domain spans exons 1 to 4 [**Figure 9A**]. We decided to flank exons 2 and 3 with loxP sites, because these two exons encode for a larger part of the kinase domain that includes important functional motives [**Figure 12A**]. Upon Cre-mediated recombination these two exons are deleted, leading to a frame shift and a premature stop, which creates a loss-of-function allele. In addition to the conventional loxP sites, we also introduced the heterotypic loxP sites loxP511 and loxP2722 next to the loxP sites to allow us to perform recombinase mediated cassette exchange (RMCE) on this genomic locus (Branda and Dymecki, 2004) (Osterwalder et al, unpublished data).

The *Pkdcc* genomic locus was isolated as a 12.5 kb *EcoRI* fragment from a BAC and subcloned into a pKS vector. The 5' recombination arm spans from just downstream of exon 1 to just upstream of exon 2. Exon 1 was not included in the recombination arm because it is very GC rich. The 3' recombination arm spans from just downstream of exon 3 to the end of the gene and 1.5 kb of downstream sequence. The recombination arms were subcloned into pGEM vectors. The sequence around exons 2 and 3 was modified such that they are flanked by the loxP sites and were cloned into a pGEM vector. A PGK-neoR cassette flanked by FRT sites was inserted 3' of exon3 but 5' of the second loxP site to allow concurrent excision of exons 2 and 3 and the PGK-neoR by Cre-mediated recombination. The final targeting vector was constructed by assembling these three fragments in a pKS vector [**Figure 12A**].

The targeting vector was linearized with *NotI* and electroporated into R1 ES-cells. ES cell clones were selected in medium containing G418. In

A

Targeting Vector
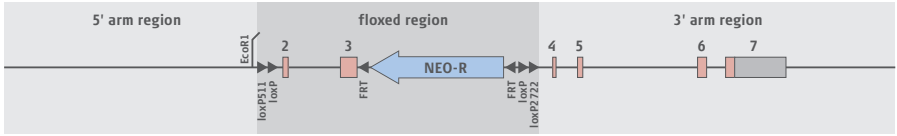
Genomic Locus

Targeted allele (*Pkdcc^floxedneo* allele)

+FLP

***Pkdcc^floxed* allele**

+CRE

***Pkdcc^Δ* allele**

63
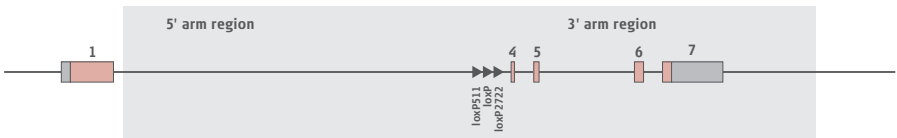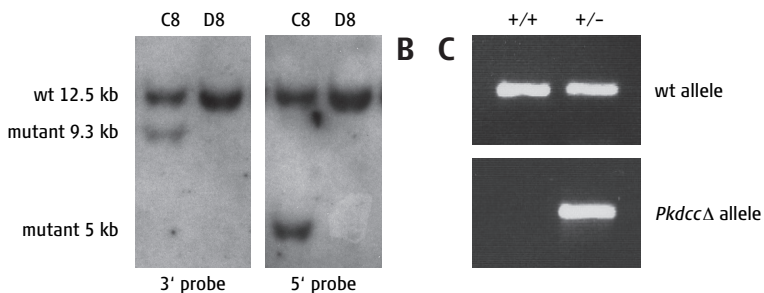
[**Figure 12**] Generation of a *Pkdcc* conditional and null allele. (**A**) The *Pkdcc* targeted allele (or *Pkdcc^floxedneo* allele) was generated by homologous recombination in ES cells. The targeting vector was electroporated into ES cells, where it recombined with the genomic locus (crossed arrows). The *Pkdcc* genomic locus consists of 7 exons. Exons are depicted as boxes; grey areas represent non-coding regions and pink areas coding regions in exons. Exons 2 and 3 were flanked by conventional loxP and the heterotypic loxP511 and loxP2722 sites (arrowheads). A neomycin resistance cassette (blue NEO-R arrow) flanked by FRT sites was introduced for positive selection. Also an additional *EcoR1* site was introduced just upstream of the 5' loxP site for easier screening. The *Pkdcc^floxed* allele was generated by crossing *Pkdcc^floxedneo* mice to a line carrying the flippase transgene (FLP). The *Pkdcc* null allele (*PkdccΔ*) was obtained by crossing P*kdcc^floxedneo* or *Pkdcc^floxed* mice to mice carrying the Cre recombinase transgene leading to excision of the loxP flanked region. The 5' and 3' genomic probes used for screening ES cells by genomic southern blotting are shown as blue boxes. (**B**) Genomic southern blot analysis of a correctly targeted ES cell carrying the *Pkdcc^floxedneo* allele (C8) and non-recombined ES clone (D8) with 5' and 3' probes. The wild-type (wt) band is detected at 12.5 kb, the mutant band detected by the 3'probe is 9.3 kb and the mutant band detected by the 5'probe is 5 kb. (**C**) PCR genotyping of a heterozygous *PkdccΔ/+* pup (+/-) compared to a wild-type littermate (+/+).

total 838 clones were picked and screened by genomic southern blot for correct homologous recombination events. Through the recombination event an additional *EcoR1* restriction site was inserted at one loxP site for easier screening [**Figure 12A**] The DNA from the ES cell clones was digested with *EcoR1* and probed with an external 5' and 3' probe. The 5' probe detects a 12.5 kb wild-type band and a 5 kb mutant band, while the 3' probe detects the same wild-type band and a 9.3 kb mutant band [**Figure 12B**]. Four of the 838 clones have undergone homologous recombination corresponding to a frequency of 0.5%. Correct recombination was confirmed by extensive Southern blot and PCR analysis (data not shown). 3 of the 4 clones were positive for all tests and were expanded and injected into C57BL/6 blastocysts (injections into blastocysts were performed by the transgenic mouse core facility at the Biozentrum, Basel). Following germline transmission mice heterozygous for the recombined locus (*Pkdcc^floxedneo/+*) were crossed to mice expressing the ubiquitously expressed CMV-Cre transgene to generate the *PkdccΔ/+* allele [**Figures 12A+C**]. Mice heterozygous for the *PkdccΔ* allele appear normal and are fertile. *Pkdcc^floxedneo/+* mice were kept to also allow conditional inactivation of *Pkdcc*. Furthermore the PGK-neoR cassette can be removed by flippase-mediated recombination.

Analysis of the skeletal phenotype of *Pkdcc∆/∆* newborns – Mice heterozygous for the *Pkdcc∆*-allele were intercrossed to generate *Pkdcc∆/∆* mice. *Pkdcc∆/∆* mice are born alive but die within the first day due to respiratory failure. They display cyanosis and do not suckle. Furthermore *Pkdcc∆/∆* newborns appear smaller than their littermates.

To examine the skeletal abnormalities in *Pkdcc∆/∆* newborns we prepared whole mount skeletal stainings. Most strikingly, the limbs of *Pkdcc∆/∆* newborn mice are severely shortened when compared to wild-type littermates [**Figure 13A**]. The mineralized regions of the bones (stained in alizarin red) are affected while the cartilage (stained in alcian blue) does not seem to differ from wild-type controls. Anterior-posterior patterning of limb development is not affected and all five digits are formed correctly. To further analyze the ossification defect, we processed the skeletons of embryos at E14.5. Already at this stage, the size reduction of the limb bones is visible [**Figure 13A**]. In addition a delay in ossification can be observed, since in the stylopod of *Pkdcc∆/∆* embryos alizarin red staining is absent (humerus) or barely visible (femur), while in wild-type littermates there is a clear domain of mineralized bone present [**Figure 13A**, **arrowheads**]. This delay in ossification can also be observed in newborns. In the forelimb and hindlimb autopod mineralization of the second phalanges was absent or decreased [**Figure 13B**, **arrowheads**] and the caudal vertebrae display delayed mineralization [**Figure 13C**, **arrowheads**]. In more rostral vertebrae the mineralized region is thinner in *Pkdcc∆/∆* newborns. These observations show that the observed ossification phenotype is not restricted to the limbs [**Figure 13C**]. The delay and decrease of mineralized regions of bones in *Pkdcc∆/∆* mice might lead to the smaller size of these mutants.

Another characteristic phenotype of *Pkdcc∆/∆* newborns is a cleft palate. The secondary palate fails to fuse, leading to a large cleft in the midline [**Figure 13D**]. Moreover, some *Pkdcc∆/∆* newborns display mild phenotypes in the fusion of the sternum (data not shown). These data indicate that *Pkdcc* is indeed important for skeletal development.
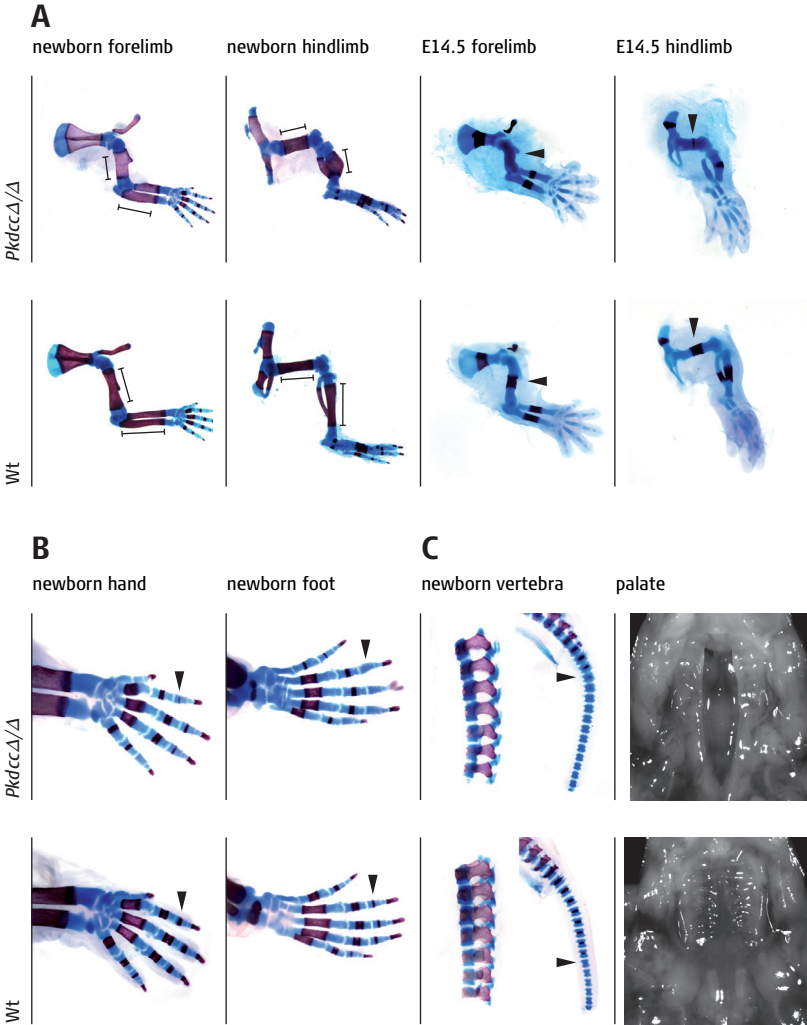
[**Figure 13**] Phenotype of *Pkdcc*-deficient newborns and embryos. (**A**) Skeletal preparations of forelimbs and hindlimbs of *PkdccΔ/Δ* mice were compared to wild-type limbs at newborn stage and at E14.5. *PkdccΔ/Δ* limbs show a severe reduction of the mineralized region (in red) both at the newborn stage (brackets) and at E14.5. Furthermore a delay of the appearance of the mineralized region is visible in *PkdccΔ/Δ* limbs at E14.5 when compared to wild-type littermates (arrowheads). The cartilage (in blue) does not seem to be affected. (**B**) Forelimb and hindlimb autopods of *PkdccΔ/Δ* newborns show a delay or reduction of ossification in the 2nd phalanges (arrowheads). (**C**) Mineralization is also reduced and delayed in vertebrae (arrowheads point to delayed mineralization). (**D**) *PkdccΔ/Δ* mice display a cleft of the secondary palate (ventral view of the palate). Brackets indicate the length of mineralized regions of limb bones. Arrowheads indicate reduced or delayed mineralization.

Analysis of *Pkdcc;Gli3* double mutant embryos – *Pkdcc* expression was found to be up-regulated in *Shh*-deficient limb buds. During limb development *Shh* is essential for AP patterning of the limb bud (Chiang et al., 2001). *Pkdcc* mutant embryos do not display an AP patterning phenotype. Nevertheless *Pkdcc* could function as a modulator of *Shh* pathway activity. To establish if *Pkdcc* has a function in the SHH signalling pathway we crossed the *Pkdcc*D mice to several members of the SHH pathway. *PkdccΔ/Δ;ShhΔ/Δ* embryos phenocopy *ShhΔ/Δ* embryos and *PkdccΔ/Δ;ShhΔ/+* newborns look like *PkdccΔ/Δ*. Likewise *PkdccΔ/Δ;PtchΔ/+* newborns do not display any novel phenotypes (data not shown).

Interestingly the mineralized regions of the limb bones of *PkdccΔ/Δ;Gli3Δ/+* newborns are shortened compared to the limbs of *PkdccΔ/Δ* newborns [Figure 14A]. We measured the lengths of the mineralized region of all limb bones of wild-type, *Gli3Δ/+*, *PkdccΔ/Δ*, and *PkdccΔ/Δ;Gli3Δ/+* newborns [Figure 14B]. The tibia is the most affected bone as in *Pkdcc*-deficient limbs its length is only 59.9% of the wild-type control, while in *PkdccΔ/Δ;Gli3Δ/+* limbs the tibia measures only 37.6% of the wild-type. Furthermore the humerus is strongly affected as *PkdccΔ/Δ* humeri measure 64.4% of wild-type controls and *PkdccΔ/Δ;Gli3Δ/+* humeri 51.3%. All other limb bones were also reduced in length in *PkdccΔ/Δ* and *PkdccΔ/Δ;Gli3Δ/+* limbs compared to wild-type, but they were more affected in *PkdccΔ/Δ;Gli3Δ/+* limbs [Figure 14B]. Limbs of *Gli3* heterozygous newborns display mild preaxial polydactyly, which was also observed in *PkdccΔ/Δ;Gli3Δ/+* limbs (Mo et al., 1997) [Figure 14A]. The skeletal elements of *Gli3Δ/Δ* limbs are slightly shorter than those of wild-type mice (Koziel et al., 2005), but we did not observe a shortening of the limb bones in *Gli3Δ/+* mice [Figure 14B].

To further study this interaction between *Pkdcc* and *Gli3* we generated *Pkdcc;Gli3* double mutant embryos. We first analyzed these embryos at E14.5, but the skeletal development of the limb in these double mutants is strongly delayed. We therefore collected embryos at E16.5 and compared the skeletal defects of the limbs. The mineralized region of *PkdccΔ/Δ;Gli3Δ/Δ* limb bones is strongly affected. Humerus, tibia and fibula show no mineralized regions whereas in wild-type controls these regions are already well developed. In ulna, radius and femur small domains of mineralization can be observed [Figure 15]. Because of the dramatic shortening of all bones, all double mutant limbs are much smaller. The mineralized region of the scapula is sometimes deformed in both *PkdccΔ/Δ;Gli3Δ/+* and *PkdccΔ/Δ;Gli3Δ/Δ* limbs, although this is not the case in all embryos [Figure 15, arrow, panel PkdccΔ/Δ;Gli3Δ/Δ]. Moreover the mineralization in the spine is strongly reduced in double mutant embryos (data not shown), showing that this delay in mineralization is again not limited to the limbs (as observed in *PkdccΔ/Δ* embryos). *Gli3Δ/Δ* embryos

A

Wt PkdccΔ/Δ PkdccΔ/Δ;Gli3Δ/+

forelimb

hindlimb
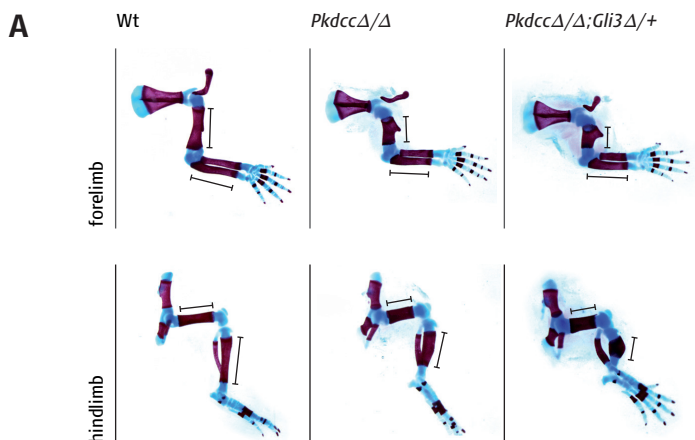
B

	Wt (n=7)	Gli3Δ/+ (N=4)	PkdccΔ/Δ (n=10)	PkdccΔ/Δ;Gli3Δ/+ (n=7)
humerus	2.61	2.68	1.68	1.34
ulna	2.91	2.88	2.5	2.33
radius	2.55	2.53	1.96	1.67
femur	2.3	2.28	1.62	1.46
tibia	2.74	2.63	1.64	1.03
fibula	2.64	2.6	1.74	1.53

[**Figure 14**] *PkdccΔ/Δ;Gli3Δ/+* newborn limbs are more severely shortened than *PkdccΔ/Δ* newborn limbs. (A) Wt, *PkdccΔ/Δ*, and *PkdccΔ/Δ;Gli3Δ/+* forelimbs and hindlimbs are shown. *PkdccΔ/Δ;Gli3Δ/+* limbs display shorter mineralized regions (red) compared to *PkdccΔ/Δ* limbs, which are shorter than Wt limbs. Brackets indicate the length of the mineralized region of limb bones. (B) The mean values (in mm) of the measurement of all limb bones in several Wt, *Gli3Δ/+*, *PkdccΔ/Δ*, and *PkdccΔ/Δ;Gli3Δ/+* newborns are indicated (number of limbs measured (n) for the different genotypes is stated in the table).
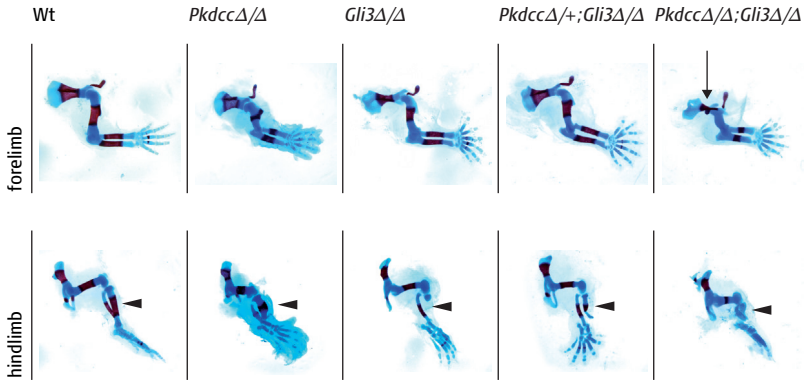
[**Figure 15**] Limb-phenotype of *PkdccΔ/Δ;Gli3Δ/Δ* embryos at E16.5. *PkdccΔ/Δ;Gli3Δ/Δ* fore- and hindlimbs are compared to Wt, *PkdccΔ/Δ*, *Gli3Δ/Δ*, and *PkdccΔ/+;Gli3Δ/Δ* limbs. Wt limbs exhibit well-developed mineralized regions (red) at this stage. In *PkdccΔ/Δ* and *Gli3Δ/Δ* (Koziel et al., 2005) the mineralized regions are shortened. *Gli3Δ/Δ* limbs display tibial hemimelia (panel *Gli3Δ/Δ* hindlimb, arrowhead) and polydactyly. The mineralized regions of *PkdccΔ/+;Gli3Δ/Δ* limbs are similar in length to *Gli3Δ/Δ*, but in some *PkdccΔ/+;Gli3Δ/Δ* embryos the *Gli3Δ/Δ* tibial hemimelia is rescued (n=2/6, panel *PkdccΔ/+;Gli3Δ/Δ* hindlimb, arrowheads indicate the position of the tibia). *PkdccΔ/Δ;Gli3Δ/Δ* limbs are severely delayed in ossification, visible by the absence or the reduction in length of mineralized regions. Furthermore the mineralized region of the scapula is deformed in some of the *PkdccΔ/Δ;Gli3Δ/Δ* embryos (arrow in panel *PkdccΔ/Δ;Gli3Δ/Δ* forelimb). The tibia also seems to be present in these mutants (panel *PkdccΔ/Δ;Gli3Δ/Δ* hindlimb). *Gli3Δ/Δ* polydactyly is not affected by the removal of one or two copies of *PkdccΔ/Δ* (panels *PkdccΔ/+;Gli3Δ/Δ* and *PkdccΔ/Δ;Gli3Δ/Δ*).

exhibit severe polydactyly with 6 to 8 fingers (Mo et al., 1997), which can be observed in both *Gli3Δ/Δ* and *Pkdcc;Gli3* double mutant embryos. In addition *Gli3*-deficient hindlimbs display tibial hemimelia [**Figure 15A**]. Interestingly in some of the *PkdccΔ/+;Gli3Δ/Δ* embryos the tibia is restored (n=2/6) [**Fig. 9 panel PkdccΔ/+;Gli3Δ/Δ, arrowhead**]. In *PkdccΔ/Δ;Gli3Δ/Δ* the tibia also seems to be present, although in these embryos the tibia and fibula are much shortened and their development is delayed. These results point to an interaction of *Pkdcc* and *Gli3* during endochondral bone formation.

Discussion

In this study we have analyzed the function of the novel gene *Pkdcc* and show that it is necessary for embryonic development. *Pkdcc* expression was found to be up-regulated in *Shh*-deficient limb buds by microarray analysis. It is expressed in the proximal limb bud and expands distally in *ShhΔ/Δ* limb buds, suggesting that this gene might be negatively regulated by SHH. Furthermore *Pkdcc* shows a dynamic and spatially restricted expression pattern during embryonic development. These observations indicated that *Pkdcc* could be important during development. To evaluate the function of *Pkdcc* in vivo we have generated a conditional null-allele in the mouse.

We have created a *Pkdcc* null allele by deleting exons 2 and 3, which contain a large part of the predicted kinase domain of PKDCC (see below). At the time when we started analyzing the phenotype of the *Pkdcc* mutant embryos, two studies were published that describe a targeted deletion of the same gene (Imuta et al., 2009; Kinoshita et al., 2009). Both groups generated a *Pkdcc* null-allele by deleting exon1, which should lead to disruption of gene expression from this locus. The phenotypes described in these two studies match the phenotype we observe in *PkdccΔ/Δ* mice, suggesting that all three targeting strategies lead to a complete disruption of PKDCC function.

To gain insight into the possible function of *Pkdcc*, we analyzed its sequence in online databases. The PKDCC protein is an orthologue of the human SGK493. SGK493 constitutes a unique protein kinase group, because it does not fit with any of the major protein kinase groups. In each species there is only one member of this SGK493 group (*Pkdcc* in the mouse). BLAST searches show that this protein is well conserved in vertebrate species (i.e. human, mouse, gorilla, dog, platypus, zebrafish) and that orthologues are also found in some invertebrate species like amphioxus, sea urchin and certain worms. Interestingly the SGK493 is not conserved in Drosophila or C. elegans.

The kinase domain of PKDCC is lacking some of the highly conserved motifs of a canonical kinase domain. To evaluate the molecular function of PKDCC we performed kinase assays, which were not conclusive, since we detected only a faint signal in the autophosphorylation assay and no substrate phosphorylation was observed. These results do not exclude the possibility that PKDCC functions as a kinase. It is possible that the conditions we chose for performing the in vitro assays were not optimal for this atypical kinase. For example the CASK protein, which was thought to contain an inactive kinase domain, was recently shown to function as

a kinase in the absence of Mg2+ (Mukherjee et al., 2008). Furthermore one of the other studies describing PKDCC function has shown that overexpressed PKDCC was tyrosine phosphorylated as detected by an anti-phosphotyrosine antibody. No tyrosine phosphorylation was detected on a PKDCC protein with a mutated ATP binding site. The mutated form of PKDCC was phosphorylated if co-transfected with wild-type PKDCC (Kinoshita et al., 2009). These results show that PKDCC probably functions as a kinase, but that the conditions and substrates still need to be evaluated.

Co-localization experiments in cells expressing myc-tagged PKDCC have shown that PKDCC localizes to the Golgi apparatus. Kinoshita et al. have also shown that PKDCC is found in some compartments of the golgi apparatus (in the ER-golgi intermediate compartment and the cis-golgi, but not in the trans-golgi). In addition, they showed that overexpression of PKDCC inhibits transport of a GFP-fused protein from the Golgi apparatus to the plasma membrane (Kinoshita et al., 2009). PKDCC might thus be part of the secretory pathway. It has to be kept in mind though that all these experiments were performed in transfected cells overexpressing PKDCC. It is possible that these results do not reflect functions of the endogenous protein in non-transfected cells. To have the possibility to detect the endogenous protein and further study the cell-biological functions of PKDCC, we are generating an antibody against PKDCC.

PkdccΔ/Δ mice display several phenotypes including respiratory failure during the first day after birth, cleft palate and a delay and reduction in endochondral bone formation. Most strikingly, the ossification defect reduces the length of long bones in the limbs. We focused our further studies on the analysis of the limb phenotypes. Endochondral bone formation begins when mesenchymal cells form condensations and become *Sox9* expressing chondrocytes. The cartilage grows through chondrocyte proliferation and production of extra-cellular matrix. At the centre of the growing bone the chondrocytes cease to proliferate and become hypertrophic. Hypertrophic chondrocytes (HC) are important regulatory cells for bone growth and formation. Finally, HCs undergo apoptosis and the cartilage matrix is invaded by osteoblasts and blood vessels that will form the bone matrix. In the long bones of the limbs, a subset of the proliferating chondrocytes (PC) assume a flattened shape and form stacks with a clear orientation directing the bone growth (reviewed by (Kronenberg, 2003)). Imuta et al. have shown that in *Pkdcc*-deficient limbs, the differentiation of PC into HC was delayed by two days. Specifically, the formation of flat proliferating chondrocytes (FPC) from round PCs was delayed, but they eventually formed. Pkdcc is expressed in PCs but not HCs at E15.5 (Imuta et al., 2009). These data indicate that *Pkdcc*

functions in the process of endochondral bone formation.

Most interestingly, we observe a worsening of the limb phenotype if *PkdccΔ* mice are crossed to *Gli3Δ* mice. Both *PkdccΔ/Δ;Gli3Δ/+* newborns and *PkdccΔ/Δ;Gli3Δ/Δ* embryos exhibit shorter limbs than their *PkdccΔ/Δ* littermates. *Ihh*, a closely related member of *Shh*, is an important regulator of bone development (St-Jacques et al., 1999). IHH binds to the same receptor as SHH, PTCH-1, thus releasing repression of SMO which then activates the transcription factors GLI1 to 3 (reviewed by (Lai and Mitchell, 2005)). Ihh-deficient mice display reduced chondrocyte proliferation, delayed chondrocyte maturation, and absence of mature osteoblasts in endochondral bones (St-Jacques et al., 1999). It was shown that in the absence of IHH signalling, GLI3 acts as a repressor and the phenotype observed in *Ihh*-deficient limbs can be partially rescued by *Gli3* removal (Koziel et al., 2005). *Gli3*-deficient mice exhibit only a slight reduction in bone length, but the limb bones of *Gli2Δ/Δ;Gli3Δ/+* embryos are more severely shortened (Mo et al., 1997). We observe a very similar synergistic reduction of long bones by crossing *PkdccΔ* mice to *Gli3Δ* mice. This indicates that *Pkdcc* might be involved in one of the processes regulated by IHH and might itself be regulated by IHH signalling. This hypothesis is supported by the observation that *Pkdcc* expression is increased in absence of SHH signalling and by the fact that there seems to be a genetic interaction between *Gli3* and *Pkdcc* during long bone development. Strikingly, the phenotypes of *Pkdcc* mutants are similar to the phenotypes of *Gli2*-deficient embryos. Both mutants have shortened limb bones, exhibit a cleft palate and delayed ossification of vertebrae and skull (Mo et al., 1997). It will be interesting to further study the interactions of *Pkdcc* with *Ihh* and the *Gli* transcription factors by detailed morphological analysis of the developing bones of single and double mutant embryos and by molecular analysis of bone development. Further information on the function of *Pkdcc* during endochondral bone formation could be gained from the analysis of the expression patterns of factors known to be involved in the processes regulated by *Ihh* (and *Gli3*) in *PkdccΔ/Δ*, *PkdccΔ/Δ;Gli3Δ/+*, and *PkdccΔ/Δ;Gli3Δ/Δ* limb bones. These studies are currently being initiated and will continue beyond the research for this PhD thesis. In addition, the different cell populations important for endochondral ossification should be analysed morphologically. Analysing the interactions of GLI3 or IHH with PKDCC or GLI3 processing in a cellular system could give further indications for the possible interactions between these factors.

7 SHH signalling coordinates antero-posterior with proximo-distal limb bud development by ensuring retinoic acid clearance

Introduction

Identification of the key molecular interactions that control the spatially coordinated expansion of progenitors during vertebrate embryogenesis remains a major challenge. During vertebrate limb bud development, the proximo-distal (PD) and antero-posterior (AP) limb skeletal axes develop from specified mesenchymal progenitors by proliferative expansion in combination with progressive determination and differentiation as chondrocytes (Tabin and Wolpert, 2007; Towers et al., 2008; Zeller et al., 2009; Zhu et al., 2008).

Two signalling centres control limb bud outgrowth and patterning: the apical ectodermal ridge (AER) at the distal tip of the limb bud and the zone of polarizing activity (ZPA) at the posterior margin of the mesenchyme (reviewed by (Tickle, 2006)). Experimental and genetic studies established that several fibroblast growth factors (FGF4, 8, 9 and 17) secreted by the AER (AER-FGFs) control outgrowth and are involved in the specification of distal identities (see e.g. (Mariani et al., 2008)). Loss or reduction of AER-FGFs in mouse limb buds leads to truncations or to complete loss of the limb skeleton due to their dual role in promoting cell survival and distal limb identities (Mariani et al., 2008; Sun et al., 2002). In contrast, retinoic acid (RA) produced by the flank mesenchyme is thought to specify proximal identities (Mercader et al., 2000; Tamura et al., 1997). RA, the active form of vitamin A is essential for embryonic development as vitamin A deficiency in mothers during gestation leads to severe fetal malformations while an excess of RA is teratogenic (Wilson et al., 1953). RA interacts with the nuclear retinoic acid receptors (RARs), which form heterodimers with retinoic X receptors (RXRs) to elicit a transcriptional response by binding to RA response elements (RARE) (reviewed by (Niederreither and Dolle, 2008)). Understanding the function of endogenous RA during embryogenesis has proved elusive for years and the breakthrough came in particular from the inactivation in mice of enzymes catalyzing RA synthesis and degradation (reviewed in (Niederreither and Dolle, 2008)). Of these, the retinaldehyde dehydrogenase 2 enzyme (RALDH2), which catalyzes a critical step in the biosynthesis of RA, seems the most important, as

Raldh2-deficient mouse embryos die at E9.5 from severe cardiac defects and suffer multiple developmental abnormalities including hindbrain and somite patterning defects (Niederreither et al., 1999). The Cyp26 family of enzymes belonging to the cytochrome P450 proteins catalyzes RA inactivation; *Cyp26a1*- and -*b1*-deficient mice display developmental defects reminiscent of the teratogenic effects of RA, suggesting that endogenous RA levels in the embryo are critical for embryogenesis (Abu-Abed et al., 2001; Yashiro et al., 2004). During limb development, RA is produced in the flank mesoderm by RALDH2 and diffuses into the proximal limb bud mesenchyme. *Raldh2* mutant embryos lack limb buds due to developmental arrest hindering the understanding of its function during limb bud development. However the molecular defects observed in forelimb buds of embryos rescued by maternal RA dietary supplementation suggest that RA is required for AP pattering (Niederreither et al., 2002). *Cyp26b1* is expressed in the distal limb bud mesenchyme and non-AER ectoderm (MacLean et al., 2001) and targeted loss of *Cyp26b1* function in mice leads to strong malformations of the limb skeleton. These defects can be phenocopied by exposure to excess RA during embryonic development, suggesting that in *Cyp26b1*-deficient embryos, an excess of RA levels in limb buds causes the primary defect (Yashiro et al., 2004). Taken together, these genetic data suggest that the levels of RA in limb buds are determined by a balance between its synthesis by RALDH2 in the flank and its degradation by CYP26b1 in the distal limb bud. This balance is critical for limb bud outgrowth and patterning. The *Meis* genes are likely mediators of RA signalling in the proximal limb bud mesenchyme and they are initially expressed throughout the limb bud while during subsequent limb bud outgrowth their expression becomes restricted to the proximal mesenchyme (Capdevila et al., 1999; Mercader et al., 1999). In chicken limb buds, ectopic distal expression of *Meis* causes distal to proximal transformations of skeletal elements while increase of RA signalling or reduction of FGF signalling results in distal expansion of the *Meis* expression domain (Capdevila et al., 1999; Mercader et al., 1999; Mercader et al., 2000). Genetic evidence in mice supports these interactions as the distal *Meis1*-negative domain is reduced in limb buds of embryos deficient for *Cyp26b1* or for AER-*Fgfs* (Mariani et al., 2008; Yashiro et al., 2004). Taken together, these results have led to a two-signal model whereby opposing RA and FGF signalling gradients from the proximal mesenchyme and AER respectively control patterning of limb skeletal elements along the PD axis (reviewed by (Benazet and Zeller, 2009)). However, few of the genes controlling formation and/or marking specific compartments of the PD limb bud axis are known.

SHH signalling by the ZPA has on the other hand been proposed to mainly control AP patterning of the limb bud. Both gain- and loss-of-function studies in chick and mouse embryonic limb buds have demonstrated the essential requirement of the SHH pathway during patterning of the AP limb bud axis and in controlling digit numbers and identities (reviewed by (Benazet and Zeller, 2009)). In particular, *Shh* deficiency in mouse embryos causes loss of the digit arch in the autopod and agenesis of the posterior zeugopodal bone (Chiang et al., 2001; Kraus et al., 2001). During limb bud outgrowth, *Shh* expression by the ZPA is propagated by a positive SHH/GREM1/FGF feedback loop operating between the mesenchyme and the AER (reviewed by (Benazet and Zeller, 2009)). This feedback loop enables SHH-dependent growth and patterning of distal limb skeletal elements as a consequence of GREM1-mediated reduction of BMP4 activity and increased AER-FGF signalling (Benazet et al., 2009). Recent genetic analysis of the temporal requirement of SHH signalling in mouse embryos revealed its dual functions, the early specification of AP limb bud axis polarity and the subsequent proliferative expansion of the specified progenitors (Zhu et al., 2008).

The effects of SHH signal transduction on target genes are mediated by the GLI transcriptional regulators (GLI1 to GLI3), which are all expressed in the limb bud mesenchyme. However, genetic analysis reveals that only GLI3 is on its own essential for autopod development as *Gli3*-deficient mouse embryos display polydactylies with associated loss of AP identity (Mo et al., 1997). Normally, constitutive processing of the full-length GLI3 protein into a GLI3 transcriptional repressor isoform (GLI3R) is inhibited in the posterior limb bud mesenchyme by SHH signalling. This was proposed to result in an unequal distribution of the GLI3R and full-length GLI3 (activator, GLI3A) isoforms in the limb bud mesenchyme (Wang et al., 2000). That study and others indicated that one major function of SHH signalling during specification of AP digit identities involves the formation of an anterior/high to posterior/low GLI3R activity gradient as a consequence of inhibiting the processing of GLI3A into Gli3R (reviewed by (Zuniga and Galli, 2005).

While a large number of studies have resulted in the identification of the essential functions of the major players and pathways in limb development, many of the underlying gene networks and inter-pathway interactions remain rather ill defined and understood (reviewed by (Zeller et al., 2009)). In this study we have investigated the alterations of the transcriptome of *Shh*-deficient limb buds at E10.5. We show that the expression of proximal genes and RA pathway activity is up-regulated and distally expanded *Shh*-deficient limb buds. In parallel, the expression of the RA inactivation enzyme *Cyp26b1* is decreased in the distal mesen-

chyme. We have investigated the possible SHH-RA interactions using a combination of experimental manipulation, genetics and mathematical simulations. Our findings reveal a SHH-dependent signalling module that normally enhances RA clearance by increasing AER-FGF signalling, which in turn up-regulates *Cyp26b1* expression. Disruption or reduction of CYP26b1-mediated RA clearance interferes with distal limb bud development leading to molecular proximalization of *Shh*-, AER-*Fgf*- and *Cyp26b1*-deficient limb buds. In addition we provide molecular evidence for early specification of the PD axis by a mutually inhibitory interaction of RA and AER-FGFs. Subsequently AP and PD limb bud patterning becomes interlinked via SHH mediated regulation of the AER-FGF/CYP26b1/RA signalling module, which enables spatially coordinated progression of limb bud development.

Results

Transcriptome analysis of *Shh*-deficient mouse limb buds

Recent studies have revealed the dual function of SHH in specification and expansion of the autopod primordial (Zhu et al., 2008). To gain a comprehensive overview of how SHH signalling regulates gene expression, we have profiled the transcriptome in *Shh*-deficient mouse forelimb buds using GeneChip Mouse Gene 1.0 ST Arrays. These GeneChips cover the whole genome and contain over 28,000 well-annotated genes. Forelimb buds of embryos at E10.5 (35-36 somites) were chosen as the identities of individual digits are specified around this period in mouse embryos (Zhu et al., 2008). In addition, the distal progression of limb bud development and proliferative expansion of the autopod primordia is ongoing under the influence of the SHH/GREM1/FGF signalling feedback loop (Benazet and Zeller, 2009; Panman et al., 2006). Statistical evaluation of the data sets revealed that the expression of ~800 transcripts was altered ≥1.2-fold in *Shh*-deficient in comparison to wild-type limb buds (p <0.03). The cut-off was set at 1.2-fold as tests revealed that such differences are reliably detected by whole mount in situ hybridisation and real-time (RT) PCR. For example, changes in *Hoxc6* and *Pbx1* transcripts [**Table 5**], which are up-regulated about 1.25 fold in *Shh*Δ/Δ limb buds are readily detected by in situ hybridisation and RT-PCR [**Figures 18 + 19**]. The selected pool of over 800 significantly altered genes contained all major SHH signalling pathway components whose transcription depends on SHH signalling ([**table 4**]: *Ptch1*, *Ptch2*, *Hip*, *Gli1*) and many established positive transcriptional targets of SHH ([**table 4**]: *5'Hoxd* genes, *Grem1*, *Hand2*, *Prdm1* and *Fgf4*, *-8*, *-9*) (Chiang et al., 2001; te Welscher et al., 2002b; Vokes et al., 2008; Zuniga et al., 1999) revealing the biological significance of the data sets. In total ~400 genes were down-regulated ≥1.2-fold in *Shh*-deficient limb buds consistent with a role of SHH as a positive transcriptional regulator. Rather unexpected from the limb skeletal phenotype, the expression of over 400 genes is up-regulated ≥1.2-fold in *Shh*-deficient limb buds. This result reveals that SHH signal transduction inhibits the transcription of a large number of genes in limb buds.
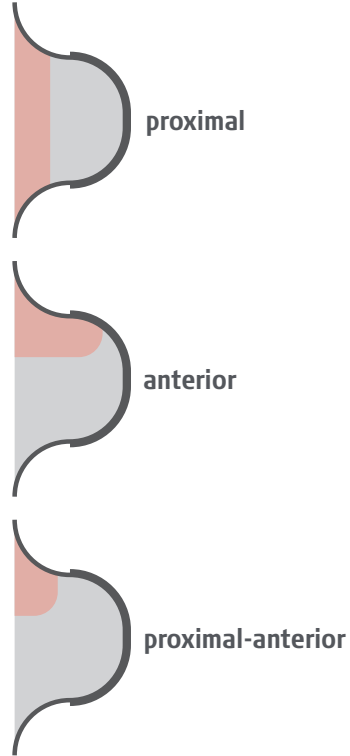
Genes downregulated in *Shh*$^{\Delta/\Delta}$ limb buds

Gene	Fold Change	P-Value	Distribution
Hoxa13	4.9	≤ 4.8×10^{-5}	distal
Sall1	2.9	≤ 6.2×10^{-5}	distal
Sall3	1.9	≤ 1.2×10^{-2}	distal
Cyp26b1	1.7	≤ 1.4×10^{-3}	distal
Sall4	1.7	≤ 1.4×10^{-2}	distal
Spry4	1.6	≤ 2.0×10^{-2}	distal
Hey1	1.6	≤ 1.7×10^{-3}	distal
Jag1	1.5	≤ 9.8×10^{-3}	distal
Sost	1.5	≤ 3.0×10^{-3}	distal
Wnt5a	1.3	≤ 2.8×10^{-3}	distal
Hes1	1.3	≤ 1.4×10^{-2}	distal
Slit3	1.3	≤ 2.4×10^{-2}	distal
Hoxd13	20	≤ 6.7×10^{-7}	post-distal
Hoxd12	17	≤ 4.3×10^{-5}	post-distal
Grem1	3.7	≤ 3.0×10^{-5}	post-distal
Rspo3	2.1	≤ 3.7×10^{-5}	post-distal
Cyp1b1	1.8	≤ 7.0×10^{-4}	post-distal
Evx1	1.3	≤ 5.9×10^{-3}	post-distal
Fmn1	1.2	≤ 7.7×10^{-3}	post-distal
Ptch2	5.7	≤ 5.9×10^{-5}	posterior
Ptch1	4.4	≤ 6.8×10^{-6}	posterior
Gli1	3.8	≤ 1.2×10^{-5}	posterior
Hhip	2.7	≤ 3.5×10^{-4}	posterior
Hand2	2.6	≤ 1.6×10^{-4}	posterior
Prdm1/Blimp1	2.3	≤ 4.7×10^{-3}	posterior
Bmp2	1.3	≤ 1.8×10^{-2}	posterior
Cdc25b	1.3	≤ 2.8×10^{-2}	posterior
Osr1	2.6	≤ 3.2×10^{-3}	prox-post
Fgf4	2.7	≤ 4.9×10^{-4}	distal (AER)
Fgf8	2	≤ 8.7×10^{-3}	distal (AER)
Fgf9	1.5	≤ 1.0×10^{-2}	distal (AER)

posterior

posterior-distal
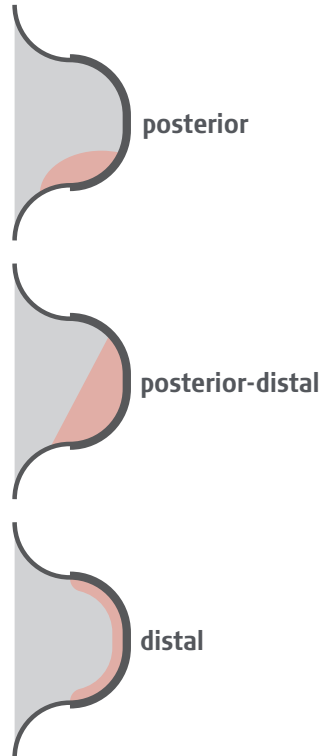
distal

[**Table 4**] Classification and spatial distribution of genes down-regulated in *Shh*-deficient limb buds. The limb schemes define what is considered posterior, posterior-distal and distal respectively in this classification. Underlined genes are components of the SHH pathway. ant: anterior. dist: distal. post: posterior

Gene	Fold Change	P-Value	Distribution
Gria	2.1	$\leq 1.0 \times 10^{-2}$	prox-ant
Hoxc5	1.9	$\leq 9.5 \times 10^{-3}$	prox-ant
Igf1	1.8	$\leq 7.0 \times 10^{-3}$	prox-ant
Alx4	1.8	$\leq 1.5 \times 10^{-6}$	prox-ant
Pax1	1.7	$\leq 2.5 \times 10^{-2}$	prox-ant
Irx3	1.6	$\leq 5.2 \times 10^{-5}$	prox-ant
Irx5	1.6	$\leq 1.1 \times 10^{-4}$	prox-ant
Alx3	1.5	$\leq 2.1 \times 10^{-3}$	prox-ant
Efna3	1.5	$\leq 1.2 \times 10^{-3}$	prox-ant
Zfhx3	1.4	$\leq 7.2 \times 10^{-3}$	prox-ant
Efna5	1.4	$\leq 4.2 \times 10^{-4}$	prox-ant
Gas1	1.3	$\leq 3.0 \times 10^{-4}$	prox-ant
Epb4.1l3	1.3	$\leq 1.3 \times 10^{-2}$	prox-ant
Glis3	1.3	$\leq 5.3 \times 10^{-3}$	prox-ant
Cdon	1.3	$\leq 4.9 \times 10^{-3}$	prox-ant
Boc	1.3	$\leq 1.2 \times 10^{-3}$	prox-ant
Pbx1	1.3	$\leq 2.4 \times 10^{-2}$	prox-ant
Hoxc6	1.3	$\leq 1.9 \times 10^{-2}$	prox-ant
Pbx3	1.2	$\leq 3.7 \times 10^{-3}$	prox-ant
Efnb2	1.2	$\leq 3.5 \times 10^{-2}$	prox-ant
Epha3	1.7	$\leq 1.6 \times 10^{-2}$	prox-ant and prox-post
Slit2	1.4	$\leq 2.2 \times 10^{-2}$	prox-ant and prox-post
Angptl1	2.1	$\leq 1.7 \times 10^{-3}$	prox
Pitx2	1.8	$\leq 1.2 \times 10^{-2}$	prox
Wif1	1.5	$\leq 7.6 \times 10^{-3}$	prox
Angptl4	1.5	$\leq 3.9 \times 10^{-4}$	prox
Glis1	1.5	$\leq 4.9 \times 10^{-3}$	prox
Zfhx4	1.4	$\leq 1.6 \times 10^{-3}$	prox
Hand1	1.4	$\leq 1.9 \times 10^{-3}$	prox
Rarb	1.3	$\leq 3.9 \times 10^{-4}$	prox
Met	1.3	$\leq 2.8 \times 10^{-2}$	prox
Mab21l1	1.2	$\leq 1.8 \times 10^{-3}$	prox
Meis1	1.2	$\leq 3.5 \times 10^{-3}$	prox
Pkdcc	1.2	$\leq 5.6 \times 10^{-3}$	prox
Epha7	1.2	$\leq 8.2 \times 10^{-3}$	prox
Meis2	1.2	$\leq 2.3 \times 10^{-4}$	prox
Hoxb9	1.5	$\leq 2.8 \times 10^{-2}$	ant
Col1a2	1.4	$\leq 2.1 \times 10^{-3}$	ant
Disp1	1.3	$\leq 1.6 \times 10^{-3}$	ant
Sox6	1.3	$\leq 6.0 \times 10^{-3}$	ant
Msx2	1.8	$\leq 9.0 \times 10^{-4}$	high ant and low post
Igfbp5	1.5	$\leq 9.6 \times 10^{-4}$	dist (AER)
Dlx5	1.4	$\leq 1.1 \times 10^{-2}$	dist (AER)
Dlx3	1.2	$\leq 2.4 \times 10^{-5}$	dist (AER)

Genes upregulated in _Shh_$^{\Delta/\Delta}$ limb buds

proximal

anterior

proximal-anterior

[**Table 5**] Classification and spatial distribution of genes up-regulated in _Shh_ mutant limb buds. The limb schemes define what is considered proximal, anterior and proximal-anterior respectively in this classification. Underlined genes are components of the SHH pathway. ant: anterior. Dist: distal. post: post. proximo: proximal.

Proliferation networks are affected in *Shh*-deficient limb buds–
Recent analysis has revealed a major role of SHH in the proliferative
expansion of the specified limb bud mesenchymal progenitors (Towers et
al., 2008; Zhu et al., 2008). These studies also indicated that SHH exerts
its effects on the G1 to S phase transition of the cell-cycle as is known
from other systems (reviewed by (Roy and Ingham, 2002)). However, a
genome-wide analysis of the gene networks controlling cell-cycle and
proliferation was lacking. Therefore, we analyzed the microarray data
using the Ingenuity pathway analysis program suite to gain insight
into the global transcriptional changes affecting the cell-cycle [**Figure 16**].
This analysis reveals that the transcription of cell-cycle genes is strongly
affected in *Shh* limb buds. The positive cell-cycle control genes *CyclinD*
and *CyclinE* and the interacting *Cdk6* are transcribed at lower levels in
*Shh*Δ/Δ than wild-type limb buds [**Figure 16, indicated in green**]. In contrast, the
expression of *Tgf-β* (Massague and Gomis, 2006) and the transcriptional
regulators *Zfhx3* and *Zfhx4* (Jung et al., 2005), which contribute to cell-cycle
arrest are up-regulated specifically in *Shh*-deficient limb buds [**Figure 16,
indicated in red**]. The expression of the tumour suppressor gene *Rb* (see e.g.
(Roy and Ingham, 2002)) is not significantly altered [**Figure 16, indicated in
white**]. In summary, the transcriptional alterations affect a large number,
but not all cell-cycle genes and are consistent with disruption of the G1
to S phase transition and cell-cycle arrest in *Shh*-deficient mouse limb
buds [**Figure 16**] (see also (Zhu et al., 2008)).

Interestingly, several members of the inhibitors of differentiation
(*Id*) gene family (reviewed by (Lasorella et al., 2001)) are up-regulated in
Shh-deficient mouse limb buds at E10.5 [**Figure 16**]. These alterations might
reflect the effects of SHH signalling on initiation of cell differentiation.

In addition to altered expression levels, the potential changes in
the spatial distributions of select transcripts were assessed in *Shh*- and
in *Gli3*-deficient limb buds [**Figure 17**]. GLI3 is one of the major intracel-
lular transducers of SHH and is processed to a repressor form in the
absence of SHH signalling. This analysis reveals a general reduction in
CyclinD1 (*Ccnd1*) and *N-myc* expression in *Shh*-deficient limb buds, while
their expression is increased particularly in the anterior mesenchyme
of *Gli3*-deficient limb buds [**Figure 17A, black arrows**]. Furthermore *Zfhx3* and
Zfhx4, which inhibit cell proliferation (Jung et al., 2005), are expressed
in the anterior-proximal mesenchyme of wild-type limb buds [**Figure
17B**]. In *Shh*-deficient limb buds, their expression is up-regulated and
expands into posterior-distal regions, while their expression is reduced in
Gli3-deficient limb buds ([**Figure 17B, arrowheads**]. Finally, the differentiation
inhibiting *Id1* and *Id2* genes are expressed predominantly in the distal,
sub-AER mesenchyme of wild-type limb buds and their expression is

up-regulated **down-regulated**
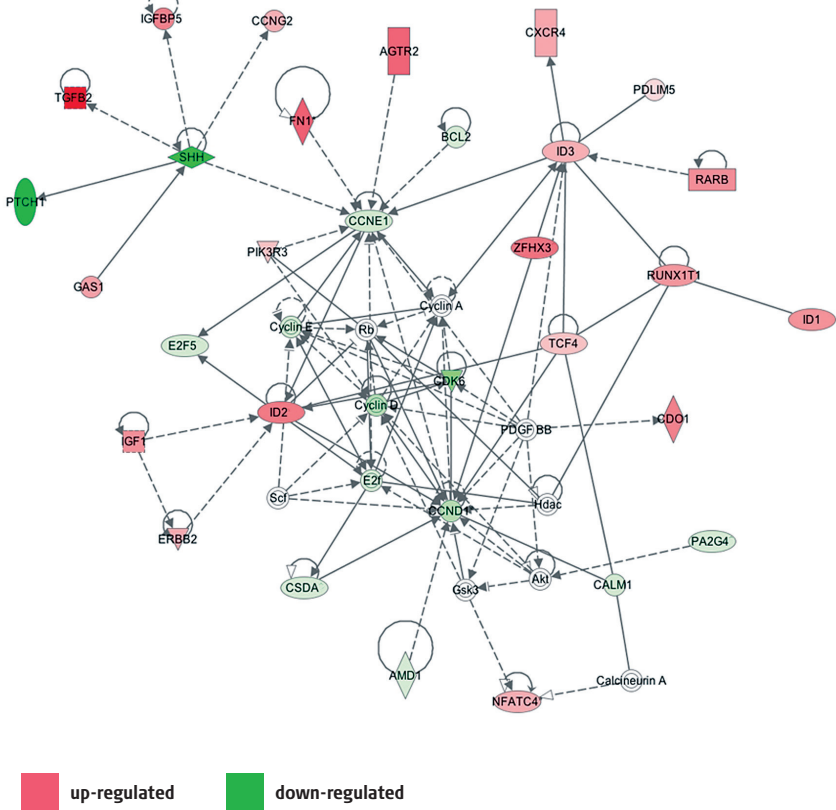
[**Figure 16**] The transcriptional alterations of cell-cycle genes in *Shh*-deficient limb buds. IPA analysis of the gene networks involved in cell-cycle and proliferation regulation. Genes whose transcription is up-regulated in *Shh* mutant limb buds are displayed in shades of red, genes whose expression is down-regulated are indicated in green. The intensity of the colouring is proportional to the fold change, weakest hues representing the minimal fold change while the strongest hues correspond to the highest fold change. Fold changes range from 1.2 to 64. Solid lines show direct interactions, while dotted lines represent indirect interactions. A complete legend to this IPA diagram is shown below (figure provided by A. Zuniga).
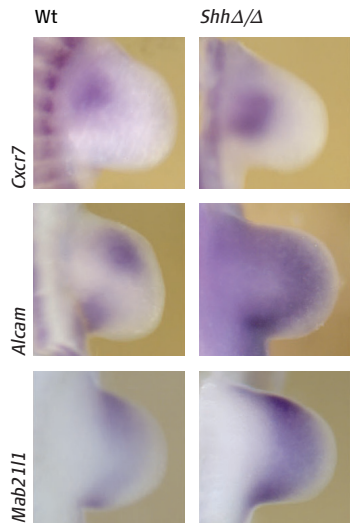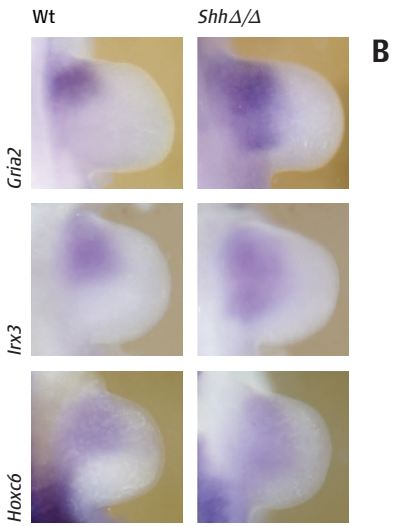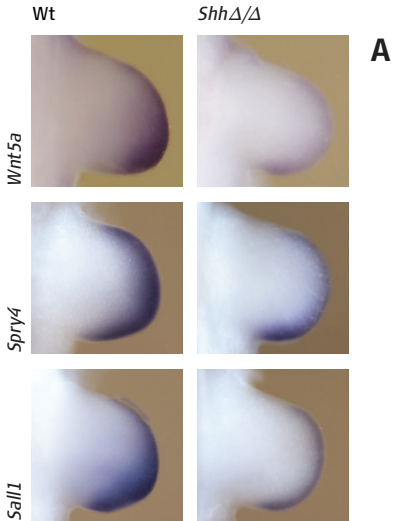
up-regulated and expanded in *Shh* mutants. In *Gli3*-deficient limb buds, their expression is specifically reduced in the anterior mesenchyme [**Figure 17C and data not shown**]. Taken together, these results reveal that SHH signalling stimulates the cell-cycle transcriptome, in particular genes involved in the G1 to S phase transition.

	Wt	Shh△/△	Gli3 Xt/Xt	
Ccnd1				A
N-myc				
Zfhx3				B
Zfhx4				
Id1				C
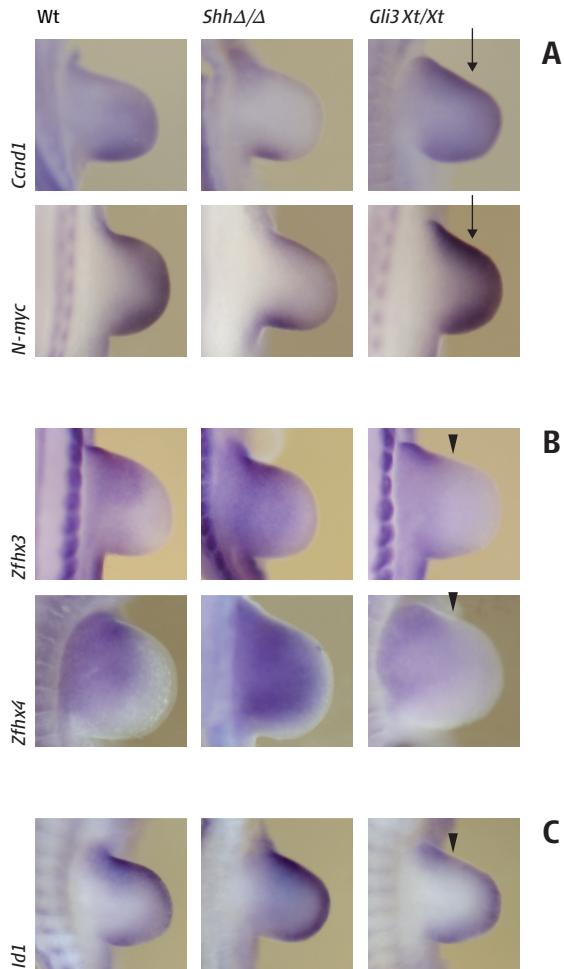
[**Figure 17**] The expression of select key regulators of the cell-cycle and differentiation is altered in a largely opposing manner in *Shh△/△* and *Gli3Xt/Xt* limb buds at E10.5. (**A**) Expression of the cell-cycle regulators *Ccnd1* and *N-myc* is down-regulated in *Shh△/△* and up-regulated in the anterior mesenchyme of *Gli3Xt/Xt* limb buds. (**B**) Expression of the proliferation inhibitory genes *Zfhx3* and *Zfhx4* is posterior-distally expanded in *Shh△/△* and down-regulated in the anterior part of *Gli3Xt/Xt* limb buds. (**C**) The differentiation inhibitory *Id1* gene is up-regulated in *Shh△/△* and down-regulated in *Gli3Xt/Xt* limb buds. Wt: wild-type; arrowheads: reduced expression; black arrows: increased expression. All limb buds are oriented with anterior to the top.

Alteration of genes marking the PD limb bud axis – While SHH is known to up-regulate transcription of posteriorly expressed genes such as *5'Hoxd* genes and *Grem1* and to promote their distal-anterior expansion (Chiang et al., 2001; Zuniga et al., 1999), little is known about the genes whose transcription is inhibited by SHH signalling. Given the high number of genes up-regulated in *Shh*-deficient limb buds, understanding if they have a common denominator might provide insight into the role of SHH signal transduction in transcriptional repression. Intriguingly *Meis2*, a known marker for proximal identity and *Pbx1*, a gene whose disruption in mice leads to proximal limb skeletal malformations are both up-regulated ~1.2 fold [**Table 5**](Selleri et al., 2001; Tabin and Wolpert, 2007). This is surprising as SHH was not known to regulate proximal genes. Therefore, systematic annotation was combined with an in situ hybridisation screen to categorize the transcripts altered in *Shh*-deficient limb buds. The majority of spatially restricted genes down-regulated in *Shh*-deficient limb buds are posterior, distal or AER expressed genes. These genes include in particular *5'Hoxd* genes, FGF pathway genes (*Fgf4, 8, 9* and *Spry4*) and Notch pathway genes (*Jag1*, *Hey1*, *Hes1*) [**Table 4**]. Intriguingly, 36 of the up-regulated genes were proximally restricted, about half of which were also anteriorly restricted [**Table 5**]. Taken together, these results indicate that SHH signal transduction negatively regulates the expression of proximal and/or anterior genes, while it propagates the expression of posterior and/or distal genes during limb bud development.

The spatial alterations of select genes are shown in Figure 18. Genes, whose expression is down-regulated often retain their spatial distribution, but levels are reduced as shown for *Wnt5a* (Yamaguchi et al., 1999), *Spry4*, a transcriptional target of AER-FGFs (Minowada et al., 1999) and *Sall1*, a transcription factor required for limb bud development (Kawakami et al., 2009) [**Figure 18A**]. In contrast, the expression of *Gria2*, a member of the glutamate receptor family (Jia et al., 1996) expands posteriorly in *Shh*-deficient limb buds [**Figure 18B, panel Gria2**]. Similarly, the anterior domains of the transcription factors *Irx3* and *Hoxc6* expand posteriorly in *Shh*-deficient limb buds [**Figure 18B**] (Houweling et al., 2001; Jegalian et al., 1992). The chemokine receptor *Cxcr7* (Maksym et al., 2009) is expressed in the proximal mesenchyme and its domain is enlarged in *Shh*-deficient limb buds. *Alcam*, a member of the immunoglobulin super-family (Bowen et al., 1995) is expressed in a distinct anterior and posterior domain in wild-type limb buds, while its expression is rather diffuse and distally expanded in *Shh*-deficient limb buds [**Figure 18B**]. Furthermore, *Mab21L1* (Wong et al., 1999) is expressed in a graded fashion in the proximal/medial limb bud mesenchyme of wild-type limb buds and its expression is distally expanded in *Shh*-deficient limb buds [**Figure 18C**]. Notably, its

Wt   Shh∆/∆

Wnt5a

Spry4

Sall1

A

Wt   Shh∆/∆

Gria2

Irx3

Hoxc6

B

Wt   Shh∆/∆

Cxcr7

Alcam

Mab21l1

[**Figure 18**] Analysis of distal and proximal genes in *Shh*-deficient limb buds at E10.5 (34-36 somites). (**A**) Expression of distal genes is generally reduced in *Shh*-deficient limb buds. (**B**) Changes in the spatial distribution of proximal genes up-regulated in *Shh*-deficient limb buds. Proximal genes expand distally and/or posteriorly. Wt: wild-type.

expression domain is similar to *Hoxa11*, which indicates that *Mab21L1* might mark the zeugopod domain like *Hoxa11* (Zakany and Duboule, 2007). Taken together, this expression analysis reveals that anterior and proximal expression domains expand in general towards posterior and distal in *Shh*-deficient limb buds.

RA pathway activity is increased in *Shh*-deficient limb buds – In an attempt to gain insight into the cause underlying the apparent proximalisation of *Shh*Δ/Δ limb buds, we analyzed the status of potential regulators of PD patterning. Two morphogenetic signals are important for patterning the PD axis: FGFs, which signal from the AER to promote distal limb structures and RA, which signals from the flank mesenchyme and is thought to promote formation of proximal skeletal elements (Mariani et al., 2008; Mercader et al., 2000). Expression of AER-*Fgfs* and their downstream mesenchymal target *Spry4* is reduced in *Shh* mutant limb buds (Chiang et al., 2001; Zuniga et al., 1999) [**Table 4 and Figure 18A**] in agreement with loss of distal structures. To evaluate the status of RA pathway in *Shh*Δ/Δ limb buds we determined the spatial distribution of RA pathway components and possible targets of RA signalling by in situ hybridisation and expression levels by RT-qPCR [**Figure 19**].

The RA receptor *Rarb* is expressed in the proximal limb bud mesenchyme. Since the *Rarb* promoter contains a RARE, it is a direct positive transcriptional target of RA signalling and most importantly an established sensor for RA activity (de The et al., 1990; Rossant et al., 1991; Sucov et al., 1990). In *Shh*Δ/Δ limb buds *Rarb* expression is distally expanded [**Figure 19 left panel**] and transcript levels are increased about 1.5 fold [**Figure 19 right panel and Table 5**]. This indicates that RA activity is significantly increased in *Shh*Δ/Δ limb buds. To evaluate whether this results in a downstream response to RA signalling, we determined the spatial distribution and expression levels of the proximal gene *Meis2*, an established downstream target of RA signalling (Mercader et al., 2000)[**Table 5**]. Indeed, its distribution is expanded along the AP and PD axis and its expression levels are increased [**Figure 19**]. Expression of the two newly identified RA-response genes *Pbx1* and *Pkdcc* (see below) is also expanded distally and their expression levels are up-regulated around 1.5 fold [**Figure 19**]. Thus, elevated RA activity correlates with increased expression of established and novel RA targets in limb buds. These data show that the signals controlling PD limb bud axis development are altered such that AER-FGF signalling (distal) is reduced while RA activity (proximal) is increased in *Shh*-deficient limb buds.

In the distal mesenchyme of wild-type limb buds, RA is hydroxylated to its inactive form by CYP26b1, which is an intra-cellular enzyme
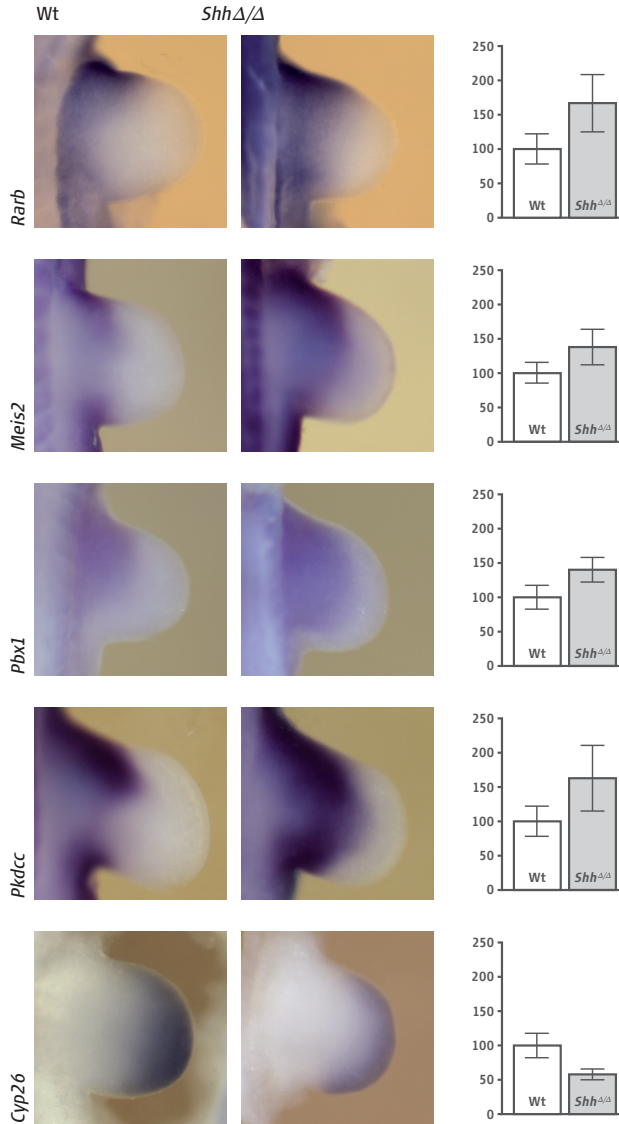
[**Figure 19**] RA target genes are up-regulated and distally expanded in *Shh*-deficient limb buds at E10.5 (34-36 somites). *Rarb, Meis2, Pbx1, Pkdcc* and *Cyp26b1* (*Cyp26*) expression in wild-type (Wt) and *Shh*$^{\Delta/\Delta}$ forelimb buds. The dotted red lines demarcate the distal limits of the expression domains. *Rarb, Meis2, Pbx1, Pkdcc* expression is increased and distally expanded in *Shh*$^{\Delta/\Delta}$ limb buds. Expression of *Cyp26b1* (*Cyp26*) is reduced in *Shh*-deficient limb buds. Real-time PCR was used to determine the relative gene expression levels in limb bud extracts (n=7 limb bud pairs at E10.5 35 to 36 somites). Means ± standard deviations are shown. All differences between Wt and *Shh*$^{\Delta/\Delta}$ limb buds are highly significant (p <0.001, except p <0.01 for *Meis2*).

(White et al., 2000). In mouse limb buds lacking *Cyp26b1*, the expression of proximal genes is increased and distally expanded and all skeletal elements are hypoplastic due to apoptosis of chondrogenic precursors (Yashiro et al., 2004). Intriguingly *Cyp26b1* (*Cyp26*) expression shows a reduction of about 1.6 fold in *Shh*-deficient limb buds [**Figure 19**], which likely decreases the inactivation of RA. This provides a straightforward explanation for the observed elevation in RA activity in *Shh*-deficient limb buds.

Expression of the proximal genes *Pbx1* and *Pkdcc* is positively regulated by RA signalling and increased expression of proximal genes in *ShhΔ/Δ* limb buds depends on RA activity – *Pbx1* encodes a transcription factor of the same TALE homeodomain protein family as *Meis* genes and *Pbx1*-deficient mice exhibit proximal limb scapular and humeral defects (Selleri et al., 2001). Embryos treated with maternal RA dietary supplementation show elevated *Pbx1* transcripts levels in limb buds by RT-PCR (Qin et al., 2002). *Pkdcc* encodes a putative kinase and its expression domain in the limb bud is highly similar to *Meis2* expression [**Figure 19**, **Wt**, ***Meis2* compared to *Pkdcc***]. The limbs of *Pkdcc*-deficient mice display shortened stylopod and zeugopod bones (chapter 7, and (Imuta et al., 2009; Kinoshita et al., 2009). To test whether these proximal genes [**Figure 19**] are RA responsive in wild-type mouse limb buds, we examined the effects of implanting beads loaded with RA into the distal mesenchyme [**Figure 20**]. Indeed, the expression of *Pbx1* and *Pkdcc* expands distally in response to ectopic RA activity, similar to *Meis2*, which has been previously shown to expand distally upon implantation of a RA-bead (Mercader et al., 2000).

We investigated whether the increased expression of these proximal RA-responsive genes in *Shh*-deficient limb buds could be inhibited by implanting beads loaded with an RA antagonist [**Figure 21**, **RAA**] (Mercader et al., 2000). The expression of the RA sensor *Rarb* and the RA targets *Pbx1* and *Pkdcc* was reduced around the RAA bead in wild-type and in *Shh*-deficient limb buds [**compare to contra-lateral control**, **Figure 21A and B**]. Interestingly the RAA effect was more pronounced in *Shh*-deficient limb buds than in wild-types. In *Cyp26b1*-deficient limb buds, RA activity is increased due to the absence of RA hydroxylation. As a consequence, *Meis2* and *Rarb* expression are distally expanded in limb buds [**Figure 21C**] (Yashiro et al., 2004). Similarly, the expression of both *Pbx1* and *Pkdcc* is distally expanded, which reveals that *Pbx1* and *Pkdcc* respond to alterations in RA activity in vivo in mouse limb buds [**Figure 21C**]. These results support the hypothesis that elevated RA activity is the main cause of the transcriptional up-regulation of these proximal genes in *Shh*-deficient limb buds.

RA bead

Meis2

Pbx1

Pkdcc
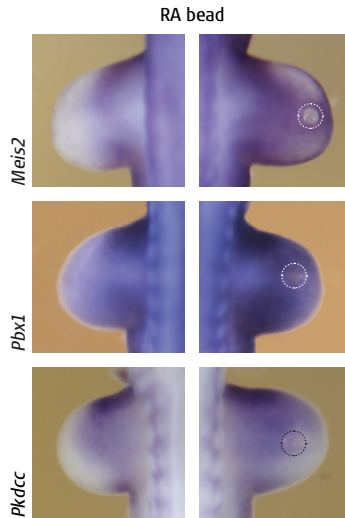
[**Figure 20**] Proximal genes respond to RA signalling in limb buds. Left panels: contra-lateral control limb buds (ungrafted). Right panels: Wild-type forelimb buds received distal grafts of RA beads (1mg/ ml) at E10.25 to E10.5 (32-35 somites) and were cultured for 6 hours. The dotted circles indicate the positions of the implanted beads. The expression of proximal genes, *Pbx1* (n=6/6) and *Pkdcc* (n=10/12) expands and is up-regulated similarly to *Meis2* (n=6/6).

Genetic evidence that AER-FGFs inhibit distal expression of proximal RA responsive genes and up-regulate *Cyp26b1* expression – *Cyp26b1* is expressed in the distal limb bud and in the two signal model for PD axis specification, RA and FGF have opposing effects, suggesting the possibility that *Cyp26b1* could be regulated by FGF signalling from the AER. Furthermore, it was recently shown in the context of interdigital cell death that *Cyp26b1* is positively regulated by FGFs (Hernandez-Martinez et al., 2009). Therefore we investigated whether AER-FGF signalling is able to regulate *Cyp26b1* expression [**Figure 22**]. Culturing wild-type limb buds in the presence of an inhibitor of FGF signal transduction (Zuniga et al., 2004) causes almost complete loss of *Cyp26b1* expression[**Figure 22, top row**]. However, as *Shh* expression is also down-regulated in wild-type limb buds treated with this inhibitor (Zuniga et al., 2004), the decrease in *Cyp26b1* expression could be caused by loss of FGF and/or SHH signalling. Therefore, we determined whether AER-FGFs could up-regulate *Cyp26b1* expression in a SHH-independent manner by implanting beads soaked in FGF4 into *Shh*-deficient limb buds. This restores the *Cyp26b1* expression domain to a considerable extent [**Figure 22, middle row**], which
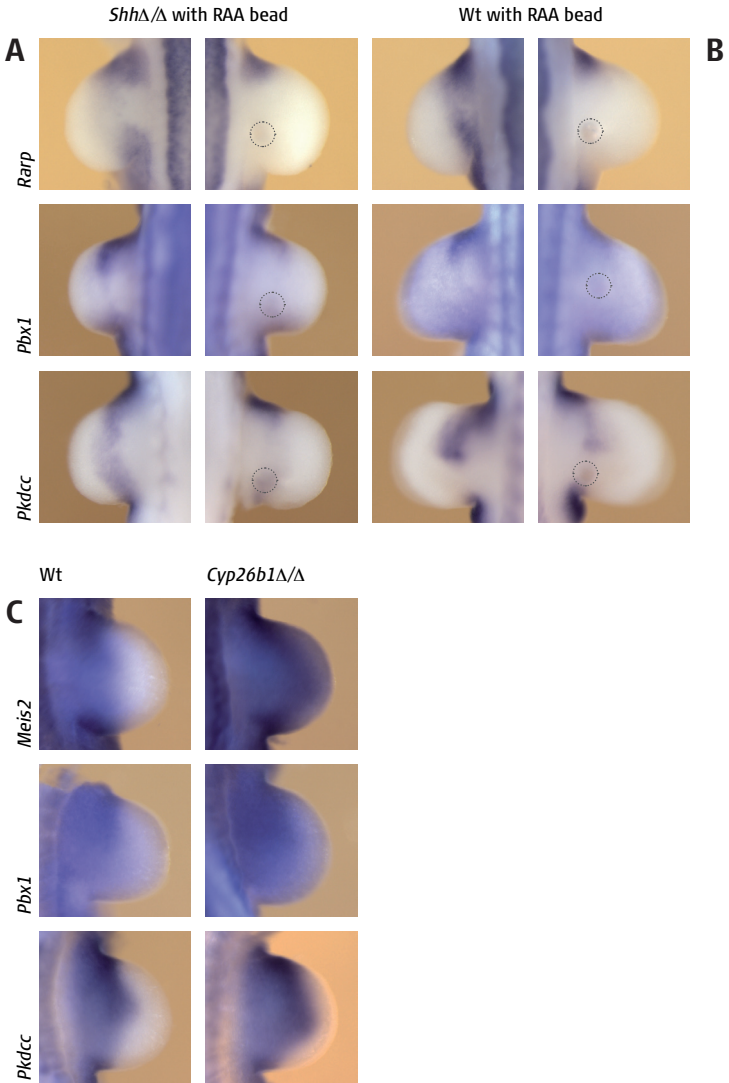
[**Figure 21**] Inhibition of RA signalling reduces the expression of proximal genes in both wild-type and *Shh*-deficient limb buds. (A + B) *Shh*-deficient and Wt forelimb buds (E10.5; 34-36 somites) 16-20 hrs after implantation of a carrier bead loaded with 2 mg/ml RA antagonist (RAA; dotted circle) (right panels). The left panels show the non-grafted contra-lateral forelimb bud as a control. (**A**) The expression of the proximal genes *Rarb* (n= 7/8), *Pbx1* (n= 5/6) and *Pkdcc* (n= 5/6) is reduced by implantation of RAA beads into *ShhΔ/Δ* limb buds. (**B**) The expression of the proximal genes *Rarb* (n= 14/14), *Pbx1* (n= 6/6) and *Pkdcc* (n= 4/6) is reduced by implantation of RAA beads into Wt limb buds. (**C**) Expression of RA responsive genes is up-regulated in limb buds lacking *Cyp26b1*. *Meis2*, *Pbx1* and *Pkdcc* expression in wild-type (left panels) and *Cyp26b1*-deficient forelimb buds (right panels). The expression of *Meis2*, *Pbx1* and *Pkdcc* is distally expanded in *Cyp26b1*-deficient forelimb buds at E10.5 (34-35 somites).

establishes that AER-FGFs can up-regulate *Cyp26b1* expression in the absence of SHH signalling. Interestingly, implantation of FGF4 beads into wild-type limb buds resulted in an only modest increase in *Cyp26b1* expression [**Figure 22,bottom row**], which suggests that it is transcribed at close to maximal levels. These data show that FGF can rescue *Cyp26b1* expression in the absence of SHH, suggesting that diminished AER-FGF signalling in *Shh*-deficient limb buds (Zuniga et al., 1999) [**Table 4**] could be the cause of the reduced levels of *Cyp26b1*.

To further investigate the role of AER-FGFs, we analysed the expression of RA response genes in forelimb buds that lack *Fgf8* and *Fgf4* in the AER (as a consequence of *Msx2*-Cre mediated conditional inactivation) and are heterozygous for an *Fgf9* null allele (hereafter referred to as AER-*Fgfmut*, [**Figure 23**]) (Mariani et al., 2008). Mariani et al. showed that *Meis1*,
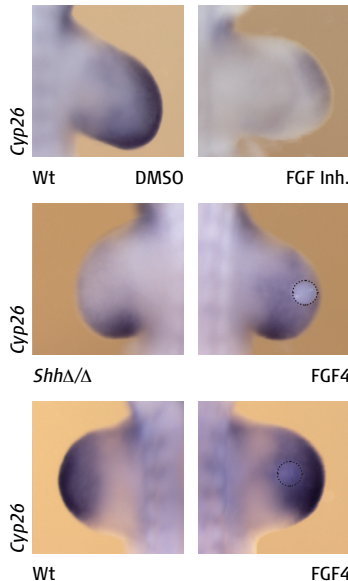

[**Figure 22**] *Cyp26b1* expression is positively regulated by AER-FGFs. All panels show *Cyp26b1* expression. Top row: forelimb buds (37-38 somites) cultured in the presence of 10 mM SU5402, an inhibitor of FGF signal transduction. *Cyp26b1* expression is down-regulated (n= 6/6; right panel) in comparison to limb buds cultured in solvent (DMSO; left panel). Middle row: implantation of an FGF4-soaked bead (demarcated by a dotted line) restores the *Cyp26b1* expression domain in *Shh*-deficient limb buds (n= 5/6; 34 somites). Bottom row: implantation of a carrier bead soaked in 1 mg/ml FGF4 only minimally up-regulates *Cyp26b1* expression in wild-type limb buds (n= 6/6; 34 somites).

which has a very similar distribution to *Meis2* (Mercader et al., 1999) is expanded distally and that the *Meis1* negative distal domain is reduced in these limb buds. We show that also the *Rarb* and *Pbx1* expression domains

are distally expanded in these AER-*Fgfmut* forelimb buds[**Figure 23A, panels Rarb and Pbx1**]. Furthermore, *Cyp26b1* expression is much more distally restricted in AER-Fgfmut than in *Shh*-deficient forelimb buds [**Figure 23A, panel Cyp26b1**], which agrees with the more severe PD skeletal defects in AER-*Fgfmut* than *Shh*-deficient forelimbs (Chiang et al., 2001; Mariani et al., 2008). These results provide genetic evidence for the proposal that AER-FGFs regulate *Cyb26b1* expression (**Figure 22**).

Early establishment of a distal state during limb bud development independent of SHH – In wild-type limb buds, *Cyp26b1* expression is activated under the *Fgf8*-expressing AER during initiation of limb bud development [**Figure 23B, 23 somites**]. At this early stage, *Rarb* is detected throughout the nascent limb bud mesenchyme, but only slightly later the *Rarb* and *Cyp26b1* expression domains become complementary and delineate the proximal and distal mesenchyme [**Figure 23C, 26 somites**]. These observations provide molecular support for the early specification of the PD limb bud axis (Mariani et al., 2008; Sun et al., 2002). The observed up-regulation of *Cyp26b1* and concurrent loss of *Rarb* expression in the distal mesenchyme creates an "RA-free" domain in the distal-most mesenchyme [**Figure 23B, C**]. This is a likely consequence of the positive effect of AER-FGF signalling (monitored by broad *Spry4* expression (Minowada et al., 1999) on *Cyp26b1* expression. In parallel to this early specification of the PD axis, SHH signalling is activated, but *Cyb26b1*, *Rarb* and AER-*Fgf8* expression are not affected in *Shh*-deficient limb buds at this early stage [**Figure 23C**]. By E9.75, *Shh* expression is detectable and the strong expression of its direct transcriptional target *Gli1* indicates that SHH signal transduction is ongoing [**Figure 24A**]. At as similar stage, the distalization of the *Rarb* expression becomes apparent in *Shh*-deficient limb buds in concert with slightly reduced *Cyp26b1* expression [**Figure 24B, compare to Figure 23C**]. This indicates that PD (i.e. distal; [**Figure 23B, C**]) and AP (i.e. posterior) (Galli et al., 2010; te Welscher et al., 2002a) identities are specified early by independent mechanisms. Only during initiation of the SHH/GREM1/AER-FGF feedback signalling system (Michos et al., 2004; Zuniga et al., 1999), do *Rarb*, *Cyp26b1* and AER-*Fgfs* become dependent on SHH signalling[**Figure 24**]. This molecular interlinking of the AP and PD axes enables spatially coordinated progression of limb bud outgrowth and patterning.

Numerical simulation of an AER-FGF/CYP26b1/RA signalling module in wild-type and mutant limb buds – Taken together, our analysis reveals the functional relevance of the up-regulation of *Cyb26b1* expression by AER-FGF signalling [**Figure 25B, green arrow**] for the specification of a "non-proximal", i.e. distal region in the nascent limb bud
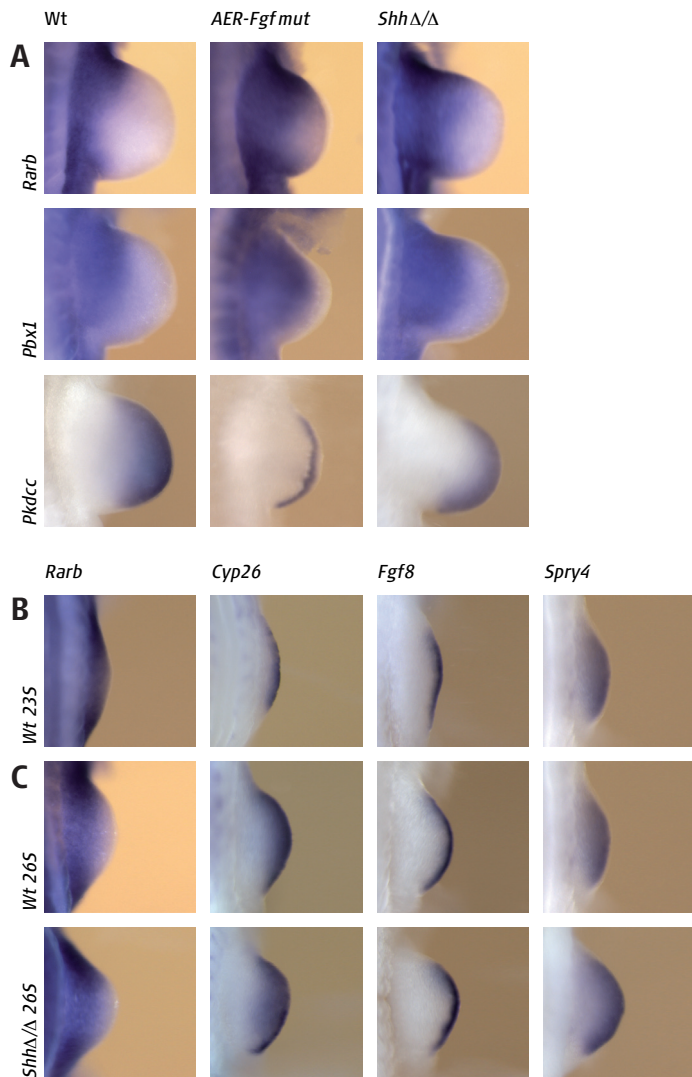
[**Figure 23**] Molecular evidence for the early specification of the PD limb bud axis. (A) Comparative analysis of the expression of *Rarb*, *Pbx1* and *Cyp26b1* in wild-type, AER-Fgfmut and *Shh*-deficient forelimb buds at E10.5 (34-35 somites). AER-*Fgfmut* forelimb buds are of the following genotype: *Msx2-CreTg/0;Fgf4Δ/flox; Fgf8Δ/flox; Fgf9Δ/+*. (B) Expression of *Rarb*, *Cyp26b1*, *Fgf8*, and *Spry4* in wild-type forelimb buds at 23 somites. *Cyp26b1* expression is activated in the distal-most mesenchyme at this early stage. (C) During early limb bud development (25-26 somites) the expression of *Rarb*, *Cyp26b1*, AER-*Fgf8* and *Spry4* is not affected in *ShhΔ/Δ* forelimb buds.
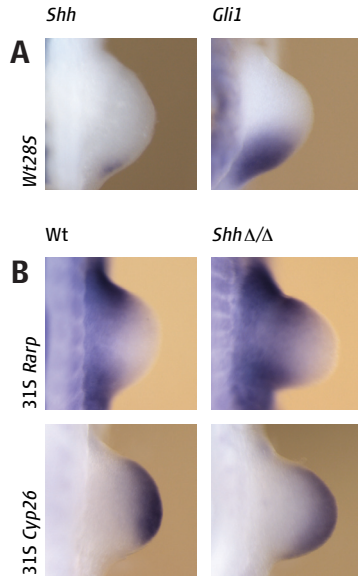
[**Figure 24**] (**A**) *Shh* and the downstream target *Gli1* are expressed in wild-type limb buds at E9.75 (28 somites). (**B**) The expression patterns of *Rarb* and *Cyp26b1* in wild-type and *Shh*-deficient limb buds at E10.0 (31 somites). At this stage, the expression of both genes starts to be altered in a complementary fashion due to the *Shh* deficiency.

mesenchyme [**Figure 23**]. In an attempt to define the simplest signalling module consistent with all genetic and experimental analysis, C. Kraemer and D. Iber (D-BSSE, ETH Systems Biology Institute) simulated the identified regulatory interactions in two spatial dimensions (AP and PD axes) and at four different time points during limb development using four reaction-diffusion type partial differential equations [**Figure 25C**, **D and Figure 26**](for formulas see material and methods). Initially, only the inactivation of RA by CYP26b1 (White et al., 2000) and the newly discovered positive regulation of *Cyp26b1* by AER-FGFs [**Figure 22**, **23A**] were considered [**Figure 25, solid black and green arrows**]. While these initial simulations reproduced many aspects of the experimentally observed expression and activity domains there were important discrepancies: in wild-type limb buds, the domains of *Cyp26b1* and AER-*Fgfs* extended proximally resulting in lower *Rarb* expression especially at an earlier time point [**Figure 26, without mutual inhibition**]. The match between the simulations and observed spatial distributions in mouse limb buds was significantly improved by postulating that high RA activity inhibits AER-FGFs [**Figure 25, red inhibitory line; Figure 26 with mutual inhibition**]. We verified this predicted inhibitory effect experimentally by implanting RA beads into the distal mesenchyme of wild-type limb buds [**Figure 25A**]. RA beads caused local reduction of AER-*Fgf8* and mesenchymal *Spry4* expression [**Figure 25A**]. *Fgf4* expression

93

in the AER was more broadly down-regulated after implantation of a RA bead (data not shown). This inhibitory effect of RA on AER-*Fgfs* was best observed in embryos of 33-34 somites, at later stages the reduction effects were less obvious, most likely due to high amounts of CYP26b1 in the distal limb bud (data not shown). These results demonstrating that RA inhibits AER-*Fgfs* are consistent with a previous study showing that high RA activity disrupts AER morphology and function in chicken limb buds (Tickle et al., 1989). RA seems to exert its effect via an RA-response element (RARE) in the cis-regulatory region of the *Fgf8* gene (Zhao et al., 2009). In addition, AER-*Fgf4* expression is reduced in *Cyp26b1*-deficient limb buds (Yashiro et al., 2004). Taken together, these results provide good evidence that high RA activity inhibits AER-*Fgf* expression.

Simulations including this inhibitory interaction [**Figure 25B, red line**] (material and methods) rather accurately reproduce the *Rarb*, *Cyp26b1* and AER-*Fgf* domains in wild-type limb buds at four different time points during limb development from initiation to a stage where the SHH/GREM1/FGF feedback loop is functional [**compare Figure 25C to Figure 23B and C**]. In the absence of SHH, AER-*Fgf* expression is significantly reduced [**Table 4**](Chiang et al., 2001; Zuniga et al., 1999). Our simulations accurately predict the increase in RA activity (monitored by the expansion of the *Rarb* domain) and proximalization due to reduced CYP26b1 activity as observed in *Shh*-deficient and in AER-*Fgfmut* limb buds [**Figure 25D, compare to Figure 19 and Figure 23**]. Furthermore, the simulations reproduce the spatial alterations observed in *Cyp26b1*-deficient limb buds [**Figure 26B, compare to Figure 21C**]. In conclusion, these mathematical simulations reproduce the observed expression domains of *Rarb*, *Cyp26b1* and *Fgfs* in both wild-type and mutant situations at different time points and thus confirm the described interactions.

A

Fgf8   RA   *Spry4*   RA
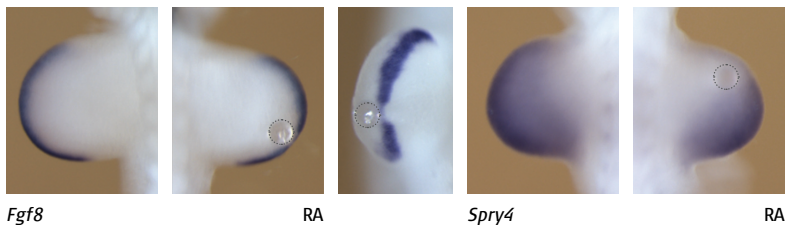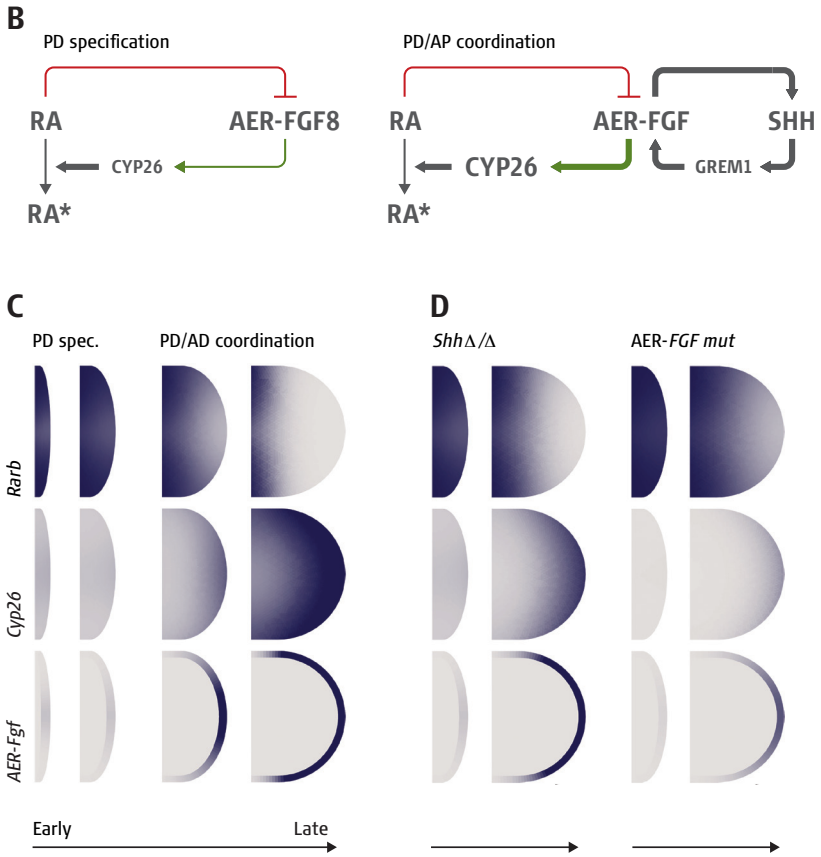
[**Figure 25**] The SHH/AER-FGF/CYP26b1/RA signalling module regulates spatially coordinated PD and AP limb axis development as plug-in to the self-regulatory limb bud signalling system defined by the SHH/ GREM1/AER-FGF feedback loop. (**A**) High RA activity inhibits AER-Fgf8 signalling locally. Implantation of a RA bead (1mg/ml) into wild-type forelimb buds at E10.25 (32-33 somites, 8 hours culture) inhibits AER-*Fgf8* (n=3/4) and *Spry4* (n=3/3) expression locally. (**B**) Schematic representation of the newly identified signalling module during PD axis specification (independent of SHH, left panel) and spatially coordinated axes development (regulated by SHH via the SHH/GREM1/AER-FGF feedback loop, right panel). RA is synthesized by RALDH2 in the embryonic flank mesenchyme and inactivated distally by CYP26b1-mediated hydroxylation (RA*). The propagation of AER-*Fgf* expression via the SHH/GREM1/ AER-FGF feedback loop is indicated (right panel). The green arrow indicates the positive regulation of *Cyp26b1* expression by AER-FGF signalling and the red inhibitory line the predicted inhibition of AER-FGF activity by RA. (**C**) Schematic representation of the simulation of dynamic spatial distributions of RA activity (*Rarb*), *Cyp26b1* and AER-*Fgfs* along the PD and AP axis in wild-type limb buds at four different time points during limb development (for equations see materials and methods). The left panels show the initial phase during which the PD axis is specified in a SHH-independent manner. The right panels show how the expression domains evolve during SHH-mediated coordinated PD/AP limb bud axis development during progression of limb bud development. (**D**) Dynamic simulations of the *Rarb*, *Cyp26b1* and AER-*Fgf* expression patterns in *Shh* deficient and AER-*Fgfmut* limb buds at ~E9.5 and ~E10.5. The simulated activities are shown in blue (dark: high, grey: low) in all panels C, D. All limb bud schemes are oriented with proximal to the left and anterior to the top. Arrows in panels C, D represent developmental time. (Panels C and D were provided by C. Kraemer and D. Iber)
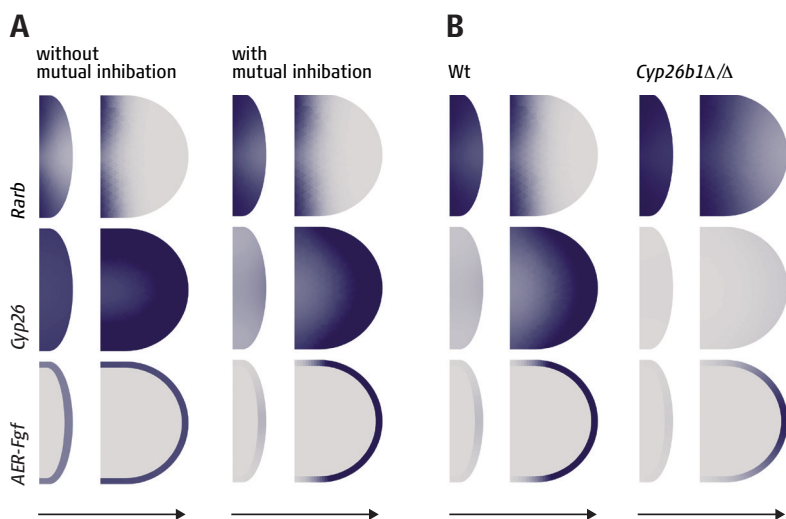
[**Figure 26**] Modelling the RA/FGF pathway interactions. [**A**] Comparison of simulated expression patterns in Wt limb buds without or with the postulated inhibition of AER-FGF by high RA activity at ~E9.5 and ~E10.5. Without RA-mediated inhibition, AER-*Fgf* expression extends very proximally together with *Cyp26b1* resulting in a decrease of *Rarb* distribution. With RA inhibition of AER-*Fgfs* the expression domains of *Cyp26b1* and AER-*Fgfs* extend less proximal especially at earlier stages. [**B**] Numerical simulations of the spatial distributions of the *Rarb*, *Cyp26b1* and AER-*Fgf* domains in *Cyp26b1*-deficient limb buds in comparison to wild-types. The simulated expression patterns are represented by color intensity, i.e. high/low concentrations correspond to blue/white. Orientation of each limb is with proximal to the left and anterior to the top. Arrows represent developmental time. (Figure provided by C. Kraemer and D. Iber)

Discussion

In this study, we combine molecular analysis with genetics and mathematical simulations to uncover a novel function of SHH in PD limb bud axis development via positive regulation of an AER-FGF/CYP26b1/RA signalling module. To gain a comprehensive overview of how SHH regulates gene expression, we have profiled the transcriptome in mouse forelimb buds lacking *Shh*. This analysis revealed that in addition to its known function in AP patterning, *Shh* is also important for PD axis patterning, as *Shh*-deficient limb buds were proximalized. The expression of proximal genes and RA activity in the proximal limb bud is increased while distal AER-FGFs are decreased. Furthermore, expression of the RA inactivating enzyme *Cyp26b1* in the distal mesenchyme is reduced. We show that *Cyp26b1* expression in the distal mesenchyme is regulated by AER-FGFs. Functional analysis and mathematical simulations reveal a SHH-dependent signalling module that normally enhances RA clearance by increasing AER-FGF signalling, which in turn up-regulates *Cyp26b1* expression. In addition, we provide molecular evidence that the limb is patterned very early along the PD axis by FGF-induced up-regulation of *Cyp26b1*, which creates a distal RA-free domain. Subsequently, when *Shh* expression is activated in the posterior mesenchyme, AP and PD axes become interlinked via SHH mediated up-regulation of AER-FGFs through the SHH/GREM1/FGF feedback loop, which is crucial for the maintenance of the AER-FGF/CYP26b1/RA signalling module.

Transcriptome analysis of *Shh*-deficient limb buds reveals a role of SHH in transcriptional repression – We have compared the transcriptome of *ShhΔ/Δ* to wild-type limb buds by performing a microarray analysis at E10.5 (35 to 36 somites). Our data sets of genes up- and down-regulated largely match those from a previous microarray study performed at E11.5, particularly for genes with a very high fold change ((Vokes et al., 2008) up-regulated: i.e. *Gria2*, *Hoxc6*, *Alx4* or *Pax1*; down-regulated: i.e. 5'*Hoxd* genes, *Hand2* or *Sall* genes). Characteristically, in both data sets, a rather large number of genes were up-regulated in *Shh* mutant limb buds. This implies that transcriptional repression by SHH is not transient but persists at E11.5 despite the fact that at this stage the *ShhΔ/Δ* limb bud is considerably smaller than wild-type limb buds and has undergone massive apoptosis (Galli et al., 2010). However, we noted some important differences between the data sets. Although fold changes cannot be compared due to stage differences, the data sets from Vokes et al. contained more up-regulated genes than our data sets,

while several genes that are present in ours were not present in theirs. For example, from the genes shown in figures 18 and 19, *Alcam*, *Wnt5a*, *Spry4*, *Cyp26b1* and *Rarb* were not present in the Vokes et al. data set, suggesting that these genes may not be expressed anymore at E11.5 and/or that the choice of cut-off for the fold change accounts for the difference.

Our microarray analysis revealed that important networks such as the cell-cycle are dependent on SHH for their maintenance [**Figure 17**], corroborating two recent studies showing that SHH controls proliferation during limb bud development (Towers et al., 2008; Zhu et al., 2008). As a large number of genes is up-regulated in *Shh*-deficient limb buds, we decided to analyze these genes, because a role for SHH signalling in mediating transcriptional repression had not been previously addressed. A striking feature of our data sets is the presence of many AP markers as well as PD markers. In agreement with previous studies we find that *Shh* is critical for maintaining the expression of posterior and distal genes in the mesenchyme and AER-expressed genes (Chiang et al., 2001; Litingtung and Chiang, 2000; te Welscher et al., 2002b; Zuniga et al., 1999). More surprisingly, we find that many known and novel anterior markers are up-regulated and posteriorly expanded (e.g. *Hoxc6*, *Pax1*, *Gria2*, *Igfbp2*) [**Table 5**], while in *Gli3*-deficient limb buds, their expression is reduced or lost (data not shown). Thus, SHH controls AP patterning by a combination of transcriptional activation and repression that are most likely a consequence of the antagonistic GLI3R/SHH interactions.

SHH acts on PD limb axis patterning through the SHH/GREM1/FGF feedback loop – Interestingly, the analysis of up-regulated genes has shown that *Shh* mutant limb buds are proximalized and that RA activity is elevated and expanded distally. More precisely, the data in support for an increase of RA activity in *ShhΔ/Δ* limb buds are the following: 1. *Rarb* expression, a sensor for RA activity is increased and distally expanded. 2. *Cyp26b1* expression in the distal limb bud is decreased. 3. The expression of RA responsive proximal genes such as *Meis2*, *Pbx1*, and *Pkdcc* is also up-regulated and distally expanded. 4. The distal expansion of these genes in *Shh*-deficient limb buds can be inhibited by the implantation of a bead loaded with a RA antagonist (BMS493 (Germain et al., 2002)). RA activity has also been shown to be elevated and distally expanded in *Cyp26b1Δ/Δ* and AER-*Fgfmut* limb buds as monitored by expansion of *Rarb*, Meis, *Pbx1* and *Pkdcc* expression ((Mariani et al., 2008; Yashiro et al., 2004) and this study). Both *Cyp26b1* null and AER-*Fgfmut* mouse embryos display severe skeletal defects that affect all elements along the PD limb axis. In *Cyp26b1*-deficient embryos, these limb phenotypes are caused by excess RA activity during development (Yashiro et al., 2004). Experimental manipulation
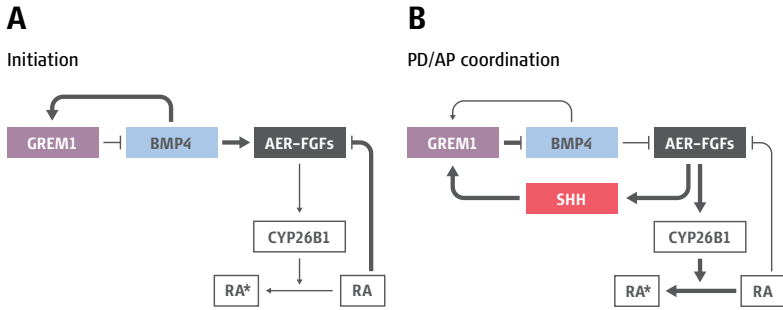
in chicken limb buds and genetic evidence has revealed that AER-FGFs play an instructive role in PD limb bud patterning (Mariani et al., 2008; Mercader et al., 2000). In this study, we provide evidence that this role may be mediated by the CYP26b1 enzyme. We show that AER-FGFs positively regulate the expression of *Cyp26b1* in the distal limb bud mesenchyme. These data strongly suggest that AER-FGFs promote clearance of RA in the distal limb bud mesenchyme by inducing *Cyp26b1* expression and thereby counteract the proximalizing activity of RA [**Figure 27**]. In *Shh*-deficient limb buds, the SHH/GREM1/FGF feedback loop is disrupted, which results in reduced AER-FGF signalling and consequently in a reduction of *Cyp26b1* expression. Disruption of CYP26b1-mediated RA clearance interferes with distal limb bud development and molecularly proximalizes *Shh*, AER-*Fgfmut* and *Cyp26b1*-deficient limb buds. While the role of endogenous RA in determining proximal structures has been the subject of some controversy (Lewandoski and Mackem, 2009) it is clear from our analysis and the severe limb phenotypes caused by increased RA activity in *Cyp26b1*-deficient mice (Yashiro et al., 2004) that distal limb bud development depends critically on AER-FGF mediated increased *Cyp26b1* expression and RA clearance. Indeed, treatment of pregnant mice with teratogenic doses of RA disrupts mesenchymal cell proliferation, which together with massive apoptosis causes severe truncations of the distal limb skeleton (PD axis) and autopod (AP axis) (Zhou and Kochhar, 2004).

Early establishment of the PD limb axis by the creation of a distal RA-free domain – Our genetic analysis and mathematical simulations shows that a signalling module based on mutual inhibition between RA and FGFs controls the early establishment of proximal and distal limb bud identities [**Figure 25B, left panel and Figure 27A**]. The fact that CYP26b1-mediated clearance of RA in the distal limb bud enables distal progression of limb development makes *Cyp26b1* expression an excellent marker of the distal mesenchymal domain in the limb bud. Regions of distinct RA and CYP26b1 activities are established already during initiation of limb bud development [**Figure 23**]. Our study indicates that proximal and distal identities of the nascent limb bud are specified early by activating *Cyp26b1* expression under the influence of FGF8 signalling by the AER. *Fgf8* expression is restricted from the proximal-most ectoderm by RA activity. CYB26b1-mediated clearance of RA from the distal-most mesenchyme then creates a distal RA-free domain and a proximal domain with high RA activity. This prepatterning of the PD limb bud axis by the RA/CYP26b1/AER-FGF module takes place before activation of *Shh* expression. Our data expands the two-signal model for PD limb bud development, which states that the PD axis of the limb bud

is patterned by RA and FGF signals (Mercader et al., 2000). We provide evidence that the distal domain established by AER-FGFs during prepatterning of the limb bud is a likely consequence of CYP26b1 mediated clearance of RA. Our observations also fit to the early specification model of PD limb axis development (Dudley et al., 2002). The early specification model predicts that the three segments (stylopod, zeugopod, and autopod) along the PD axis are specified very early (reviewed by (Tabin and Wolpert, 2007). The main difference between our observations and this model is that our data indicates that not all three segments along the PD are specified early, but rather that two states, a proximal and a distal state, are created. In fact, it was already proposed by Mariani et al. that the initial PD axis patterning might only establish two segments and that the third intermediate domain is established later (Mariani et al., 2008). Prepatterning of the PD axis is reminiscent of prepatterning of the AP axis, which also occurs during initiation of limb bud outgrowth and also depends on mutual inhibition (between *Hand2* and *Gli3*) (Galli et al., 2010). This shows that these two limb bud axes are specified from the initiation of outgrowth onwards. The early specification of the PD and AP limb bud axes occurs independent of one another and prior to the onset of SHH-mediated regulation of the AER-FGF/CYP26b1/RA signalling module that integrates PD with AP limb bud development.

SHH-RA interactions are not mediated by GLI3 repression

During the transition from the early, prepatterned limb bud to SHH-dependent AP patterning, one of the main functions of SHH is to antagonize the formation of the GLI3R. This becomes obvious from the phenotype of *Shh/Gli3* double mutant limbs (Litingtung et al., 2002; te Welscher et al., 2002b). These limbs display the same phenotype as *Gli3*-deficient limbs, which exhibit severe polydactyly with loss of digit identity. Our transcriptome analysis and the in situ hybridisation screen have revealed that many genes are regulated in an opposing manner in *Shh*- and *Gli3*-deficient limb buds. For example, the cell-cycle genes and many of the anterior restricted genes show opposite regulation by SHH signalling and GLI3 repression [**Figure 17 and 18, and data not shown**]. Interestingly, many of the proximal genes that are up-regulated and expanded in *Shh*-deficient limb buds are not significantly affected in *Gli3*-deficient limb buds (data not shown). This indicates that the distal expansion observed in *Shh*-deficient limb buds is not due to altered GLI3 activity, but is indeed caused by a loss of CYP26b1-mediated RA clearance in the distal limb bud.

A

Initiation

GREM1 — BMP4 → AER–FGFs

CYP26B1

RA* ← RA

B

PD/AP coordination

GREM1 — BMP4 → AER–FGFs

SHH

CYP26B1

RA* ← RA

[**Figure 27**] Schematic representation of the RA/CYP26b1/AER-FGF signalling module that functions as a plug in to the self-regulatory limb bud signalling system (Benazet et al., 2009). RA is inactivated by CYP26b1-mediated hydroxylation to inactive forms of RA (RA*). The fast feedback loop between BMP4 (blue) and GREM1 (purple) enabling progression of early limb development is indicated. [**A**] Initiation phase: Early PD axis specification is independent of SHH. The AER (expressing AER-*Fgfs* (dark grey)) is induced by high levels of BMP4 and by FGF10 (not shown). AER-FGFs induce the expression of *Cyp26b1* in the distal mesenchyme, which creates a distal RA-free domain. In addition, high RA in the proximal limb inhibits *Fgf* expression in the proximal ectoderm. [**B**] After activation of SHH (red) signalling in the posterior mesenchyme, the interlinked signalling feedback loops are functional and the development of the AP and PD axes are coordinated. SHH regulates the propagation of AER-*Fgf* expression via the SHH/GREM1/AER-FGF feedback loop. AER-FGFs are crucial for the maintenance of *Cyp26b1* expression in the distal limb bud to ensure RA clearance and thus to enable distal progression of limb development in a coordinated manner along both the AP and PD axes.

SHH signalling integrates AP and PD axes patterning – When SHH signalling is initiated in the posterior limb bud mesenchyme, the SHH/GREM1/FGF epithelial-mesenchymal signalling feedback loop is activated. This loop is necessary for maintenance of both AER-*Fgfs* and *Shh* expression. At this time, the AER-FGF/CYP26b1/RA signalling module becomes dependent on SHH, as SHH-mediated maintenance of *Fgf* expression in the AER via SHH/GREM1/FGF feedback loop is essential for up-regulation of *Cyp26b1* expression [**Figure 27B**]. This shows that the AER-FGF/CYP26b1/RA signalling module functions as a plug-in to the self-regulatory limb bud signalling system (Benazet et al., 2009) [**Figure 25B**, **right panel and Figure 27B**]. The interlinking of these two feedback signalling systems assures that the distal limb bud stays free of RA while the AP and distal patterns are laid down. In addition, these interactions constitute a further connection between the AP and PD axes, enabling coordinated outgrowth and patterning along these axes.

Mutually inhibitory interactions between RA and FGFs during development – The mutually inhibitory AER-FGF/CYP26b1/RA signalling module we describe here is strikingly similar to the interactions of these two signals during vertebrate somitogenesis. During somitogenesis, RA is produced by RALDH2 in the newly formed somites and the rostral presomitic mesoderm. *Fgf8* is expressed in the most caudal region where it maintains a stem cell population for the generation of trunk tissue. *Cyp26a1* is expressed in the same region and its expression is regulated by FGF8, at least in Xenopus laevis embryos (Moreno and Kintner, 2004). CYP26a1 is important to clear RA from the undifferentiated region. These interactions are thought to be involved spacing the boundaries of the newly formed somite pairs (reviewed by (Dequeant and Pourquie, 2008)) and have been proposed to create sharp developmental thresholds by a mechanism that promotes bi-stable states (Goldbeter et al., 2007). These interactions are virtually the same interactions that others and we have described for limb bud development (Mariani et al., 2008; Mercader et al., 2000; Yashiro et al., 2004). In fact, it seems that the mutually inhibitory interactions between RA and FGFs have been co-opted for the spatially coordinated development of diverse embryonic structures such as limb buds, the somites, the neural tube and the heart and that these interactions are also involved processes like neurogenesis (neural differentiation of stem cells) and interdigital cell death (this study and (Dequeant and Pourquie, 2008; Diez del Corral et al., 2003; Hernandez-Martinez et al., 2009; Mercader et al., 2000; Ryckebusch et al., 2008; Stavridis et al., 2010). During these interactions, FGFs generally keep a stem cell population or progenitor cells in an undifferentiated state, while RA counteracts these effects to control differentiation. This is most likely also the case during limb bud development, where it is generally assumed that FGFs keep the distal mesenchyme in an undifferentiated state. The role of RA during the patterning phase is not clear, but RA could be involved in the proximal to distal sequence of the generation of chondrogenic condensations observed during limb development and thus together with AER-FGFs define the differentiation front (Tabin and Wolpert, 2007). These interactions are also potentially interesting for developing cancer treatments, as FGFs are involved in a variety of cancers (Turner and Grose, 2010). One study has shown that treatment with RA can inhibit *Fgf4* expression in a cell-line from male germ cell cancers that strongly overexpress FGF4 (Maerz et al., 1998). In conclusion, the mutually inhibitory interaction between the RA and FGF signalling pathways seems to represent a fundamental signalling mechanism for the establishment of distinct embryonic domains.

Conclusions and outlook

The identification and the analysis of the signals involved in limb bud development have provided insight into how the limb bud is patterned along its three axes. SHH has been shown to be crucial for AP patterning of the limb bud, as loss of SHH function during limb development results in a collapse of the AP axis (Chiang et al., 2001; Kraus et al., 2001). On the other hand FGFs have been shown to be essential for limb bud outgrowth and specification along the PD axis (Mariani et al., 2008). Many more factors have been identified to be essential for limb development (e.g. BMPs, BMP antagonists, *Hox* genes) (reviewed by (Zeller et al., 2009). Nevertheless, still little is known about how these different signals interact to govern limb bud development in a coordinated way. Furthermore, only few studies have looked at how cells of the limb bud respond to these different signals. To analyze the genome-wide effects of SHH signalling on the limb bud we have performed a transcriptome analysis of *Shh*-deficient limb buds. We have combined genetics with molecular analysis, experimental manipulation of limb buds and mathematical simulations to study a novel, unexpected function of SHH during limb development. The main conclusions of this study are:

— SHH also regulates PD limb bud patterning: loss of SHH signalling during limb bud development leads to molecular proximalization of the limb bud at E10.5 as observed by the distal expansion of many proximally expressed genes. Furthermore, *Shh*-deficient limb buds show an increase in proximal RA-activity most likely due to a decrease of the RA inactivating enzyme CYP26b1 in the distal limb bud, leading to up-regulation and distal expansion of RA responsive genes.

— SHH signalling integrates PD with AP limb bud patterning: we show that *Cyp26b1* expression is regulated by AER-FGFs. This illustrates that the effect of SHH on *Cyp26b1* expression is mediated through the SHH/GREM1/FGF feedback loop. These interactions integrate PD and AP limb axes development, as AER-FGF mediated up-regulation of *Cyp26b1* expression in the distal limb bud is dependent on the SHH/GREM1/FGF feedback loop.

— The PD axis is established very early during limb bud outgrowth: mutually inhibitory interactions between RA from the flank and AER-FGFs establish the PD axis at the beginning of limb bud development. Activation of *Cyp26b1* expression in the distal mesenchyme by AER-FGFs leads to the formation of a RA-free distal domain as soon as FGF8 is activated in the AER. This happens independently of SHH and before the integration of PD and AP limb axis development.

— Clearance of RA from the distal domain of the limb bud is crucial for distal progression of limb bud development: the establishment of the distal RA-free domain by AER-FGF-induced CYP26b1 activity is absolutely necessary for coordinated PD and AP limb bud development. This is also corroborated by the phenotypes of *AER-FGF^mut* and *Cyp26b1*-deficient limbs, which both display severe phenotypes along the PD and AP axes (Mariani et al., 2008; Yashiro et al., 2004).

These insights into the interactions of the SHH, FGF and RA pathways raise many new questions about their function and regulation during limb development. One major conclusion from our transcriptome and experimental analysis is that SHH impacts on RA pathway activity. Interactions between the SHH and RA pathways in the limb bud have only been studied in the context of experiments that have shown that RA could be involved in *Shh* activation in the limb bud. Originally it was shown that *Shh* is ectopically induced in the anterior limb bud by application of beads soaked in RA (Riddle et al., 1993). Experiments performed in *Raldh2* mutant embryos, which were rescued by maternal RA supplementation have shown that correct RA signalling seems to be important for proximal restriction of *Shh* expression (Niederreither et al., 2002). Here we show for the first time that SHH signalling influences the RA pathway through regulation of *Cyp26b1* expression. However, these observations only provide a first idea of the regulation of these interactions. The interactions between these pathways can be further studied by generating compound mutants of SHH and RA pathway members. Generating *Shh;Cyp26b1* compound mutants (*ShhΔ/Δ ;Cyp26b1Δ/Δ* or *ShhΔ/Δ ;Cyp26b1Δ/+)* should lead to an increase of the proximalization we observe in *Shh*-deficient limb buds. RA synthesis by RALDH2 in the flank is the source of RA in the limb bud. *Raldh2*-deficient embryos die at E9.5, which is the time when limb bud outgrowth only starts (Niederreither et al., 1999). This makes analysis of double mutant embryos impossible. Nevertheless removal of one copy of *Raldh2* has been shown to have an effect in a mutant background (Ribes et al., 2007). Heterozygosity for *Raldh2* in a *Shh* mutant background might to some extent rescue the PD phenotype that we observe in *Shh*-deficient limb buds. This might be detectable by changes in the expression of the molecular markers for the proximal limb bud we have established and might even have an impact on the skeletal phenotype of *Shh*-deficient limbs. In addition, these compound mutants might reveal unknown aspects of the SHH-RA interactions. These studies will provide further insights into the regulation of SHH and RA interactions and how AP and PD axis patterning are integrated during progression of limb bud development.

The function of endogenous RA during limb bud development is still unclear and it is not known whether RA is important during the early specification phase of limb bud development (Lewandoski and Mackem, 2009). To rescue the early lethality of embryos deficient for *Raldh2*, conditional inactivation of RA-synthesis in the lateral plate mesoderm would be necessary. This is complicated further as it has been shown that RA is important for limb bud induction in the flank mesenchyme before limb bud outgrowth (Niederreither et al., 1999; Zhao et al., 2009). Conditional inactivation of RALDH2 function would thus have to happen at a rather defined time point after limb bud induction but before limb bud outgrowth. Inducible Cre-lines for conditional inactivation in the lateral plate mesoderm at precise time points would have to be used. For the lateral plate mesoderm at the level of the hindlimb bud a tamoxifen-inducible Cre-line already exists (*Hoxb6CreER^T* (Zhu et al., 2008). For conditional inactivation in the lateral plate mesoderm at the level of the forelimb bud, a Cre under the control of the *Rarb* promoter exists, however this is not an inducible Cre (Kobayashi et al., 2005). Using tamoxifen-inducible Cre recombinases has not always been straightforward, making it not applicable in all situations (unpublished data, our lab). The efficient removal of RA synthesis would thus have to be carefully evaluated. Even though it might not be straightforward to perform these experiments, it would be very interesting to be able to analyze the physiological functions of RA in PD and AP limb bud patterning.

In this study we have shown that AER-FGFs regulate the expression of *Cyp26b1* in the distal limb bud. This shows that the impact of SHH on *Cyp26b1* expression is mediated through the SHH/GREM1/FGF feedback loop. During somitogenesis FGF signalling controls expression of *Cyp26a1* in the tail bud (Moreno and Kintner, 2004). However, both studies do not demonstrate if the regulation of *Cyp26* by FGFs is direct or mediated by other factors. Further analysis of the regulation of *Cyp26* by FGFs is necessary to answer this question. The Cyp26 enzymes were originally discovered as RA responsive genes (White et al., 1996). Indeed, *Cyp26b1* expression is strongly induced over the whole limb bud, when a RA soaked bead is implanted into the limb bud and is also rapidly and broadly induced in Xenopus embryos exposed to RA (data not shown and (Moreno and Kintner, 2004)). Interestingly, the expression patterns of all three *Cyp26* genes are more or less complimentary to the regions where RA activity is observed (MacLean et al., 2001; Rossant et al., 1991; Tahayato et al., 2003; Uehara et al., 2007). This raises the question what represses the activation of Cyp26 expression in the domains of endogenous RA activity. It is not known which factors in the proximal limb bud repress activation of *Cyp26b1* by RA signalling. The RA activity

and *Cyp26* expression domains are also mutually exclusive at E7.0 in anterior and posterior parts of the embryo and during somitogenesis (reviewed by (Niederreither and Dolle, 2008)). The description of the interactions between the FGF and RA pathways in regulating the RA degrading activity would provide further insights into the inhibitory RA-FGF interactions in diverse embryonic structures.

Our collaborators simulated the identified regulatory interactions between RA, FGFs, and SHH in two spatial dimensions (AP and PD axes) at different times during limb bud development using four reaction-diffusion type partial differential equations. This model was able to accurately reproduce the expression domains of factors involved in both wild-type and mutant situations. In fact, the process of formulating the model revealed an additional inhibitory interaction between RA and FGFs, which we verified experimentally. A recent study by our lab has simulated the temporal kinetics of complex signalling interactions with genetic and molecular datasets as a basis (Benazet et al., 2009). The predictive power of this model and subsequent experimental analysis were able to reveal an important aspect of the complex interactions described in this study. Together with this study this shows that the inclusion of mathematical modelling in the analysis of complex regulatory interactions can provide important novel insights. Importantly, an *in silico* model can be used to simulate conditions that are not possible to generate *in vivo*. The incorporation of detailed data on expression patterns and growth together with the known signalling interactions (i.e. signalling modules) could allow modellers to formulate a detailed 3D model of limb development. A very recent study has provided a first model that incorporated the actual 3D shape of the limb bud at two different time points in conjunction with cell proliferation rates. The authors were able to show that limb bud growth and shape are not simply controlled by an uneven distribution of proliferation rates but that directional cell activities are involved in directing PD limb bud outgrowth (Boehm et al., 2010). A 3D limb model including growth and the important signals would provide an important tool to discover novel interactions and processes during limb bud development and to test experimental evidence. In addition, studying interactions between signals in the limb bud both *in vivo* and *in silico* can be expanded to other embryonic structures as the same signalling modules seem to be employed in different embryonic structures, although signalling modules might be combined in a different manner to generate diverse functions and structures.

Dagmar Iber, Rolf Zeller and Aimée Zuniga (2011). **SHH propagates distal limb bud development by enhancing CYP26B1-mediated retionic acid clearance via AER-FGF signalling.** Development 138, 1913-1923.

8. Acknowledgments

9. References

Abu-Abed, S., Dolle, P., Metzger, D., Beckett, B., Chambon, P., and Petkovich, M. (2001). The retinoic acid-metabolizing enzyme, CYP26A1, is essential for normal hindbrain patterning, vertebral identity, and development of posterior structures. Genes Dev *15*, 226-240.

Adams, S.L., Cohen, A.J., and Lassova, L. (2007). Integration of signaling pathways regulating chondrocyte differentiation during endochondral bone formation. J Cell Physiol *213*, 635-641.

Ahn, K., Mishina, Y., Hanks, M.C., Behringer, R.R., and Crenshaw, E.B., 3rd (2001). BMPR-IA signaling is required for the formation of the apical ectodermal ridge and dorsal-ventral patterning of the limb. Development *128*, 4449-4461.

Ahn, S., and Joyner, A.L. (2004). Dynamic changes in the response of cells to positive hedgehog signaling during mouse limb patterning. Cell *118*, 505-516.

Benazet, J.D., Bischofberger, M., Tiecke, E., Goncalves, A., Martin, J.F., Zuniga, A., Naef, F., and Zeller, R. (2009). A self-regulatory system of interlinked signaling feedback loops controls mouse limb patterning. Science *323*, 1050-1053.

Benazet, J.D., and Zeller, R. (2009). Vertebrate Limb Development: Moving from Classical Morphogen Gradients to an Integrated 4D Patterning System. Cold Spring Harb Perspect Biol *doi: 10.1101/cshperspect.a001339.*

Boehm, B., Westerberg, H., Lesnicar-Pucko, G., Raja, S., Rautschka, M., Cotterell, J., Swoger, J., and Sharpe, J. (2010). The role of spatially controlled cell proliferation in limb bud morphogenesis. PLoS Biol *8*, e1000420.

Bowen, M.A., Patel, D.D., Li, X., Modrell, B., Malacko, A.R., Wang, W.C., Marquardt, H., Neubauer, M., Pesando, J.M., Francke, U., et al. (1995). Cloning, mapping, and characterization of activated leukocyte-cell adhesion molecule (ALCAM), a CD6 ligand. J Exp Med *181*, 2213-2220.

Branda, C.S., and Dymecki, S.M. (2004). Talking about a revolution: The impact of site-specific recombinases on genetic analyses in mice. Dev Cell *6*, 7-28.

Capdevila, J., Tsukui, T., Rodriquez Esteban, C., Zappavigna, V., and Izpisua Belmonte, J.C. (1999). Control of vertebrate limb outgrowth by the proximal factor Meis2 and distal antagonism of BMPs by Gremlin. Mol Cell *4*, 839-849.

Capellini, T.D., Di Giacomo, G., Salsi, V., Brendolan, A., Ferretti, E., Srivastava, D., Zappavigna, V., and Selleri, L. (2006). Pbx1/Pbx2 requirement for distal limb patterning is mediated by the hierarchical control of Hox gene spatial distribution and Shh expression. Development *133*, 2263-2273.

Chen, M.H., Li, Y.J., Kawakami, T., Xu, S.M., and Chuang, P.T. (2004). Palmitoylation is required for the production of a soluble multimeric Hedgehog protein complex and long-range signaling in vertebrates. Genes Dev *18*, 641-659.

Chiang, C., Litingtung, Y., Harris, M.P., Simandl, B.K., Li, Y., Beachy, P.A., and Fallon, J.F. (2001). Manifestation of the Limb Prepattern: Limb Development in the Absence of Sonic Hedgehog Function. Developmental Biology *236*, 421-435.

Chiang, C., Litingtung, Y., Lee, E., Young, K.E., Corden, J.L., Westphal, H., and Beachy, P.A. (1996). Cyclopia and defective axial patterning in mice lacking *Sonic hedgehog* gene function. Nature *383*, 407-413.

Cooke, J., and Summerbell, D. (1980). Cell cycle and experimental pattern duplication in the chick wing during embryonic development. Nature *287*, 697-701.

Corson, L.B., Yamanaka, Y., Lai, K.M., and Rossant, J. (2003). Spatial and temporal patterns of ERK signaling during mouse embryogenesis. Development *130*, 4527-4537.

Davis, A.P., Witte, D.P., Hsieh-Li, H.M., Potter, S., and Capecchi, M. (1995). Absence of radius and ulna in mice lacking *hoxa-11* and *hoxd-11*. Nature *375*, 791-795.

de The, H., Vivanco-Ruiz, M.M., Tiollais, P., Stunnenberg, H., and Dejean, A. (1990). Identification of a retinoic acid responsive element in the retinoic acid receptor beta gene. Nature *343*, 177-180.

Dequeant, M.L., and Pourquie, O. (2008). Segmental patterning of the vertebrate embryonic axis. Nat Rev Genet *9*, 370-382.

Diez del Corral, R., Olivera-Martinez, I., Goriely, A., Gale, E., Maden, M., and Storey, K. (2003). Opposing FGF and retinoid pathways control ventral neural pattern, neuronal differentiation, and segmentation during body axis extension. Neuron *40*, 65-79.

Dudley, A.T., Ros, M.A., and Tabin, C.J. (2002). A re-examination of proximodistal patterning during vertebrate limb development. Nature *418*, 539-544.

Eisenhart, C. (1947). The assumptions underlying the analysis of variance. Biometrics *3*, 1-21. Fromental-Ramain, C., Warot, X., Messadecq, N., LeMeur, M., Dollé, P., and Chambon, P. (1996). Hox-a13 and Hox-d13 play a crucial role in patterning of the limb autopod. Development *122*, 2997-3011.

Galli, A., Robay, D., Osterwalder, M., Bao, X., Benazet, J.D., Muhammad, T., Paro, R., Mackem, S., and Zeller, R. (2010). Distinct Roles of Hand2 in Initiating Polarity and Posterior Shh Expression during the Onset of Mouse Limb Bud Development. PLoS Genetics *6*, e1000901.

Galloway, J.L., Delgado, I., Ros, M.A., and Tabin, C.J. (2009). A reevaluation of X-irradiation-induced phocomelia and proximodistal limb patterning. Nature *460*, 400-404.

Germain, P., Iyer, J., Zechel, C., and Gronemeyer, H. (2002). Co-regulator recruitment and the mechanism of retinoic acid receptor synergy. Nature *415*, 187-192.

Goldbeter, A., Gonze, D., and Pourquie, O. (2007). Sharp developmental thresholds defined through bistability by antagonistic gradients of retinoic acid and FGF signaling. Dev Dyn *236*, 1495-1508.

Goodrich, L.V., Milenkovic, L., Higgins, K.M., and Scott, M.P. (1997). Altered neural cell fates and medulloblastoma in mouse patched mutants. Science *277*, 1109-1113.

Harfe, B.D., Scherz, P.J., Nissim, S., Tian, H., McMahon, A.P., and Tabin, C.J. (2004). Evidence for an expansion-based temporal Shh gradient in specifying vertebrate digit identities. Cell *118*, 517-528.

Hernandez-Martinez, R., Castro-Obregon, S., and Covarrubias, L. (2009). Progressive interdigital cell death: regulation by the antagonistic interaction between fibroblast growth factor 8 and retinoic acid. Development *136*, 3669-3678.

Houweling, A.C., Dildrop, R., Peters, T., Mummenhoff, J., Moorman, A.F., Ruther, U., and Christoffels, V.M. (2001). Gene and cluster-specific expression of the Iroquois family members during mouse development. Mech Dev *107*, 169-174.

Hui, C., and Joyner, A. (1993). A mouse model of greig cephalopolysyndactyly syndrome: the extra-toesJ mutation contains an intragenic deletion of the Gli3 gene. Nat-Genet *3*, 241-246.

Imuta, Y., Nishioka, N., Kiyonari, H., and Sasaki, H. (2009). Short limbs, cleft palate, and delayed formation of flat proliferative chondrocytes in mice with targeted disruption of a putative protein kinase gene, Pkdcc (AW548124). Dev Dyn *238*, 210-222.

Jegalian, B.G., Miller, R.W., Wright, C.V., Blum, M., and De Robertis, E.M. (1992). A Hox 3.3-lacZ transgene expressed in developing limbs. Mech Dev *39*, 171-180.

Jia, Z., Agopyan, N., Miu, P., Xiong, Z., Henderson, J., Gerlai, R., Taverna, F.A., Velumian, A., MacDonald, J., Carlen, P., et al. (1996). Enhanced LTP in mice deficient in the AMPA receptor GluR2. Neuron *17*, 945-956.

Jiang, J., and Hui, C.C. (2008). Hedgehog signaling in development and cancer. Dev Cell *15*, 801-812.

Johnson, D.R. (1967). *Extra-toes*: a new mutant gene causing multiple abnormalities in the mouse. J Embryol exp Morph *17*, 543-581.

Jung, C.G., Kim, H.J., Kawaguchi, M., Khanna, K.K., Hida, H., Asai, K., Nishino, H., and Miura, Y. (2005). Homeotic factor ATBF1 induces the cell cycle arrest associated with neuronal differentiation. Development *132*, 5137-5145.

Kawakami, Y., Uchiyama, Y., Rodriguez Esteban, C., Inenaga, T., Koyano-Nakagawa, N., Kawakami, H., Marti, M., Kmita, M., Monaghan-Nichols, P., Nishinakamura, R., et al. (2009). Sall genes regulate region-specific morphogenesis in the mouse limb by modulating Hox activities. Development *136*, 585-594.

Khokha, M.K., Hsu, D., Brunet, L.J., Dionne, M.S., and Harland, R.M. (2003). Gremlin is the BMP antagonist required for maintenance of Shh and Fgf signals during limb patterning. Nat Genet *34*, 303-307.

Kinoshita, M., Era, T., Jakt, L.M., and Nishikawa, S. (2009). The novel protein kinase Vlk is essential for stromal function of mesenchymal cells. Development *136*, 2069-2079.

Kmita, M., Tarchini, B., Zakany, J., Logan, M., Tabin, C.J., and Duboule, D. (2005). Early developmental arrest of mammalian limbs lacking HoxA/HoxD gene function. Nature *435*, 1113-1116.

Kobayashi, A., Kwan, K.M., Carroll, T.J., McMahon, A.P., Mendelsohn, C.L., and Behringer, R.R. (2005). Distinct and sequential tissue-specific activities of the LIM-class homeobox gene Lim1 for tubular morphogenesis during kidney development. Development *132*, 2809-2823.

Koziel, L., Wuelling, M., Schneider, S., and Vortkamp, A. (2005). Gli3 acts as a repressor downstream of Ihh in regulating two distinct steps of chondrocyte differentiation. Development *132*, 5249-5260.

Kraus, P., Fraidenraich, D., and Loomis, C.A. (2001). Some distal limb structures develop in mice lacking Sonic hedgehog signaling. Mech Dev *100*, 45-58.

Kronenberg, H.M. (2003). Developmental regulation of the growth plate. Nature *423*, 332-336.

Lai, L.P., and Mitchell, J. (2005). Indian hedgehog: its roles and regulation in endochondral bone development. J Cell Biochem *96*, 1163-1173.

Lasorella, A., Uo, T., and Iavarone, A. (2001). Id proteins at the cross-road of development and cancer. Oncogene *20*, 8326-8333.

Laufer, E., Nelson, C.E., Johnson, R.L., Morgan, B.A., and Tabin, C. (1994). Sonic hedgehog and Fgf-4 act through a signaling cascade and feedback loop to integrate growth and patterning of the developing limb bud. Cell *79*, 993-1003.

Lettice, L.A., Heaney, S.J., Purdie, L.A., Li, L., de Beer, P., Oostra, B.A., Goode, D., Elgar, G., Hill, R.E., and de Graaff, E. (2003). A long-range Shh enhancer regulates expression in the developing limb and fin and is associated with preaxial polydactyly. Hum Mol Genet *12*, 1725-1735.

Lewandoski, M., and Mackem, S. (2009). Limb development: the rise and fall of retinoic acid. Curr Biol *19*, R558-561.

Lewandoski, M., Sun, X., and Martin, G.R. (2000). Fgf8 signalling from the AER is essential for normal limb development. Nat Genet *26*, 460-463.

Li, Y., Zhang, H., Litingtung, Y., and Chiang, C. (2006). Cholesterol modification restricts the spread of Shh gradient in the limb bud. Proc Natl Acad Sci U S A *103*, 6548-6553.

Litingtung, Y., and Chiang, C. (2000). Specification of ventral neuron types is mediated by antagonistic interaction between Shh and Gli3. Nat Neurosci *3*, 979-985.

Litingtung, Y., Dahn, R.D., Li, Y., Fallon, J.F., and Chiang, C. (2002). Shh and Gli3 are dispensable for limb skeleton formation but regulate digit number and identity. Nature *418*, 979-983.

MacLean, G., Abu-Abed, S., Dolle, P., Tahayato, A., Chambon, P., and Petkovich, M. (2001). Cloning of a novel retinoic-acid metabolizing cytochrome P450, Cyp26B1, and comparative expression analysis with Cyp26A1 during early murine development. Mech Dev *107*, 195-201.

Maerz, W.J., Baselga, J., Reuter, V.E., Mellado, B., Myers, M.L., Bosl, G.J., Spinella, M.J., and Dmitrovsky, E. (1998). FGF4 dissociates anti-tumorigenic from differentiation signals of retinoic acid in human embryonal carcinomas. Oncogene *17*, 761-767.

Maksym, R.B., Tarnowski, M., Grymula, K., Tarnowska, J., Wysoczynski, M., Liu, R., Czerny, B., Ratajczak, J., Kucia, M., and Ratajczak, M.Z. (2009). The role of stromal-derived factor-1--CXCR7 axis in development and cancer. Eur J Pharmacol *625*, 31-40.

Mariani, F.V., Ahn, C.P., and Martin, G.R. (2008). Genetic evidence that FGFs have an instructive role in limb proximal-distal patterning. Nature *453*, 401-405.

Marigo, V., Johnson, R.L., Vortkamp, A., and Tabin, C.J. (1996a). Sonic hedgehog Differentially Regulates Expression of *GLI* and *GLI3* during Limb Development. Dev Biol *180*, 273-283.

Marigo, V., Scott, M.P., Johnson, R.L., Goodrich, L.V., and Tabin, C.J. (1996b). Conservation in *hedgehog* signaling: induction of a chicken *patched* homolog by *Sonic hedgehog* in the developing limb. Development *122*, 1225-1233.

Mark, M., Ghyselinck, N.B., and Chambon, P. (2009). Function of retinoic acid receptors during embryonic development. Nucl Recept Signal *7*, e002.

Massague, J., and Gomis, R.R. (2006). The logic of TGFbeta signaling. FEBS Lett *580*, 2811-2820.

Medina-Martinez, O., Bradley, A., and Ramirez-Solis, R. (2000). A large targeted deletion of Hoxb1-Hoxb9 produces a series of single-segment anterior homeotic transformations. Dev Biol *222*, 71-83.

Mercader, N., Leonardo, E., Azpiazu, N., Serrano, A., Morata, G., Martinez, C., and Torres, M. (1999). Conserved regulation of proximodistal limb axis development by Meis1/Hth. Nature *402*, 425-429.

Mercader, N., Leonardo, E., Piedra, M.E., Martinez, A.C., Ros, M.A., and Torres, M. (2000). Opposing RA and FGF signals control proximodistal vertebrate limb development through regulation of Meis genes. Development *127*, 3961-3970.

Mercader, N., Selleri, L., Criado, L.M., Pallares, P., Parras, C., Cleary, M.L., and Torres, M. (2009). Ectopic Meis1 expression in the mouse limb bud alters P-D patterning in a Pbx1-independent manner. Int J Dev Biol *53*, 1483-1494.

Michos, O., Panman, L., Vintersten, K., Beier, K., Zeller, R., and Zuniga, A. (2004). Gremlin-mediated BMP antagonism induces the epithelial-mesenchymal feedback signaling controlling metanephric kidney and limb organogenesis. Development *131*, 3401-3410.

Min, H., Danilenko, D.M., Scully, S.A., Bonlon, B., Ring, B.D., Tarpley, J.E., DeRose, M., and Simonet, W.S. (1998). Fgf-10 is required for both limb and lung development and exhibits striking functional similarity to Drosophila branchless. Genes & Development *12*, 3156-3161.

Minowada, G., Jarvis, L.A., Chi, C.L., Neubuser, A., Sun, X., Hacohen, N., Krasnow, M.A., and Martin, G.R. (1999). Vertebrate Sprouty genes are induced by FGF signaling and can cause chondrodysplasia when overexpressed. Development *126*, 4465-4475.

Mo, R., Freer, A.M., Zinyk, D.L., Crackower, M.A., Michaud, J., Heng, H.H.Q., Chik, K.W., Shi, X.M., Tsui, L.C., Cheng, S.H., et al. (1997). Specific and redundant functions of *Gli2* and *Gli3* zinc finger genes in skeletal patterning and development. Development *124*, 113-123.

Moon, A.M., and Capecchi, M.R. (2000). Fgf8 is required for outgrowth and patterning of the limbs. Nat Genet *26*, 455-459.

Moreno, T.A., and Kintner, C. (2004). Regulation of segmental patterning by retinoic acid signaling during Xenopus somitogenesis. Dev Cell *6*, 205-218.

Mukherjee, K., Sharma, M., Urlaub, H., Bourenkov, G.P., Jahn, R., Sudhof, T.C., and Wahl, M.C. (2008). CASK Functions as a Mg2+-independent neurexin kinase. Cell *133*, 328-339.

Niederreither, K., and Dolle, P. (2008). Retinoic acid in development: towards an integrated view. Nat Rev Genet *9*, 541-553.

Niederreither, K., McCaffery, P., Drager, U.C., Chambon, P., and Dolle, P. (1997). Restricted expression and retinoic acid-induced downregulation of the retinaldehyde dehydrogenase type 2 (RALDH-2) gene during mouse development. Mech Dev *62*, 67-78.

Niederreither, K., Subbarayan, V., Dolle, P., and Chambon, P. (1999). Embryonic retinoic acid synthesis is essential for early mouse post- implantation development. Nat Genet *21*, 444-448.

Niederreither, K., Vermot, J., Schuhbaur, B., Chambon, P., and Dolle, P. (2002). Embryonic retinoic acid synthesis is required for forelimb growth and anteroposterior patterning in the mouse. Development *129*, 3563-3574.

Nissim, S., Hasso, S.M., Fallon, J.F., and Tabin, C.J. (2006). Regulation of Gremlin expression in the posterior limb bud. Dev Biol *299*, 12-21.

Niswander, L., Jeffrey, S., Martin, G.R., and Tickle, C. (1994). A positive feedback loop coordinates growth and patterning in the vertebrate limb. Nature *371*, 609-612.

Niswander, L., Tickle, C., Vogel, A., Booth, I., and Martin, G.R. (1993). FGF-4 replaces the apical ectodermal ridge and directs outgrowth and patterning of the limb. Cell *75*, 579-587.

Noji, S., Nohno, T., Koyama, E., Muto, K., Ohyama, K., Aoki, Y., Tamura, K., Ohsugi, K., Ide, H., Taniguchi, S., et al. (1991). Retinoic acid induces polarizing activity but is unlikely to be a morphogen in the chick limb bud. Nature *350*, 83-86.

Nusslein-Volhard, C., and Wieschaus, E. (1980). Mutations affecting segment number and polarity in Drosophila. Nature *287*, 795-801.

Ohuchi, H., Nakagawa, T., Yamamoto, A., Araga, A., Ohata, T., Ishimaru, Y., Yoshioka, H., Kuwana, T., Nohno, T., Yamasaki, M., et al. (1997). The mesenchymal factor, FGF10, initiates and maintains the outgrowth of the chick limb bud through interaction with FGF8, an apical ectodermal factor. Development *124*, 2235-2244.

Panman, L., Galli, A., Lagarde, N., Michos, O., Soete, G., Zuniga, A., and Zeller, R. (2006). Differential regulation of gene expression in the digit forming area of the mouse limb bud by SHH and gremlin 1/FGF-mediated epithelial-mesenchymal signalling. Development *133*, 3419-3428.

Park, H.L., Bai, C., Platt, K.A., Matise, M.P., Beeghly, A., Hui, C.C., Nakashima, M., and Joyner, A.L. (2000). Mouse Gli1 mutants are viable but have defects in SHH signaling in combination with a Gli2 mutation. Development *127*, 1593-1605.

Pascoal, S., Carvalho, C.R., Rodriguez-Leon, J., Delfini, M.C., Duprez, D., Thorsteinsdottir, S., and Palmeirim, I. (2007). A molecular clock operates during chick autopod proximal-distal outgrowth. J Mol Biol *368*, 303-309.

Pizette, S., Abate-Shen, C., and Niswander, L. (2001). BMP controls proximodistal outgrowth, via induction of the apical ectodermal ridge, and dorsoventral patterning in the vertebrate limb. Development *128*, 4463-4474.

Qin, P., Cimildoro, R., Kochhar, D.M., Soprano, K.J., and Soprano, D.R. (2002). PBX, MEIS, and IGF-I are potential mediators of retinoic acid-induced proximodistal limb reduction defects. Teratology *66*, 224-234.

Ribes, V., Otto, D.M., Dickmann, L., Schmidt, K., Schuhbaur, B., Henderson, C., Blomhoff, R., Wolf, C.R., Tickle, C., and Dolle, P. (2007). Rescue of cytochrome P450 oxidoreductase (Por) mouse mutants reveals functions in vasculogenesis, brain and limb patterning linked to retinoic acid homeostasis. Dev Biol *303*, 66-81.

Riddle, R.D., Johnson, R.L., Laufer, E., and Tabin, C. (1993). *Sonic hedgehog* mediates the polarizing activity of the ZPA. Cell *75*, 1401-1416.

Robert, B. (2007). Bone morphogenetic protein signaling in limb outgrowth and patterning. Dev Growth Differ *49*, 455-468.

Ross, S.A., McCaffery, P.J., Drager, U.C., and De Luca, L.M. (2000). Retinoids in embryonal development. Physiol Rev *80*, 1021-1054.

Rossant, J., Zirngibl, R., Cado, D., Shago, M., and Giguere, V. (1991). Expression of a retinoic acid response element-hsplacZ transgene defines specific domains of transcriptional activity during mouse embryogenesis. Genes Dev *5*, 1333-1344.

Roy, S., and Ingham, P.W. (2002). Hedgehogs tryst with the cell cycle. J Cell Sci *115*, 4393-4397.

Ryckebusch, L., Wang, Z., Bertrand, N., Lin, S.C., Chi, X., Schwartz, R., Zaffran, S., and Niederreither, K. (2008). Retinoic acid deficiency alters second heart field formation. Proc Natl Acad Sci U S A *105*, 2913-2918.

Sagai, T., Hosoya, M., Mizushina, Y., Tamura, M., and Shiroishi, T. (2005). Elimination of a long-range cis-regulatory module causes complete loss of limb-specific Shh expression and truncation of the mouse limb. Development *132*, 797-803.

Sandell, L.L., Sanderson, B.W., Moiseyev, G., Johnson, T., Mushegian, A., Young, K., Rey, J.P., Ma, J.X., Staehling-Hampton, K., and Trainor, P.A. (2007). RDH10 is essential for synthesis of embryonic retinoic acid and is required for limb, craniofacial, and organ development. Genes Dev *21*, 1113-1124.

Saunders, J.W., Jr, and Gasseling, M.T. (1968). Ectodermal-mesenchymal interactions in the origin of limb symmetry. In Epithelial-Mesenchymal Interactions, R. Fleichmeyer, and R.E. Billingham, eds. (Baltimore, Williams and Wilkin), pp. 78-97.

Saunders, J.W., Jr. (1948). The proximo-distal sequence of origin of the parts of the chick wing and the role of the ectoderm. J Exp Zool *108*, 363-403.

Scherz, P.J., Harfe, B.D., McMahon, A.P., and Tabin, C.J. (2004). The limb bud Shh-Fgf feedback loop is terminated by expansion of former ZPA cells. Science *305*, 396-399.

Scherz, P.J., McGlinn, E., Nissim, S., and Tabin, C.J. (2007). Extended exposure to Sonic hedgehog is required for patterning the posterior digits of the vertebrate limb. Dev Biol *308*, 343-354.

Sekine, K., Ohuchi, H., Fujiwara, M., Yamasaki, M., Yoshizawa, T., Sato, T., Yagashita, N., Matsui, D., Koga, Y., Itoh, N., et al. (1999). Fgf10 is essential for limb and lung formation. Nature Genetics *21*, 138-141.

Selleri, L., Depew, M.J., Jacobs, Y., Chanda, S.K., Tsang, K.Y., Cheah, K.S., Rubenstein, J.L., O'Gorman, S., and Cleary, M.L. (2001). Requirement for Pbx1 in skeletal patterning and programming chondrocyte proliferation and differentiation. Development *128*, 3543-3557.

Smith, J.C. (1980). The time required for positional signalling in the chick wing bud. J Embryol Exp Morphol *60*, 321-328.

Spitz, F., Gonzalez, F., and Duboule, D. (2003). A global control region defines a chromosomal regulatory landscape containing the HoxD cluster. Cell *113*, 405-417.

St-Jacques, B., Dassule, H.R., Karavanova, I., Botchkarev, V.A., Li, J., Danielian, P.S., McMahon, J.A., Lewis, P.M., Paus, R., and McMahon, A.P. (1998). Sonic hedgehog signaling is essential for hair development. Curr Biol *8*, 1058-1068.

St-Jacques, B., Hammerschmidt, M., and McMahon, A.P. (1999). Indian hedgehog signaling regulates proliferation and differentiation of chondrocytes and is essential for bone formation. Genes Dev *13*, 2072-2086.

Stavridis, M.P., Collins, B.J., and Storey, K.G. (2010). Retinoic acid orchestrates fibroblast growth factor signalling to drive embryonic stem cell differentiation. Development *137*, 881-890.

Sucov, H.M., Murakami, K.K., and Evans, R.M. (1990). Characterization of an autoregulated response element in the mouse retinoic acid receptor type beta gene. Proc Natl Acad Sci U S A *87*, 5392-5396.

Suemori, H., and Noguchi, S. (2000). Hox C cluster genes are dispensable for overall body plan of mouse embryonic development. Dev Biol *220*, 333-342.

Summerbell, D., Lewis, J.H., and Wolpert, L. (1973). Positional information in chick limb morphogenesis. Nature *244*, 492-496.

Sun, X., Lewandoski, M., Meyers, E.N., Liu, Y.H., Maxson, R.E., Jr., and Martin, G.R. (2000). Conditional inactivation of Fgf4 reveals complexity of signalling during limb bud development. Nat Genet *25*, 83-86.

Sun, X., Mariani, F.V., and Martin, G.R. (2002). Functions of FGF signalling from the apical ectodermal ridge in limb development. Nature *418*, 501-508.

Tabin, C., and Wolpert, L. (2007). Rethinking the proximodistal axis of the vertebrate limb in the molecular era. Genes Dev *21*, 1433-1442.

Tahayato, A., Dolle, P., and Petkovich, M. (2003). Cyp26C1 encodes a novel retinoic acid-metabolizing enzyme expressed in the hindbrain, inner ear, first branchial arch and tooth buds during murine development. Gene Expr Patterns *3*, 449-454.

Tamura, K., Yokouchi, Y., Kuroiwa, A., and Ide, H. (1997). Retinoic acid changes the proximodistal developmental competence and affinity of distal cells in the developing chick limb bud. Dev Biol *188*, 224-234.

Tarchini, B., and Duboule, D. (2006). Control of Hoxd genes' collinearity during early limb development. Dev Cell *10*, 93-103.

te Welscher, P., Fernandez-Teran, M., Ros, M.A., and Zeller, R. (2002a). Mutual genetic antagonism involving GLI3 and dHAND prepatterns the vertebrate limb bud mesenchyme prior to SHH signaling. Genes Dev *16*, 421-426.

te Welscher, P., Zuniga, A., Kuijper, S., Drenth, T., Goedemans, H.J., Meijlink, F., and Zeller, R. (2002b). Progression of Vertebrate Limb Development through SHH-Mediated Counteraction of GLI3. Science *298*, 827-830.

Tickle, C. (1981). The number of polarizing region cells required to specify additional digits in the developing chick wing. Nature *289*, 295-298.

Tickle, C. (2006). Making digit patterns in the vertebrate limb. Nat Rev Mol Cell Biol *7*, 45-53.

Tickle, C., Alberts, B.M., Wolpert, L., and Lee, J. (1982). Local application of retinoic acid in the limb bud mimics the action of the polarizing region. Nature *296*, 564-565.

Tickle, c., Crawley, A., and Farrar, J. (1989). Retinoic acid application to chick wing buds leads to a dose dependant reorganisation of the apical ectodermal ridge that is mediated by the mesenchyme. Development *106*, 691-705.

Towers, M., Mahood, R., Yin, Y., and Tickle, C. (2008). Integration of growth and specification in chick wing digit-patterning. Nature *452*, 882-886.

Turner, N., and Grose, R. (2010). Fibroblast growth factor signalling: from development to cancer. Nat Rev Cancer *10*, 116-129.

Uehara, M., Yashiro, K., Mamiya, S., Nishino, J., Chambon, P., Dolle, P., and Sakai, Y. (2007). CYP26A1 and CYP26C1 cooperatively regulate anterior-posterior patterning of the developing brain and the production of migratory cranial neural crest cells in the mouse. Dev Biol *302*, 399-411.

Varjosalo, M., and Taipale, J. (2008). Hedgehog: functions and mechanisms. Genes Dev *22*, 2454-2472.

Verheyden, J.M., and Sun, X. (2008). An Fgf/Gremlin inhibitory feedback loop triggers termination of limb bud outgrowth. Nature *454*, 638-641.

Vokes, S.A., Ji, H., Wong, W.H., and McMahon, A.P. (2008). A genome-scale analysis of the cis-regulatory circuitry underlying sonic hedgehog-mediated patterning of the mammalian limb. Genes Dev *22*, 2651-2663.

Wanek, N., Gardiner, D.M., Muneoka, K., and Bryant, S.V. (1991). Conversion by retinoic acid of anterior cells into ZPA cells in the chick wing bud. Nature *350*, 81-83.

Wang, B., Fallon, J.F., and Beachy, P.A. (2000). Hedgehog-Regulated Processing of Gli3 Produces an Anterior/Posterior Repressor gradient in the Developing Vertebrate Limb. Cell *100*, 423-434.

White, J.A., Guo, Y.D., Baetz, K., Beckett-Jones, B., Bonasoro, J., Hsu, K.E., Dilworth, F.J., Jones, G., and Petkovich, M. (1996). Identification of the retinoic acid-inducible all-trans-retinoic acid 4-hydroxylase. J Biol Chem *271*, 29922-29927.

White, J.A., Ramshaw, H., Taimi, M., Stangle, W., Zhang, A., Everingham, S., Creighton, S., Tam, S.P., Jones, G., and Petkovich, M. (2000). Identification of the human cytochrome P450, P450RAI-2, which is predominantly expressed in the adult cerebellum and is responsible for all-trans-retinoic acid metabolism. Proc Natl Acad Sci U S A *97*, 6403-6408.

Wilkinson, D.G. (1993). In situ hybridisation (IRL Press).

Wilson, C.W., and Chuang, P.T. (2010). Mechanism and evolution of cytosolic Hedgehog signal transduction. Development *137*, 2079-2094.

Wilson, J.G., Roth, C.B., and Warkany, J. (1953). An analysis of the syndrome of malformations induced by maternal vitamin A deficiency. Effects of restoration of vitamin A at various times during gestation. Am J Anat *92*, 189-217.

Wolpert, L. (1969). Positional information and the spatial pattern of cellular differentiation. J Theor Biol *25*, 1-47.

Wolpert, L., Tickle, C., and Sampford, M. (1979). The effect of cell killing by x-irradiation on pattern formation in the chick limb. J Embryol Exp Morphol *50*, 175-193.

Wong, R.L., Chan, K.K., and Chow, K.L. (1999). Developmental expression of Mab21l2 during mouse embryogenesis. Mech Dev *87*, 185-188.

Yamaguchi, T.P., Bradley, A., McMahon, A.P., and Jones, S. (1999). A Wnt5a pathway underlies outgrowth of multiple structures in the vertebrate embryo. Development *126*, 1211-1223.

Yang, Y., Drossopoulou, G., Chuang, P.T., Duprez, D., Marti, E., Bumcrot, D., Vargesson, N., Clarke, J., Niswander, L., McMahon, A., et al. (1997). Relationship between does, distance and time in Sonic Hedgehog-mediated regulation of anteroposterior polarity in the chick limb. Development *124*, 4393-4404.

Yashiro, K., Zhao, X., Uehara, M., Yamashita, K., Nishijima, M., Nishino, J., Saijoh, Y., Sakai, Y., and Hamada, H. (2004). Regulation of retinoic acid distribution is required for proximodistal patterning and outgrowth of the developing mouse limb. Dev Cell *6*, 411-422.

Zakany, J., and Duboule, D. (2007). The role of Hox genes during vertebrate limb development. Curr Opin Genet Dev *17*, 359-366.

Zeller, R., Lopez-Rios, J., and Zuniga, A. (2009). Vertebrate limb bud development: moving towards integrative analysis of organogenesis. Nat Rev Genet *10*, 845-858.

Zhao, X., Sirbu, I.O., Mic, F.A., Molotkova, N., Molotkov, A., Kumar, S., and Duester, G. (2009). Retinoic acid promotes limb induction through effects on body axis extension but is unnecessary for limb patterning. Curr Biol *19*, 1050-1057.

Zhou, J., and Kochhar, D.M. (2004). Cellular anomalies underlying retinoid-induced phocomelia. Reprod Toxicol *19*, 103-110.

Zhu, J., Nakamura, E., Nguyen, M.T., Bao, X., Akiyama, H., and Mackem, S. (2008). Uncoupling Sonic hedgehog control of pattern and expansion of the developing limb bud. Dev Cell *14*, 624-632.

Zuniga, A., and Galli, A. (2005). Limb Pattern Formation: Upstream and Downstream of Shh Signalling. In Shh and Gli Signalling and Development, S. Howie, and C. Fisher, eds. (Eurekah).

Zuniga, A., Haramis, A.P., McMahon, A.P., and Zeller, R. (1999). Signal relay by BMP antagonism controls the SHH/FGF4 feedback loop in vertebrate limb buds. Nature *401*, 598-602.

Zuniga, A., Michos, O., Spitz, F., Haramis, A.P., Panman, L., Galli, A., Vintersten, K., Klasen, C., Mansfield, W., Kuc, S., et al. (2004). Mouse limb deformity mutations disrupt a global control region within the large regulatory landscape required for Gremlin expression. Genes Dev *18*, 1553-1564.

Zuniga, A., and Zeller, R. (1999). Gli3 (Xt) and formin (ld) participate in the positioning of the polarising region and control of posterior limb-bud identity. Development *126*, 13-21.

Zwilling, E. (1956). Interaction between Limb Bud Ectoderm and Mesoderm in the Chick embryo. II. Experimental Limb Manipulation. JExp Zool, 173-188.

Curriculum vitae

Personal Details
Simone Probst
Date of birth: 04.11.1978
Nationality: Swiss

University Education

2006–2010   PhD student in the Laboratory of Dr. Aimée Zuniga and Prof. Dr. Rolf Zeller, Developmental Genetics, Department of Biomedicine, University of Basel, Switzerland. "Coordination of Limb Bud Development: The Role of SHH in PD Limb Bud Patterning"
2004–2005   Studied Medicine, University of Basel, completion of first year
1999–2003   Studied Molecular Biology, Biozentrum, University of Basel, degree: Diploma (M. Sc.), October 2003
Diploma Thesis: "Towards a Mouse System to Test the Efficacy of Vectored Measles Virus-based Divalent Vaccines" in the laboratory of Prof. Dr. Roberto Cattaneo, Mayo Clinic, Rochester, MN, USA

Work Experience

2010–2011   Postdoctoral position in the Laboratory of Dr. Aimée Zuniga and Prof. Dr. Rolf Zeller, Developmental Genetics, Department of Biomedicine, University of Basel, Switzerland.
2005–2006   Research Assistant, ENT Clinic, University Hospital Basel, Switzerland
2003–2005   Technician and Trainee at "Biotech Manufacturing" and "Preclinical CNS-Research", Roche Basel, Switzerland
1998–1999   6 Months Internship at "Laboratory Animal Services" Novartis, Basel, Switzerland
1 Month Internship in Nursing, Surgical Clinic of the University Hospital Basel

Technical Skills

Developmental biology techniques: mouse colony management, embryo isolation, genotyping, mouse genetics, surgical manipulation and embryo culture, in situ hybridization, skeletal stains, histological techniques, cell death detection, light and fluorescent microscopy
Cell culture techniques: homologous recombination in embryonic stem cells, regular cell line culture and transient transfection for overexpression of proteins, virus stock growth and purification
Molecular biology and biochemistry techniques: protein purification, protein analytics (HPLC), protein chromatography, kinase assays, immunocytochemistry, Western blotting, Southern blotting, pulse-chase labelling, DNA and RNA extraction, PCR and cloning.

Teaching experience

2006–2011   Assistant in Developmental Biology Practical, Medical Faculty, University of Basel, Switzerland. 2006
2003–2005   Presentations at the "Mitarbeiter-Weiterbildung" Seminars at „Biotech Manufacturing", Roche Basel, Switzerland (Topics: Molecular Biology and Immunology)

Presentations

2010   Selected Oral Presentation at CSHL Meeting "Mouse Development, Genetics and Genomics", Cold Spring Harbor, USA
2009   Poster Presentation at the Bio Valley Life Sciences Week, Basel, Switzerland
2008   Poster Presentation at the 10th International Conference on Limb Development and Regeneration, San Lorenzo de El Escorial, Madrid, Spain
2003   Selected Oral Presentation at the "Annual Meeting of the American Association of Virology", Davis, CA, USA

Languages
German   native
English   very good (spoken and written)
French   good
Spanish   basic

Publications

Research:
1. Simone Probst, Conradin Kraemer, Philippe Demougin, Rushikesh Sheth, Gail R. Martin, Hidetaka Shiratori, Hiroshi Hamada, Dagmar Iber, Rolf Zeller and Aimée Zuniga (2011). SHH propagates distal limb bud development by enhancing CYP26b1-mediated retinoic acid clearance via AER-FGF signalling. Development 138, 1913–1923.
2. Claude Fischer, Inti Zlobec, Edith Green, Simone Probst, Claudio Storck, Alessandro Lugli, Luigi Tornillo, Markus Wolfensberger and Luigi Terracciano (2009). Is the improved prognosis of p16 positive oropharyngeal squamous cell carcinoma dependent of the treatment modality? Int. J. Cancer 126, 1256–1262.
3. Claude Fischer, Inti Zlobec, Edith Stöckli, Simone Probst, Claudio Storck, Luigi Tornillo, Alessandro Lugli, Markus Wolfensberger and Luigi Terracciano (2008). Is immunohistochemical epidermal growth factor receptor expression overestimated as a prognostic factor in head-neck squamous cell carcinoma? A retrospective analysis based on a tissue microarray of 365 carcinomas. Hum. Pathol. 39, 1527–1534.

Reviews:
1. Aimée Zuniga, Rolf Zeller, Simone Probst (2011). The molecular basis of human congenital limb malformations. WIREs Developmental Biology, in press.